JEAE

Journal of Engineering in Agriculture and the Environment

ISSN: 1562-6946 **Volume 5. No1. 2019**

KeSEBAE **Kenya Society of Environmental, Biological and Agricultural Engineers**

JEAE

Journal of Engineering in Agriculture and the Environment

ISSN: 1562-6946 **Volume 5. No1. 2019**

Published by:

Kenya Society of Environmental, Biological and Agricultural Engineers (KeSEBAE)
P.O Box 10677-00100
GPO
Nairobi
Tel: +254 788 712 156
Email: info@kesebae.or.ke

KeSEBAE

The Journal of Engineering in Agriculture and the Environment, JEAE, is published by the **Kenya Society of Environmental, Biological and Agricultural Engineers,** KeSEBAE, as an international forum for publication of basic and applied research in engineering for the environment, agriculture and biology based production and processing industries.

CONTENTS Pages

HYDROLOGIC RESPONSE MODELLING IN LUTANANDWA RIVER CATCHMENT, LIMPOPO, SOUTH AFRICA, USING SOIL WATER ASSESSMENT TOOL (SWAT) MODEL

Obiero[1], J.P.O.; Marenya[2], M.O.; Nkuna[3], T. R

[1, 2, 3] University of Venda, Limpopo, South Africa

ABSTRACT

Flow simulation is important in planning and design of engineering hydraulic structures. The purpose of this study is to predict flow in the Lutanandwa river catchment in the Luvuvhu river basin, Limpopo, South Africa. The input data needed for SWAT model set up included Digital Elevation Model (DEM), hydro meteorological data, land cover and soils data acquired from various institutions in South Africa. The DEM was processed from contours in the Department of Hydrology and Water Resources, University of Venda. Meteorological data was acquired from the South African Weather Service (SAWS). Observed daily stream flow data was obtained from the Department of Water Affairs and Sanitation. Land cover data was acquired from processed satellite imagery obtained from the department of Environmental Affairs and ground truthing carried out to verify the land cover information. Soils information was obtained from the Agricultural Research Council – Institute of Soil, Climate, and Water (ARC-ISCW). The soils data was obtained in the form of geo referenced land type map. Based on assessment of the data status, the period 2002 to 2014 was selected for modeling. The meteorological data processed for this period was prepared in the appropriate format for model set up. Soil water characteristic calculator was used to estimate the soil properties required as input to SWAT model. The land cover types in the study area was converted to corresponding SWAT land use types. The statistical parameters required as input to the weather generator in the SWAT model was calculated using the pcpSTAT programme which was used to compute the parameters using weather information. All input data was processed and prepared in the appropriate format for model set up. The processed input data was loaded into the Geographic Information Systems (GIS) interface of the SWAT model to enable model set up for flow simulation.

Keywords: Data preparation, Model set up, hydrologic response

INTRODUCTION

Stream flow hydrographs measure the hydrologic response of catchments to the incident rainfall. Information on runoff is important in design of engineering hydraulic structures used in soil and water conservation, flood control, water storage and hydroelectric power generation. Modeling stream flow is important as it enables prediction of stream flow hydrographs. The ability to predict stream flow is needed in predicting impact of climate change and land use on catchment hydrologic response. Such prediction is important in water resources planning and management. While recognizing the importance of stream flow in information provision on problems related to design, Asati and Rathmore (2012) demonstrated the role of hydrological modelling as a means of comparing performance of various models in runoff prediction. This was accomplished by testing the models of interest on data set from the same watershed. Model comparison has been used in assessing suitability of models and conditions for their applicability to a catchment

(Jajarmizadeh *et al.,* 2015). Modelling stream flow allows for prediction of flow at outlets of ungauged catchments where such information is important in water resources planning and management. The Soil Water Assessment Tool (SWAT) model selected for use in this study is physically based and able to simulate stream flow to a high level of spatial detail through watershed division into sub basins (Santhi *et al.,* 2006). It has been used for applications that include simulation of stream flow and sediment discharge under various land used and management practices world over with notable success (Ndomba and Birhanu, 2008) including simulation of the effect of climate change (Githui *et al.,* 2008) and land use (Odira *et al.,* 2010) on hydrologic response. It has been adapted to catchments of various sizes. The SWAT model has gained publicity worldwide as excellent assessment model for hydrological modelling and water resource management (Vilaysane *et al.,* 2015). The purpose of this study is to demonstrate the role of SWAT model in predicting hydrologic response in the Lutanandwa river catchment, Limpopo, South Africa.

METHODOLOGY

Study area

The study was conducted in the Lutanandwa river catchment, a sub-catchment of the Luvuvhu river basin. The catchment lies between latitudes 22º59'12''S and 23º05'30''S and longitudes 30º09'58" 30º21'58''E and occupies an area of about 132.4km^2, a mean annual rainfall and evaporation of 1287mm and 1200-1600mm respectively. Rainfall is seasonal occurring mainly in the summer months being October to March strongly influenced by the Soutpernsberg Mountains. Temperature varies varies from 2 to 34ºC with a mean value of 18ºC. The catchment is dominated by sandy clay loam soil. Land use activities in the catchment mainly consist of forestry and agriculture in the upper reaches, and rural settlements downstream. The detailed description of the quaternary catchment designated A91D is presented by Odiyo *et al.,* (2012) and illustrated in the Figure 1. The predominant land cover types in the catchment are shown in Figure 2.

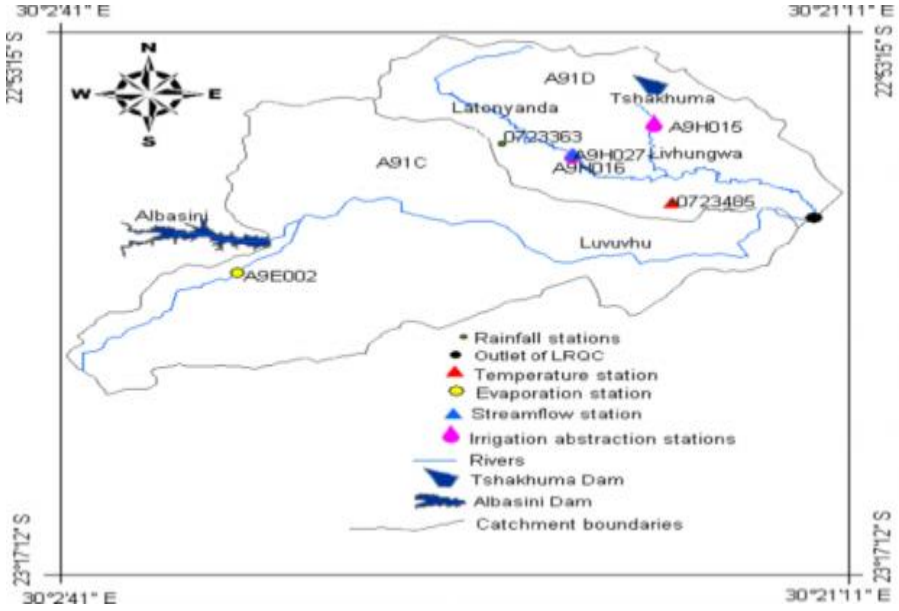

Figure 1: Location of the study area in Luvuvhu river catchment, rainfall stations, stream gauges and weather stations (Adapted from Odiyo *et al.,* 2012)

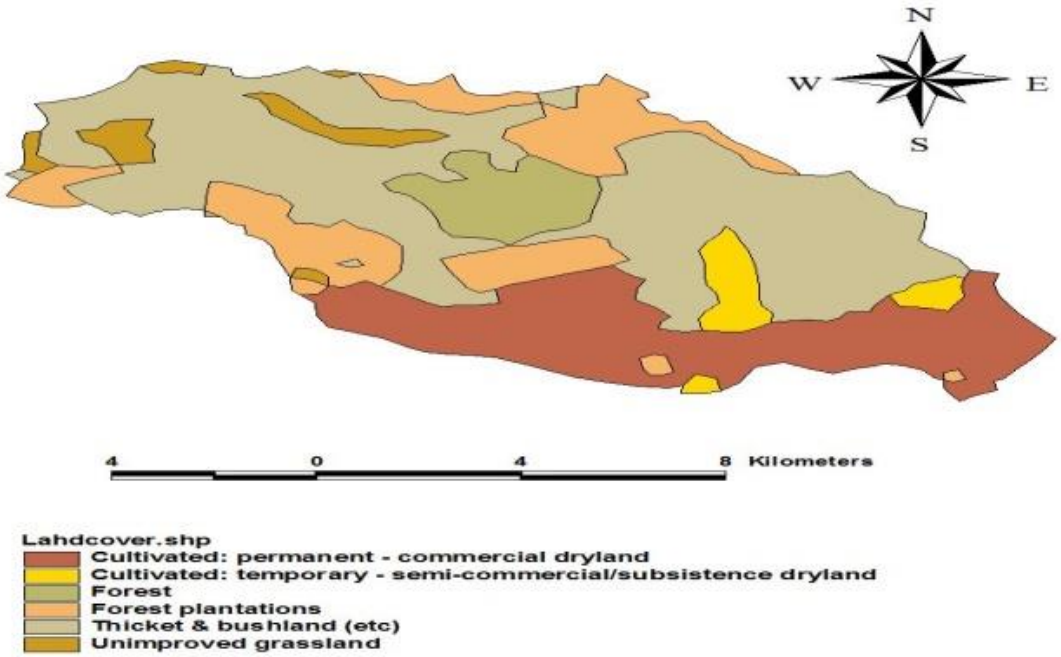

Figure 2: Land use types in the Lutanadwa river catchment

Brief Model description

SWAT model is a process based, continuous physically based distributed parameter river basin model that simulates water, sediment and pollutant yields used to assist water resources managers assess impact of land use management on water, and diffuse pollution for large ungauged catchments with different soil types, land use and management practices (Levesque *et al.,* 2008). A detailed review of the SWAT model and its historical development and applications of the SWAT model is comprehensively documented in Gassman *et al.,* (2007). The model has been used for a wide range of applications for reasons that include its computational efficiency and flexibility on input data requirements (Stehr *et al.,* 2008). Outputs from the model simulation include such hydrological variables as Stream flow, ground water flow, evapotranspiration, sediment yield, surface runoff among others.

Digital elevation model development

The Digital Elevation Model (DEM) was derived from digitized contours using appropriate tools in ArcGIS software. Figure 3 shows the DEM derived from the contours. The DEM was processed at the department of Hydrology and Water Resources, University of Venda.

Hydro meteorological data acquisition and processing

Stream flow data

Daily flow data was acquired from the department of Water Affairs and Sanitation for the station designated A9HO27. The station was damaged by floods in the year 2000 during when it was out of operation for a period of two years. This resulted into a break in the data collection

for the period 2000 to 2002. Hence the period considered for modeling commenced from the year 2002 during when discharge data was continuously recorded to date. During the period 2002 and 2014, the daily flow data had had no gaps making it ideal for model calibration and validation purposes.

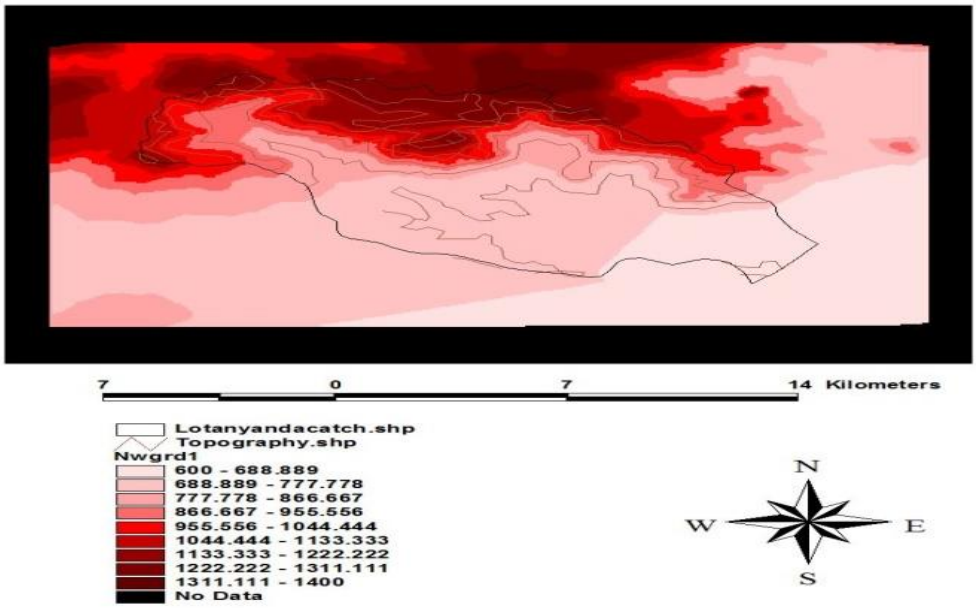

Figure 3: Digital Elevation Model (DEM) developed from contours

Weather data

This was acquired in the form of daily rainfall data and other weather information including daily maximum and minimum temperature, solar radiation, dew point temperature, relative humidity and wind speed acquired on a daily time step. The data was obtained from rainfall stations as well as automatic weather stations in the vicinity of the catchment. Sources of the weather information included the South African Weather Service (SAWS) and the Agricultural Research Council – Institute of Soil, Climate, and Water (ARC-ISCW), South Africa. The period chosen for simulation was 2002 to 2014 during when data was available continuously as required by the SWAT model. The weather data was used to compute the statistical parameters required as input to the SWAT model GIS interface. The statistical parameters computed for rainfall is tabulated below (Table 1). Similar parameters were computed for the other weather elements including temperatures (maximum and minimum), wind speed, solar radiation and relative humidity.

Statistical Analysis of Daily Precipitation Data (2002 - 2012)
Input Filename = rain0212.txt
Number of Years = 11
Number of Leap Years = 3
Number of Records = 4018
Number of NoData values = 200

Table 1 Statistical parameters for precipitation used as input data for the weather generator in the SWAT model GIS interface

Month	PCP_MM	PCPSTD	PCPSKW	PR_W1	PR_W2	PCPD
Jan.	251.62	20.4343	4.5004	0.2717	0.6561	14.27
Feb.	138.93	13.2570	5.2289	0.2825	0.5746	12.18
Mar.	207.87	20.0245	5.3895	0.2914	0.6627	15.09
Apr.	76.24	6.9295	5.0593	0.1705	0.6460	10.27
May.	20.26	3.4449	8.3582	0.0822	0.4286	4.45
Jun.	32.12	4.6497	7.8605	0.1041	0.5082	5.55
Jul.	30.07	4.5771	8.3984	0.0972	0.4340	4.82
Aug.	22.40	2.8726	6.5043	0.1219	0.4194	5.64
Sep.	35.67	3.2729	5.0687	0.1240	0.6477	8.00
Oct	90.65	7.1653	4.2074	0.2677	0.6154	13.00
Nov.	152.37	12.5932	4.8265	0.2737	0.6424	13.73
Dec.	194.53	14.0872	4.0563	0.2895	0.7354	17.18

PCP_MM = average monthly precipitation [mm]
PCPSTD = standard deviation
PCPSKW = skew coefficient
PR_W1 = probability of a wet day following a dry day
PR_W2 = probability of a wet day following a wet day
PCPD = average number of days of precipitation in month

Soil data acquisition and processing

The soils information was obtained from the land type maps acquired from Agricultural Research Council – Institute of Soil, Climate, and Water (ARC-ISCW), in which fifteen land type units were identified. Figure 4 shows the various land types in the study area. The soil texture for the land types in the study area was determined based on the detailed description of the land types provided with the soils data. Specific soil properties are required as input to the SWAT model during the model set up. The Table 2 shows the estimated soil properties based on the use of Soil Water Characteristics Calculator which uses soil texture to estimate the properties based on the use of pedotransfer functions developed by Saxton *et al.,* (2006).

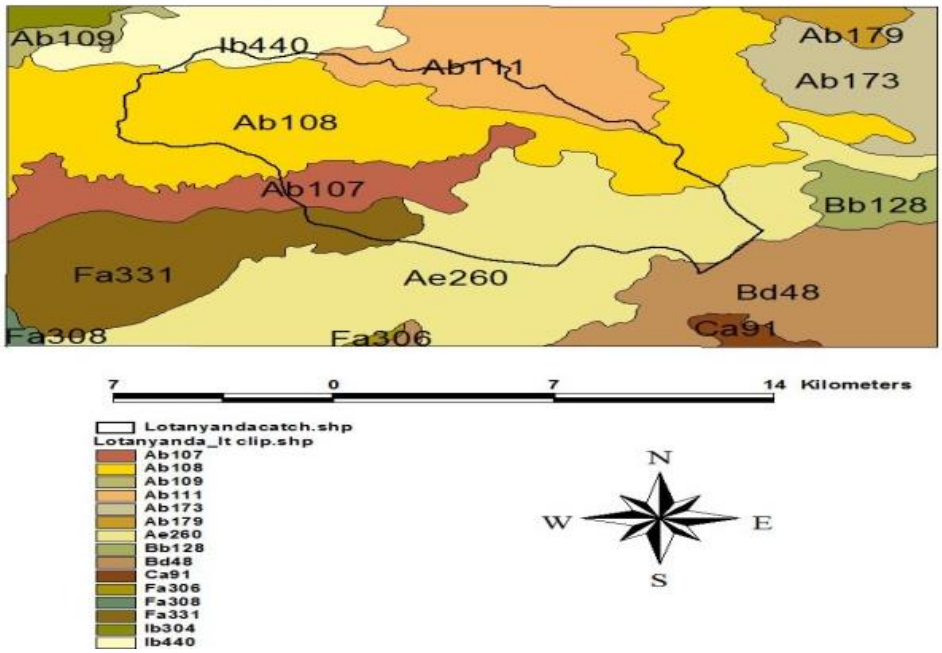

Figure 4: Land types in the study area obtained from soils information acquired

Table 2 Estimated soil properties derived from soil texture for the land types in the Lutanandwa river catchment

Land type	**Approx. Texture**					**Soil properties**					
	Depth (mm)	Ave. % clay (given)	% silt	% sand	TEX	Bulk density	K_s (mm/h)	AWC (cm/cm)	ROCK %	OM %	C
lb304	389	15.0	83.0	2.0	S-L	1.59	1.88	0.22	5	0.0	0.0
Ab109	1004	34	21	45	S-C-L	1.54	2.38	0.12	3.7	0.1	0.058
Ab108	1016	33	22	45	S-C-L	1.55	2.63	0.11	3.0	0.1	0.058
Ab173	807	36	19	45	S-C	1.53	1.86	0.12	0.0	0.1	0.058
lb440	389	15.0	83.0	2.0	S-L	1.59	1.88	0.22	5.0	0.0	0.0
Ab111	887	33	22	45	S-C-L	1.55	2.67	0.12	13	0.1	0.058
Ab179	1058	25	30	45	L	1.59	6.01	0.12	11	0.1	0.058
Fa331	738	20	2	78	S-L	1.64	5.83	0.06	1.7	0.0	0.0
Ae260	981	30	25	45	S-C-L	1.57	3.64	0.12	0.1	0.0	0.0
Bd48	580	14	3	83	S-L	1.63	39.12	0.05	0.9	0.0	0.0
Ab107	763	32	23	45	S-C-L	1.56	2.98	0.12	1.7	0.1	0.058
Bb128	518	15	2	83	S-L	1.63	35.72	0.05	0.0	0.1	0.058
Ca91	568	18	30	52	S-L	1.62	13.31	0.11	0.0	0.1	0.058
Fa306	183	15.0	83	2.0	S-L	1.59	1.88	0.22	0.0	0.0	0.0
Fa308	443	17.0	3	80	S-L	1.64	27.66	0.06	0.0	0.0	0.0

Based on the soil properties estimated from soil texture for each land type, the estimated soil properties are recorded into the GIS interface of SWAT by incorporating the land type and properties into the interface as shown in Figure 5.

Land use data acquisition and processing

The land cover information was obtained from the department of Environmental Affairs website. The land cover information was derived from processed satellite image. The land cover types were then converted to the equivalent SWAT land use types as shown in Table 3.

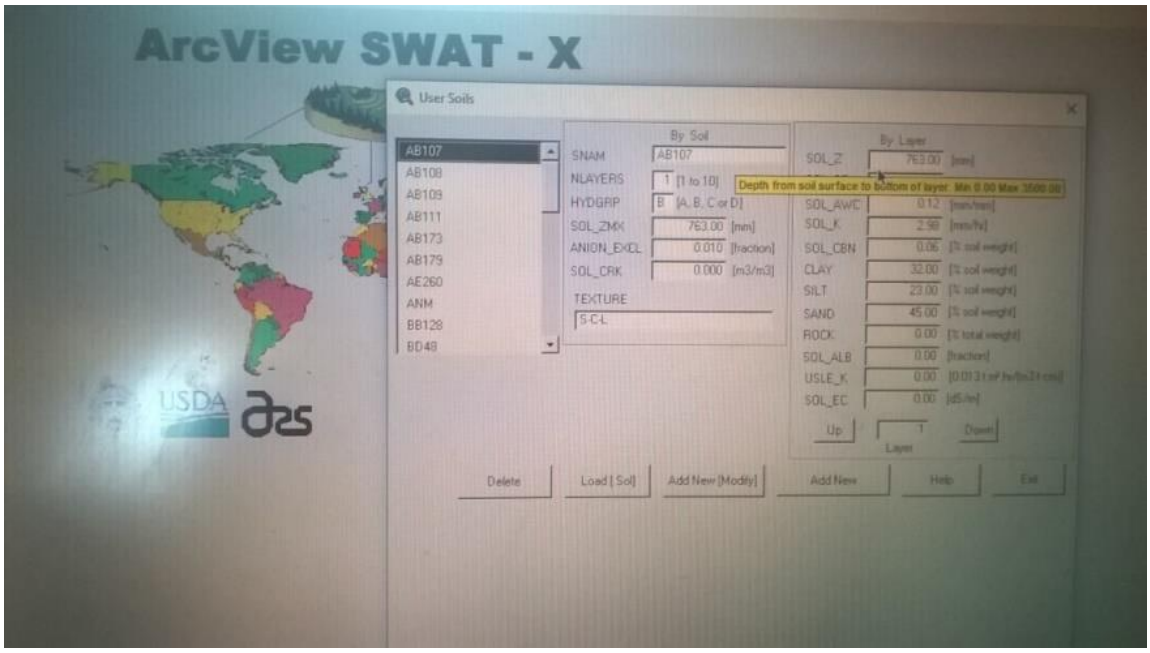

Figure 5: ArcView interface of SWAT illustrating incorporation of soil properties

Table 3 Conversion of land cover to SWAT land use types

land use	SWAT land use	SWAT land use code
Thicket and bush land	Range-grasses	RNGE
Forest plantation	Mixed forest Land	FRST
Unimproved grassland	Bermuda grass	BERM
Forest	Evergreen Forest Land	FRSE
Cultivated: Temporary – semi commercial/subsistence dryland	Agricultural Land-Generic	AGRL
Cultivated: permanent – commercial dryland	Orchard	ORCD
Urban/built-up: residential	Residential-Medium density	URMD
Degraded: Forest and Woodland	Mixed forest Land	FRST
Forest and Woodland	Forest-deciduous	FRSD

Model set up

The automatic delineation dialogue box embedded in the GIS interface of SWAT was used to load the input data that included DEM, to carry out stream definition, addition of catchment outlet and catchment delineation into sub basins and hydrologic response units. Based on the DEM and subsequent stream definition, the watershed was automatically delineated into seven sub basins from a manually digitized masked area derived from the DEM boundary. In the HRU definition, the dominant land use option was used resulting into a single HRU for each sub-basin. The input weather data included the daily rainfall, maximum and minimum temperature. Inputs to the weather generator included daily rainfall, temperatures, solar radiation, wind speed and relative humidity. The trial simulation run was performed on a daily and monthly time steps within the period 2002 to 2014 selected on the basis of availability of stream flow data on a continuous basis devoid of breaks or gaps in data acquired a requirement for calibration and validation processes.

RESULTS AND DISCUSSION

Preliminary simulation of hydrologic response

Daily flow simulations

Flow simulation was carried out after model set up. The year 2002 was used skipped for model warm up. The period 2003 to 2014 was then used for model simulations. A preliminary comparison of observed and simulated daily flow was performed in the period 2004 to 2008 to make a preliminary assessment of the model performance. This period was chosen being when the land cover was considered to be representative. Figure 6 show the hydrographs of observed and simulated total flow during this period.

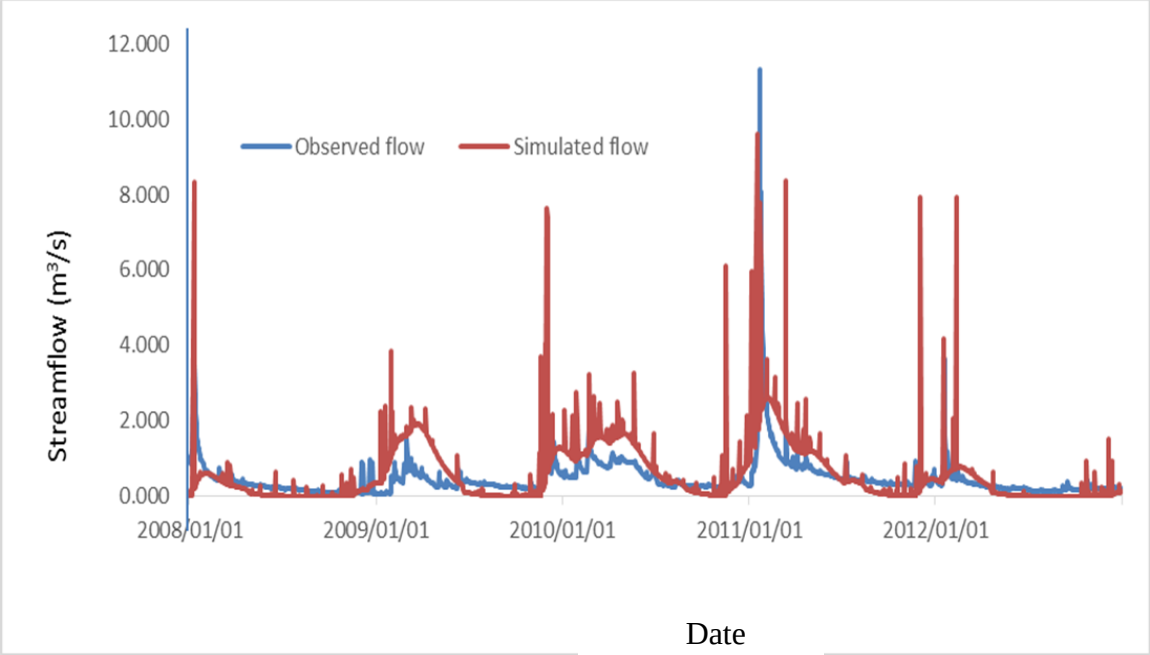

Figure 6: Observed and simulated daily flow during the period 2008 to 2012

The hydrographs of simulated and observed flows tend to follow the same pattern. In general, the model seems to over predict the high flows especially the peak flows but under-predict low flows. Possible reason for over-prediction may be attributed to the differences in the model approach to flow determination and that used in flow observation. Observation of flow is instantaneous reading while the prediction is based on average daily flow. Considering the small size of the catchment, possibility could be that the observations were made when the peak flow has already passed the catchment outlet so that a lower value than the actual peak flow is recorded when reading is taken. The extent to which the low flows are under predicted does not appear to be as pronounced as that to which the high flows are over predicted to the extent that the predicted and observed low flow almost fit. The timing of the peak flows is the same in most instances, i.e. the hydrographs are not out of phase. Figure 7 shows the comparison of observed and simulated flows based on scatter plots and using linear regression for model evaluation.

Based on this initial simulation run, prior to model calibration, the value of coefficient of determination R^2 = 0.30 (r = 0.55) while that of the Nash Sutcliffe Efficiency (NSE) = -0.64, a reflection of unsatisfactory performance based on this preliminary assessment. Values of other performance measures e.g. Root mean square error (RMSE) = 32.15 and the ratio of RMSE and the standard deviation of measured data (RSR) =1.28 also reflected unsatisfactory performance in this first instance. Reasons for unsatisfactory results are partly attributed to the assumption of a single Hydrologic Response Unit (HRU) for each sub-basin during the HRU definition in model set up. Such an assumption results into a poor representation of the sub-basin characteristics also observed by Vilaysane *et al.,* (2015) who points out that multiple scenarios would give a better stream flow estimation. Other possible reasons include poor representation of rainfall for the area in question. Over estimation or under-estimation of rainfall may cause discrepancies in runoff prediction. SWAT model allocates rainfall to a location based on the rain gauge nearest to it according the Thiesen polygon approach to areal rainfall determination which also ignores relief effects. Rainfall varies significantly spatially even within short distances, hence there is possibility of assigning more rainfall that would have occurred resulting into over-prediction of daily stream flow. However, improved performance is expected for monthly flow simulations.

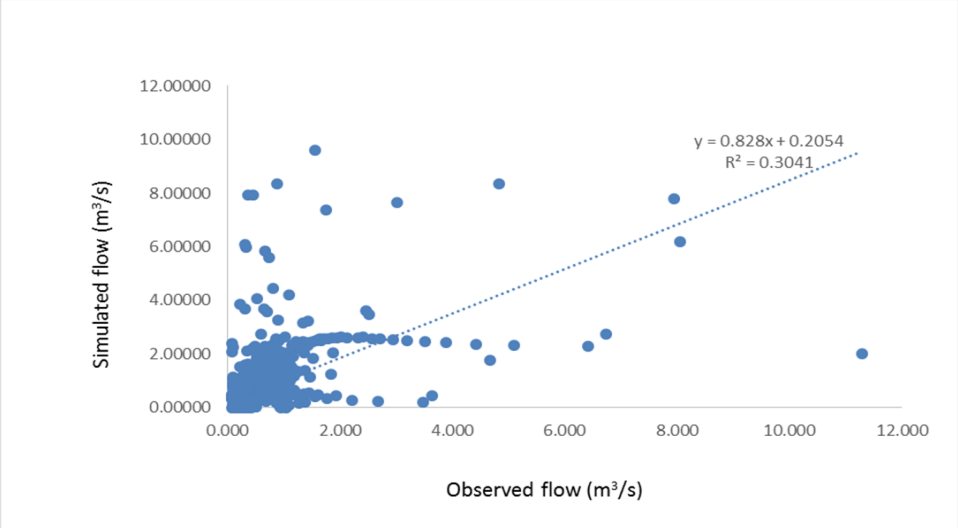

Figure 7: Scatter plot for Observed and predicted daily stream flow based on linear regression

Monthly flow simulation

Subsequent to the daily simulations, flow simulation was carried out for the same period as was done for daily flow i.e. 2008 to 2012. Figure 8 show the monthly flow hydrographs for the simulated and observed flows during this period.

It is evident from the monthly flow hydrographs that the model over predicts high flows. This is also supported by the value of deviation volume (D_v) calculated to be -122.50 which measures the extent to which a model over-predicts the observed values indicating gross over prediction. The flow patterns are however similar. The high peak values are over-predicted. However, the simulated flows closely match the observed flows during the low flows, except for a few isolated instances when there is a slight under-prediction of the low flows e.g. during the period July to October 2009 and also in the period September to October 2011. Figure 9 show the scatter plot between the observed and predicted average daily flow in month for the same period.

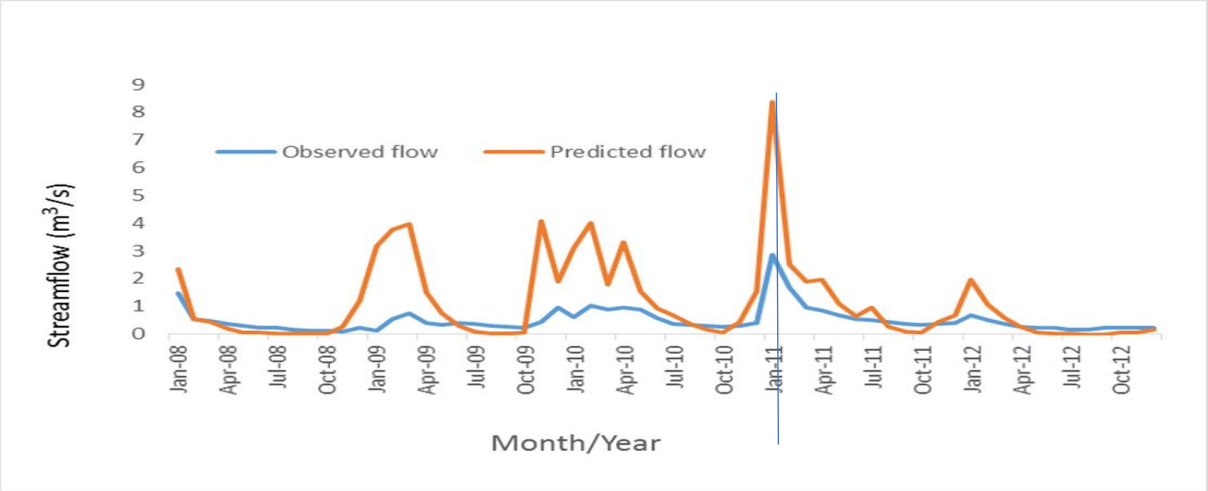

Figure 8: Observed and simulated average daily stream flow in month during preliminary simulation

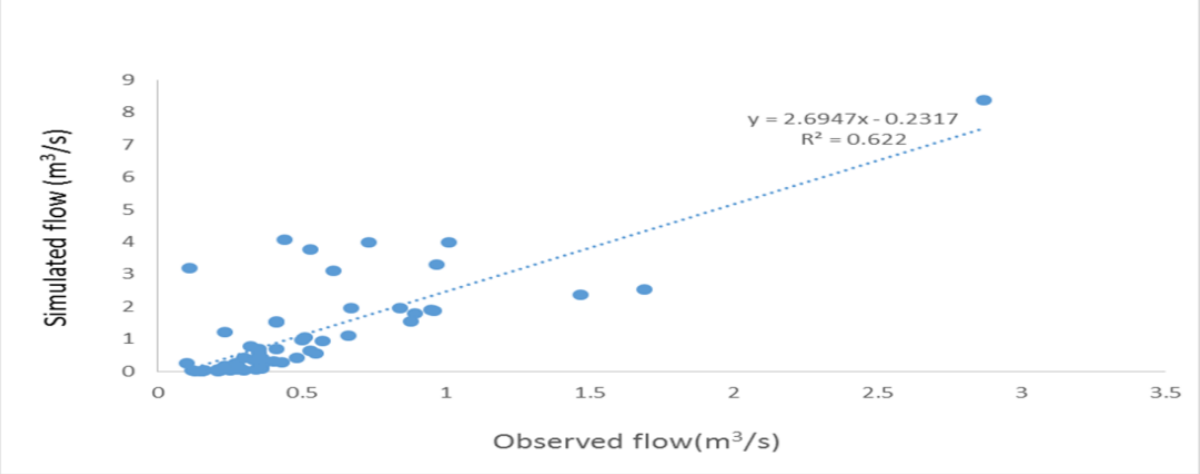

Figure 9: Comparison of observed and simulated average daily flow in month based on scatter plot

Based on the coefficient of determination R^2 = 0.62 (r=0.78), the model performance is satisfactory (>0.5) and therefore acceptable. Values of other performance measures however indicated otherwise.

The NSE = -8.15 PBIAS = -128.9 (>25), RMSE (=10.36>0.7) and RSR (= 3.03>0.7) also reflected unsatisfactory performance ((Moriasi et al., 2007. Unsatisfactory performance is partly attributed to uncertainty on input rainfall data. There are instances where high rainfall is recorded resulting into high runoff response and predicted stream flow, however the observed flows shows no such response. This may be associated with uncertainty of the rainfall data due to possible errors or misrepresentation of the rainfall in the area in question by the selected rain gauge record. Other factors could be the poor prediction of the soil properties. Such properties are required as input to SWAT model, however they were not available and had to be estimated based on soil texture information. Such estimation is approximate based on use of pedotransfer functions. Poor estimation of, say, Available Water Capacity will overestimate or underestimate the soil storage capacity and hence the amount of water available as runoff during rain storms and subsequently yield poor prediction of stream flow. Runoff is sensitive to land cover characteristics which influence the curve number (CN) values. The land cover types had to be converted to corresponding SWAT land use types during model set up. Such approximations of land use may not be representative of the actual land cover type thereby influencing the predicted stream flow. This is more pronounced with high flows that produce runoff and high stream flow. Poor representation of topographic graphical characteristics resulting from unrepresentative DEM may also cause discrepancies in stream flow prediction. Table 4 presents a summary of the performance measures during the preliminary simulation run. Unsatisfactory performance is expected during preliminary simulation runs since no adjustment has been made with regard to the sensitive model parameters. Improved performance is expected during calibration and validation processes.

The model shows promise of good performance in simulation of stream flow especially with respect to improved value for coefficient of determination (R^2) during monthly flow simulation. Also, the fact the patterns of flow are fairly well simulated except that the high flows are grossly over-predicted. The model also simulates the low flow fairly well judging from the reasonably close-fitting hydrographs for the low flows both in the case of daily and monthly flow simulations. The model shows promise for use in low flow simulation.

Table 4 Measures of model performance in stream flow prediction during preliminary flow simulation

Time step	Performance Measures					
	R^2	RMSE	RSR	D_V	PBIAS	NSE
Daily	0.30	32.15	1.28	-25.54	-25.6	-0.64
Monthly	0.60	10.4	3.02	-122.5	-128.9	-0.85

CONCLUSION

The model was able to simulate hydrological stream flow during preliminary simulation run after model set up. The initial performance of the SWAT model in simulation of hydrologic response based on the daily flow simulation is unsatisfactory in this first instance. Several reasons are associated with this performance which includes the uncertainty associated with respect to daily flow simulations owing to the differences in which the model predicts flow and the manner in which observations are made to obtain measured flows. Assumption of single HRU per sub basin during model set up was identified as another possible reason. Improved simulation is also achievable through the more representative approach to model set up which includes use of multiple scenarios in HRU definitions as opposed to the assumption of single HRU per sub basin. Other reasons cited for poor model simulation included poor rainfall

representation or uncertainty with rainfall data, used of unrepresentative land use description, estimation of soil properties etc. Improved simulation performance based on the coefficient of determination (R^2) was observed during monthly flow simulations. Better performance is expected in the subsequent calibration and validation periods. The model shows promise for use in stream flow prediction in the catchment.

ACKNOWLEDGEMENTS

The author wishes to thank the University of Venda through which funding for this project was obtained through the Directorate for Research and innovation. Special thanks to the support obtained from staff at the department of Hydrology and Water Resources for processing some of the input data for model set up. I also wish to acknowledge support obtained from various institutions in South Africa who provided the raw data for this research and included the South African Weather Service (SAWS), Department of Environmental Affairs, Department of Water and Sanitation (DWAS), ESRI South Africa for training in GIS and Agricultural Research Council – Institute of Soil, Climate, and Water (ARC-ISCW).

REFERENCES

Asati, S.R; and S.S Rathmore. 2012. *Comparative study of streamflow prediction models*. Int. J. Life Sc. Bt & Pharm. Re. Vol. 1 (2), IJLBPR: 139 – 151.

Gassman, P.W, M.R. Reyes, C.H. Green and J.G. Arnold. 2007. *The Soil water Assessment Tool: Historical Development, Applications and Future Research Directions*. Transactions of the ASABE 5(4): 1211-1250.

Githui, F; Gitau, W; Mutua, F. and W. Bauwens. 2008. *Climate Change Impact on SWAT simulated streamflow in Western Kenya*. International Journal of Climatology 29 (12): 1823-1834

Jajarmizadeh, M.K, Lafdani, S, Harun. 2015. *Application of SVM and SWAT models for monthly streamflow prediction, a case study in South of Iran*. KSCE J Civ Eng., vol 19 (1): 345 – 357.

Levesque, E., F. Anctil and A. Van Griensven. 2008. *Evaluation of the Streamflow Simulation by SWAT model for two Small Watersheds under Snowmelt and Rainfall.* Hydrological Sciences Journal 53(5): 961–976.

Moriasi, D.N., J.G. Arnold, M.W. Van Liew, R.L. Binger, R.D Harmel, and T.L. Veith. 2007. *Model Evaluation Guidelines for Systematic Quantification of Accuracy in Watershed Simulations.* Transactions of the American Society of Agricultural and Biological Engineers (ASABE*)* 50(3): 885-900.

Ndomba, P.M and B.Z. Birhanu. 2008. *Problems and Prospects of SWAT Model Applications in NILOTIC Catchments*: *A Review*. Nile Water Engineering Scientific Magazine 1: 41-52.

Odira, P.M. A, M.O. Nyadawa, B. Okello, N.A. Juma and J.P.O. Obiero. 2010. *Impact of Land Use/Cover dynamics on Stream flow: A case Study of Nzoia river Catchment, Kenya.* Nile Water Science and Engineering Journal 3(2): 64-78.

Odiyo J.O., Phangisa J.I, Makungo R. 2012. *Rainfall-runoff modeling for estimating Latonyanda River flow contributions to Luvuvhu River downstream of Albasini dam*. Phys. Chem. Earth, 50-52: 5-13.

Santhi, C., Srinivasan, R; Arnold J.G. and Williams, J. R. 2006. *A modelling approach to model the impacts of water quality management plans implemented in a watershed in Texas*, Environmental modelling and software, 21: 1141 – 1157.

Saxton, K.E and W.J. Rawls. 2006. *Soil Water Characteristic Estimates by Texture and Organic Matter for Hydrologic Solutions*. Soil Science Soc. Am. J. 70: 1569-1578.

Stehr, A., A.P. Debeles, F. Romero and H. Alcayaga. 2008. *Hydrological modeling with SWAT under conditions of limited data availability: evaluation of results from Chilean case study*. Hydrological Sciences Journal 53(5): 588-601.

Vilaysane, B., Takara, K; Luo, P; Akkharath, I and Duan, W. 2015. *Hydrological stream flow modelling for calibration and uncertainity analysis using SWAT model in the xedone river basin, Lao PDR.* Procedia Environmental Sciences 28, Elsevier B.V. :380-390.

EFFECT OF SOME PROCESS VARIABLES ON THE STRENGTH, FLOWABILITY AND THERMAL PROPERTIES OF TIGERNUT (*Cyperus Esculentus L*) FLOUR

Komolafe[1], G.O.; Osunde[2], Z.; Idah[3], P.; Chiemela[4], C

[1, 2, 3] Federal University of Technology, Minna, Nigeria

ABSTRACT

This work evaluated the effect of drying temperature, drying time and post sprouting sampling time (as the process variables) on flowability and thermal properties of tigernut flour. Response surface methodology was employed in the experimental design. The flowability of the bulk solid tigernut flour was determined by applying uniaxial compression test of granules using universal testing machine Instron 3369 and by application of the principle prescribed by Carvarlho et al., (2011) and Schulze (2011) and. thermal characteristics using thermal conducting probe and calibrated copper calorimeter. The result showed that the strength of the tigernut flour at 2.01 and 3.02g/cm^3 were higher than that at 1.62g/cm^3 in all the studied tigernut flour samples. The flow functions ranged from 4.01 to 4.86. tigernut flour sample from seeds to sprouted for 36 hours dried at 50^{o}C for 12 hours had the lowest function while tigernut flour sample from seeds sprouted for 43.53hours, dried of 56.44^{o}C for 12.02 hours (optimized sample) had the highest flow function of 4.86. The friction angles which describe the flow properties of the tigernut flour ranged from 41.50^o to 42.20^o for internal friction angle while the wall friction angles varied between 47.80 and 48.5, the angle of internal friction between the tigernut flour granules generally increased with an increase in bulk density in the range of 1.62 to 3.02 g/cm^3, frictional factor and half hopper angle ranged from 1.51 to 1.52 and 22.8 to 23^o respectively. Angle of repose, Hausner ratio and Carr's index ranged from 27.82 to 44.19; 1.17 to 1.34 and 15.34 to 26.13 respectively, with easy flowability flour. Thermal conductivity, specific heat capacity and diffusivity varied between 0.054 and 0.083Wm^{-1}K^{-1}; 390.73 and 1069.6 Jkg^{-1}K^{-1}; 1.197 × 10^{-4} and 2.713 × 10^{-4}m^{2}s^{-1} respectively. This information could be useful in the industrial processing and handling of tigernut flour.

Keywords: tigernut flour, process variables, flowability, thermal properties

INTRODUCTION

Tiger nut (*Cyperus esclentus l.)* is a tuber crop that belongs to the family *cyperaceae,* which is cultivated throughout the world and is widely found in the Northern parts of Nigeria (Chinma *et al.,* 2010). Tiger nut though an underutilized crop has been reported to contain high nutritional properties. Research studies have shown that 100g tiger nuts contain 386 kcal (1635 KJ), 7 % proteins, 35 % fat(oil), 31 % starch, 21 % glucose and 6 % fibre (Muhammad, *et al.,* 2011), minerals (mainly phosphorous and potassium) and vitamin E and C (Belewu and Belewu 2007).

Nowadays, tigernuts are also cultivated in northern Nigeria, Niger, Mali, Senegal, Ghana and Togo where they are used primarily uncooked as side dish. In Africa, Niger –Republic

is the major producer of tigernut, with 125 metric tons, followed by Ghana with 50 metric tons and about 36.3 metric tons in Nigeria, where production is concentrated in the Northern parts of the country (Balami *et al.,* 2015). In Nigeria, tigernut is popularly grown around Zaria, Katsina, Mubi and Kastina-Ala (Abano and Amoah 2011). Tigernut is not widely known as nutritive food crop. Therefore, it has been poorly investigated (Shikhov *et al*., 2011).

Sun- drying has been reported to have drawbacks of both requiring long drying time and poor product quality (Chou and Chua 2001; Soysal *et al.,*2006; Therdthai and Zhou 2009). An increase in the utilization of the crop and formulation of a wide range of possible products from tigernut will require that the traditional drying technique be replaced with efficient drying systems like industrial dryers such as solar and hot air dryers (Ertekin and Yaldiz 2004). Processing of local produce increases its economic value and also increases the gross domestic products (GDP) of her country.

Considering the well documented health benefits of tiger nut, substitution of wheat flour with tigernut flour for cake production is advocated as cakes prepared from such composite flour could help in reducing protein energy and micronutrient deficiency prevalent in developing countries such as Nigeria (Chinma *et al.,*2010).Tigernut flour has also been reported to have food applications such as in cakes, biscuits, cookies, pasta, beverage powder production, inclusion in ice-cream, soup thickener and complementary foods production(Elena *et al*., 2012; Gambo and Da'u 2014). It was also reported that the inclusion of tigernut flour in composite flour programme especially in developing countries, Nigeria in particular has the potentials to conserve foreign exchange, provide nutritious food to more people at affordable cost and widen utilization of indigenous crops in food formulation (Ade-Omowaye *et al.,* 2008). The development of tigernut flour is encouraged, as it will increase the economic value of the crops and provide health benefits to consumer (Sanchez *et al.,* 2012).

In the processing and handling of tigernut flour, the measurement of the properties of the granular solids is important because these properties inherently affect their behavior during storage, handling and processing (Fitzpatrick *et al*., 2004). Powders are the least predictable of all materials in relation to flowability because of the large number of factors that can cause changes in their rheological properties. Generally, powders are either cohesive or non-cohesive. Non-cohesive powders are free flowing, their particles are separate and when unconfined are able to move individually and generally with negligible interparticle forces with major obstruction to flow in this case being internal friction. The processing and handling of granular materials are usually aided by the use of hopper, silo or conveyor. An ideal flow pattern termed mass flow occurs when all the powder is in motion and moving downwards towards the discharge outlet, producing a "first in, first out" pattern. A problem of no flow could occur when the powder forms a cohesive arch across the opening which has sufficient strength within the arch to be self – supporting. At this funnel flow pattern there is an active channel down the centre of the vessel while there is stagnation of powder along the hopper or bin wall, creating a "last in first out" powder delivery which comes along with some operational problems such as rat-holing, segregation and flooding. Rat-holing refers to where a central void develops above the discharge outlet in place of the active flow channel. The rat-holes can collapse causing an excessive aeration of the powder and a great mechanical damage. The aeration in the active flow channel encourages both flooding and segregation which are not desirable. Under this condition, the powder becomes fluid-like and the flow properties could be governed by the physical properties such as particle size and shape, the granular surface structure and particle density and other external conditions such as moisture content, temperature and the presence of other materials or ingredients (Abu-hardan and Hill, 2010).

The flows of granular solids through a given hopper often depend on their flow properties.

Flowability is not an inherent material property, but rather the result of the combination of material physical properties that affect flow and the equipment used for its processing and handling. These properties are important in determining the flow behavior of flour Bulk density affect the structure loads and storage facilities. The angle of repose is important in designing of storage and transporting structures. The Hausner ratio and Carr" s index are two widely used measurements to indicate flowability of bulk solids and are commonly referred to as the compressibility index (Gani *et al*., 2015). The measurement of the physical properties of granular materials is an essential step during the development on the optimization of an industrial process (Lumay *et al.,* 2012). Flowability of granular material can be defined as its ability to flow in a desired manner in a specific piece of equipment (Bumiller *et al.,* 2012). The flow properties of granular solids have recently gained special importance as measures of the quality of final product online as well as during the later handling and on-shelf storage (Molenda and Stasiak 2002). Flow properties are the specific bulk characteristics and properties of the granular materials that affect flow, which can in principle be measured. The flowability of granular solids depends on the relationship between the adhesive forces to the other forces acting on them. The influence of the adhesive forces on the flow behavior increases with decrease in the particle size (Fadeyibi *et al*., 2014). An evaluation of the flow behavior of granular solids must always consider the stresses previously acting on them, the consolidation stress leading to certain adhesive forces exerted on them and hence the strength of the granular solids (Schulze, 2011). The flow function is defined as the ratio of the consolidation to the unconfirmed yield strength. A number of methods and testers exist in literature for determining the thermal, strength and flow properties of bulk solids. Schwedes, (2002) reported that choosing the right method for a specific application requires the knowledge and some experience of handling the bulk materials. The flow properties of bulk materials, either in powdered or granular form are frequently determined by performing a shear text following a slightly modified procedure proposed by Jenike (1964), Fitzpatrick *et al.,* (2004). The use of a more direct method, such as the uniaxial compression test in the measurement of flow properties of granular solids (Schwedes, 2002), use of line heat source in a thermal conductivity probe (Kara *et al*., 2011) and the use of calibrated copper calorimeters for specific heat capacity (Aviara and Haque, 2001) has been reported, but information in this regards on tigernut flour is limited, hence this present study on the effect of processing variables on the thermal properties and flowability of tigernut flour.

At present, bulk density and tapped density measurements are much more widely used than angles of repose to assess powder cohesion and flow properties (Ali, 2005).

While for thermal analysis, steady and transcient-state heat transfer methods are commonly used to analyze physical properties of food samples as a function of temperature.

The objective of this research was to determine the effect of process variables (drying temperature, drying time and post sprouting sampling time) on the flowability and thermal properties of tigernut flour.

MATERIAL AND METHODS

Material

Fifty kilogram of yellow variety of tigernut (*cyperus esculentus* L) seeds was purchased from Sheihk Gumi central market Bakindogo, Kaduna in Kaduna State Nigeria.

Preparation of tigernut flour

The seeds were sorted to remove bad seeds, stones and dirt. They were then washed with potable water, drained and spread separately on clean jute bags, covered with damp cotton cloth and left to sprout at different times. Water was sprinkled at 12 hours interval to facilitate the sprouting process. Hair were removed from the sprouted seeds and then dried as indicated in

experimental design using hot air tray dryer (LE ECHWA Model LH-1300) at 2.0m/s air velocity. At the end of the drying for each sample, they were cooled, milled and passed through a 212(micron) number 70 sieve (Laboratory EndeCott test sieve), cooled and packaged in an airtight low-density polyethylene bags and stored in freezer at -18 ^{o}C until removed for analysis.

Design of experiment

Response surface methodology according to Myers and Montgomery (2002) was adopted,

With the experimental design as shown in Table 1,

Table 1 Variable for the Tigernut Flour Process Parameters

Variable	Code	Unit	Variable levels				
			-α	-1	0	+1	+α
Drying Temp	X_1	^{o}C	46.59	50	55	60	63.41
Drying time	X_2	Hr	11.32	12	13	14	14.68
Post sprouting time	X_3	Hr	31.91	36	42	48	52.09

X_1, X_2, X_3 and their levels of variation are based on literature (Chinma *et al.,* 2009; Chinma *et al.,* 2010; Komolafe *et al.,* 2012) and preliminary experimentations.

Design Constrains**:** $46.59 \leq X_1 \leq 63.41$; $11.32 \leq X_2 \leq 14.68$; $31.91 \leq X_3 \leq 52.09$

2.4 Uniaxial compression test

The universal Testing Machine {UTM) Instron 3369 was used to carry out a compression test on the bulk samples tigernut flour at the Kwara state University Malete, Nigeria. The method described by Carvalho *et al.,* (2011) was employed in determining the consolidation, shear and unconfined yield stresses of the tigernut flour. The experimental condition was maintained at (16 ±1) ^{o}C and 50% relative humidity throughout the compression testing period.

The values of stress at peak break and yield points of compression were read from the UTM operated at the speed of 0.001mm/sec and in the loading range of 81.13 to 2,313.58N as test condition. The compressive stress at peak gave the consolidation stress of the tigernut flour under compression in a confined hollow cylindrical ring. On further compression, the sample which is now unconfined at the sides, broke at certain critical stress called shear stress of the tigernut flour sample under compression. The yield limits of the tigernut flour samples, which depend on their previous consolidation trials, gave greater values of the unconfined yield stress as the bulk density and consolidation stress increased as shown in figure 1 (Schulze, 2011).

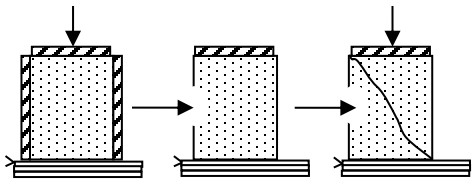

Figure 1: Uniaxial compression Test of Tigernut Flour Granule

(σ_y= unconfnded yield stress (kPa), σ_c = consolidation stress (kPa) (Schulze, 2011).

The procedure was repeated three times for all the tigernut flour samples.

2.5 Determination of flow function, friction factor, angle of internal and wall frictions.

The flow behavior of granular solids, is dependent on the flow function being friction angles, consolidation and unconfined yield stresses, can be assessed using equation (1) and (2).

$$Flowability \frac{consolidated\ stress}{unconfined\ yields\ strength} \quad \ldots (1)$$

(Schulze, 2011).

Flowabilities of the granular solids characterized with respect to their functions according to the flow classification of bulk solids proposed by Jenike (1964), is

$$ff = \frac{\delta c}{\delta y} = \frac{(1 + Sin\theta_w)\, x\, (1 - sin\theta_1}{2\,(Sin\theta_w - Sin\theta_c)} \quad \ldots (2)$$

(Jenike, 1964)

Where: δ_c = consolidated stress (Kpa), δ_y = unconfined yield strength (Kpa), θ_w = angle of wall friction (degree), θ_i = angle of internal friction (Kpa)

The flow function was computed from the inverse of the slopes of the straight lines connecting the unconfined yield strength and consolidation stress of the tigernut flour samples as obtained from the uniaxial compression test. The flow behaviors of the tigernut flour were assessed using Equations (1) and (2) which shows the dependence of the flow function on the friction angles, consolidation and unconfined yield stresses. The flowabilities of the granular solids (tigernut flour) were characterized with respect to their flow functions according to the flow classification of bulk solids proposed by Jenike (1964), as shown in Figure 2 (Schulze, 2011).

The angle of internal friction of the tigernut flour was determined from the straight lines tangent to the greatest Mohr circle (Figure 3) which defines the effective yield locus enclosing the consolidation stress axis and the angle of internal friction of the curves. The radius of the Mohr stress circle is equal to the unconfined yield stress of the granular solids (Peleg, 1981; Thalberg *et al.*, 2004; Chase, 2012; Oko *et al*., 2015). The friction angle of wall friction was determined from the effective yield locus. Based on the established empirical relationship between the flow behaviors of granular solids and the angle of internal friction, flow function and friction factor as expressed in Equation (3), the friction factors of the granular solids were computed (Fadeyibi *et al.*, 2014).

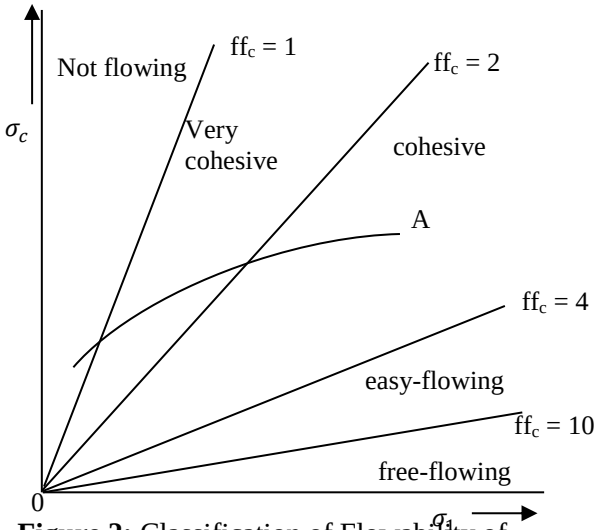

Figure 2: Classification of Flowability of Granular Solids

Granular Solid (ff_c) is flow function, σ_c is shear stress, σ_1 is consolidation stress (Schulze, 2011).

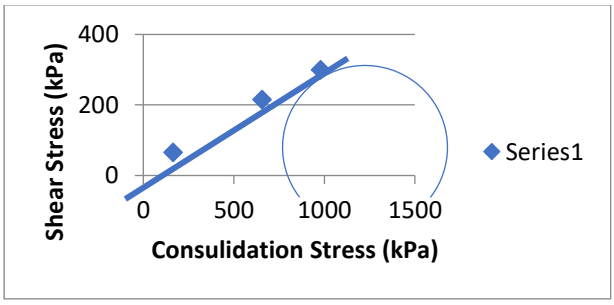

Figure 3: Consolidation-shear stress curve for tigernut flour

H (θ) = ff 4 sin θ_i / 1+ sin …(3)

Where H (θ) = friction factor accounting for the vibration in the arch thickness (dimensionless).

2.6 Determination of loose density and bulk density of tigernut flour

The loose and bulk densities were determined according to the method described by Shumaila *et al.*, (2015). The tigernut flour was carefully filled into a 100ml standard graduated cylinder of Vankle's design, initially filled up to the 25ml

volume of the cylinder and then weighed. The cylinder was tapped on a flat surface about 10 times and the cylinder further filled with the tigernut flour and weighed again. The loose bulk and tapped density were calculated based on the volume of the cylinder and weight of the material established from the expressions given by Shumaila *et al*., (2015) in Equations (4) to (7).

$$\rho_l = W_l / V_l \quad \ldots (4)$$

$$\rho_t = W_t / V_t \quad \ldots (5)$$

Where ρ_l and ρ_t are the densities (kg/m^3), W_l and W_t are the masses (kg), V_l and V_t are the volumes (m^3) of tigernut flour in loose and tapped fill respectively. The loose bulk and tapped densities were used to compute the Carr's index (CI) and Hausner ratio (HR).

$$CI = 100 \times [(\rho_t - \rho_l) / \rho_t \quad \ldots (6)$$

$$HR = \rho_t / \rho_l \quad \ldots (7)$$

Hausner ratio was expressed in decimals and is defined as the ratio of a material tapped bulk to its loose bulk density.

2.7 Determination of angle of repose

The angle of repose is the angle formed by the horizontal base of the bench surface and edge of a cone-like pile of granules. The angle of repose was determined using the method described by Shumaila *et al.,* (2015). The cylinder was placed over a plain surface and tigernut flour was carefully filled in, tapping during filling to get uniform flour packing and to minimize or prevent the wall effect. The tube was then slowly raised above the floor so that the whole material could sslide and forms a natural slope. The height of the heap above the floor and the diameter of its base were measured and the angle of repose (φ) was calculated using Equation (8).

$$\text{Angle of repose } (\phi) (^\circ) = \tan^{-1} 2h/D \quad (8)$$

Where ϕ is angle of repose (°), h is height of the pile (mm), D is the diameter of the pile (mm). The flowability was then classified using Table 2 scale of flowability (Igathinathane *et al*., 2010).

Table 2 Scale of Flowability

Carr's Index	Angle of Repose	Hausner Ratio	Flowability
10	25-30	1.00-1.11	Excellent
11-15	31-35	1.12-1.18	Good
16-20	36-40	1.19-1.25	Fair
21-25	41-45	1.26-1.34	Passable
26-31	46-55	1.35-1.45	Poor
32-37	56-65	1.46-1.69	Very poor
>38	>66	>1.60	Very very poor

Source: Igathinathane *et al*., (2011)

2.8 Determination of Thermal Properties of Tigernut Flour

2.8.1 Determination of thermal conductivity

The tigernut flour thermal conductivity test was determined according to the method described by Bozikova (2008).The thermal conductivity of the flour samples were determined at the Kwara State University, Malete, Nigeria, using TE19S thermal conductivity apparatus and applying thermal needle (hot wire) probe procedure. Known constant heat energy was passed to the flour sample, the temperature rise was recorded over a period of time. The heating wire as well as the temprtature sensor (thermocouple) is encapsulated in the probe that electically insulates the hot wire and the temperature sensor from the test material. The heat source was assumed to have a constant and uniform output along the length of the test sample. The thermal conductivity (κ) was calculated using Equation (9).

$$\kappa = \frac{Q}{4\pi}\left[\frac{dT}{d(lnt)}\right]^{-1} \quad \ldots (9)$$

Where: κ is thermal conductivity in W m^{-1}K^{-1}, Q is the heat input which is the quantity of heat applied in Wm^{-1}, dT/d(lnt) is a numerical value deduced from experimental data, T_1 is temperature at the top of the flour sample (specimen) in ^{o}C, T_2 is the temperature at the bottom of the sample in ^{o}C and t is time in s.

The heat input (Q) was expressed as in Equation (10).

$Q = VI/L$ ... (10)

Where: V is voltage in (V), I is current in (A) and L is the length of the heater wire in m.

2.8.2 Determination of specific heat capacity

The specific heat of tigernut flour was determined using calibrated copper calorimeter following method described by Aviara and Haque (2001). The experiment was carried out at the Kaduna Polytechnic, Kaduna State, Nigeria. A tigernut flour sample of known mass and moisture content was put into the calorimeter containing water of known mass and temperature. The mixture was then stirred using a copper stirrer. A constant heat input was passed through the heater to the mixture. The temperature rise with time relationship was used to calculate the heat capacity (C_p) using Equation (11)

$$C_p \approx \frac{(m_c C_c + m_w C_w)[T_w - (T_e + t'R')]}{m_s[(T_e + t'R') - T_s]} \quad \ldots (11)$$

Where; C_p, C_c and C_w are the specific heats of sample, calorimeter and water, respectively (J kg^{-1} K^{-1}); m_s, m_c and m_w are the masses of sample, calorimeter and water (kg), respectively; R' is the rate of temperature fall of the mixture after equilibrium

2.8.3 Determination of thermal diffusivity of tigernut flour

The thermal diffusivity of tigernut flour was determined by the application of time-temperature relationship obtained in the above thermal experimentation using Equation (12) as applied by Aviara, Haque and Ogunjimi (2008).

$$\alpha = \underline{k}\backslash\rho C_p \quad \ldots (12)$$

Where α is thermal diffusivity in m^2s^{-1}, κ is thermal conductivity in $Wm^{-1}K^{-1}$, ρ is the density in kgm^{-3} and C_p is the specific heat capacity in J / kg ^oK

3 Results and Discussions

3.1The strength properties of the tigernut flour at varied bulk densities are shown in Table 3.The compressive strength of the tigernut flour increases with an increase in the bulk density as shown in Table 3. The strength of the tigernut flour at 2.01 and 3.02g/cm^3 was higher than that at 1.62g/cm^3 in all the studied tigernut flour samples. Since at the bulk densities of 2.01 and 3.02g/cm^3 the compressive strengths were higher, they would likely be sufficient for the maximum compression of the tigernut flour granular solids. This observation is in agreement with the report made by Fadeyibi *et. al*., (2014) that the higher the bulk densities of granular solids, the higher the compressive strength required to form granules and agglomerates of the solids. This indicates that an increase in the density of the granular solids at constant moisture will lead to increase in the strength of the resultant structure of the material. The bulk density of 3.02g/cm^3 can therefore be used in the design of hopper and storage bin for the consistent flow of tigernut flour.

The result of the strength properties of the tigernut flour samples also showed that there is increase in the strength of the granular solids with decrease in moisture content. This observation is in line with report by Peleg *et al*., (1973); Jose *et al*., (2017) that the compressibility of granular solids (pellets) increase with a decreased in the moisture content at lower loads, but the particle size did not have any significant effect on the compressibility.

It was equally observed that the consolidation stress of the tigernut flour is higher than its corresponding shear and unconfined yield strengths at all the varied bulk densities evaluated. This is probably due to the decrease in the crossectional area of the granular solids with an increase in the vertical loads observed during the uniaxial compression test. This observation is also in line with that reported by Fadeyibi, *et al*., (2014) for cassava and yam starch-glycerol composite granular solids.

3.2 Flow Functions of Tigernut Flour Samples

The flowability of bulk solids or granular solids depends on its consolidation stress and unconfined yield strength as indicated in equations (1) and (2) and by extension flowability of granular solids therefore depends on its flow functions. The flow functions of the studied tigernut flour samples are shown in Table 4. The result of the flow functions indicated that all the tigernut flour samples at the studied experimental condition had easy flowability, the flow functions ranged from 4.01 to 4.86. tigernut flour sample from seeds to sprouted for 36 hours dried at 50°C for 12 hours had the lowest function while tigernut flour sample from seeds sprouted for 43.53hours, dried of 56.44°C for 12.02 hours (optimized sample) had the highest flow function of 4.86. the greater the flow function of a bulk solid, the better its flowability in a specific equipment (Schulze, 2011, Fadeyi *et al.*., 2014 comparing the result of flow functions of the tigernut flour samples (Table 4) with the flowability classifcaiton in Figure 2 implies that all the tigernut flour samples at the studied experimental processing condition had easy flowability. It can also be deduced that since the consolidation stress increases with increase in the unconfined yield strength, any increase in the yield strength will also results into increase in flow function of the granular solids, hence increase its flowability. Also, as shown in Figure 4 the flowability of tigernut flour increase with the increase in flow function, despite that the values of the flow functions observed for the stated three samples are not wide apart. Therefore, for this reason based on this experimental work the tigernut sprouted for 43.53 hours, dried at 56.44°C for 12.02 hours had the best and easiest flowability of 4.86 flow function. This is in agreement with the work reported by Thalberg *et al.*, 2004 on the comparison of different flowabilituy tests of powders that stated that contrary to the difficult flows in most granular solids, the higher flow function and lower force of cohesion in most powder are evidence of their higher flowabilities. The flow function can be used in the characterization of flowability of tigernut flour and in the design of the handling and processing of the tigernut flour products.

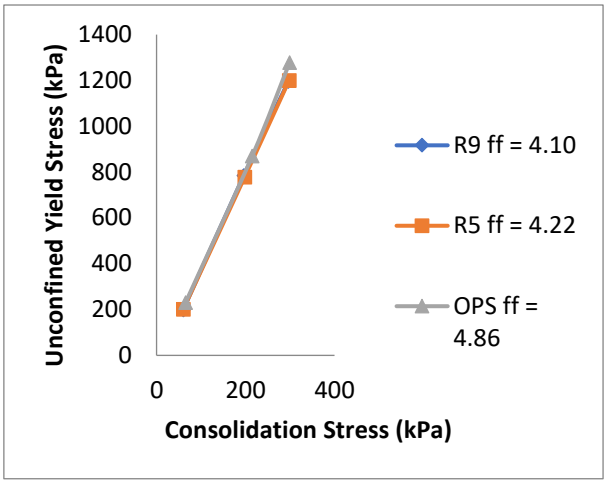

Figure 4: Flow Function of Tigernut flour

The result of the friction angles which describe the flow properties of the tigernut flour ranged from 41.50° to 42.20° for internal friction angle while the wall friction angles varied between 47.80 and 48.5, the angle of internal friction between the tigernut flour granules generally increase with an increase in bulk density in the range of 1.62 to 3.02 g/cm^3, however the values of internal friction angle obtained in this study is slightly higher (41.50 to 42.20) against 40° reported by Fadeyibi *et al.*, 2014 for cassava yam starch glycerol composite flour.

The angle of internal friction is a measure of the force required to cause the flour particles to move or slide against each other. The angle of internal friction data is useful in calculating the lateral pressure on the wall storage bins and for the design of gravity flow hopper, silo and processing of bulk solids (Jenike, 1964, Peleg, 1981; Thalberg *et. al*., 2004). Oko *et al*., 2015 reported a lower angle of wall friction of 29° for potato flour. Fadeyibi *et al.*, 2014 reported that higher angle of wall friction at 3g/cm^3 was required in the design of hopper or silo with steeper walls for the consistent flow of the granuler solids. Similar report was also made by Bamiller *et al*., (2012).

3.3 Scale flowability of the Tigernut Flour

The result of the flowability of the tigernut flour samples studied based on scale flowability by the assessment of Carr's index angle of repose and Hausner ratio is shown on Table 5. Friom the result obtained none of the tigernut flour sample within the studied process condition had poor flowability. It was observed that decrease in the angle of repose and Housner ratio result in decrease in flowability.

The result also indicated that flowability of the tigernut flour samples were influenced by their moisture content. Flowability increases with decrease in moisture content which in summary based on the moisture contents of the samples are:

$3.48\% \leq mc \leq 4.3\% \equiv$ passable flowability

$3.40\% \leq mc \leq 3.90\% \equiv$ fair flowability

$2.79\% \leq mc \leq 3.39\% \equiv$ good flowability

$2.44\% \leq mc \leq 2.78\% \equiv$ excellent flowability

Where mc is moisture content

This observation is in line with the report by Fitzpatrick et. al.; (2004) who determined the flow properties of thirteen granular solids of varied particle sizes, moisture contents, bulk densities and particle densities and moisture content markedly influenced the flowability.

Hence, based on these findings, it can be established that the flow function of granular solids (such as the tigernut flour studied) largely depend on its particle size moisture content and the cohesive force between the particles.

3.4 Thermal Properties of Tigernut Flour

The result of the thermal properties of tigernut is as shown in Table 6. Thermal conductivity varied between 0.053 wm^{-1} and 0.083 wm^{-1}/C^{-1} thermal conductivity, while that sprouted for 42 hours dried at 46.59°C for 13 hours had the highest 0.083$wm^{-1}C^{-1}$thermal conductivity.

It can be deduced from the result obtained that thermal conductivity increased with increase in bulk density. Oke *et al.,* (2007) had reported similar trend for sweet potatoes. This increase in thermal conductivity with increase in bulk density could probably be due to more mass of the sample contained per unit volume which means the greater the density of the sample the lower the volume of air in the particle intensities and the greater the contact between the particles, hence.

A lower thermal conductivity values of range 0.329 W/m °C and 0.344W/m °C was reported for cassava flour (Sanni *et al*., 2016). The highest thermal conductivity 0.083 $Wm^{-1}K^{-1}$ recorded for tigernut sample (run 9) could be attributed to its highest moisture content of 4.38% and lowest drying temperature 46.59 °C compared to 2.41% moisture content and 63.41°C drying temperature in run10 as corroborated by Nwabanne (2009).

This observation agreed with the report by Ikegwu *et al*., (2016) that temperature and moisture content significantly affect the thermal conductivity of African yam bean. Thermal conductivity range from 0.267 to 0.374 W/m °C were reported (Ikegwu *et al*., 2016) for African yam bean.

The specific heat capacity fot tigernut flour ranged from 390.73 J $Kg^{-1}K^{-1}$ to 1069.60 J $Kg^{-1}K^{-1}$. Tigernut sprouted for 42 hours dried at 63.41°C for 13 hours had the lowest 390.73 J $Kg^{-1}K^{-1}$ specific heat capacity, while tigernut sprouted for 42 hours dried at 46.59 °C for 13 hours had the highest 1069.60 J $Kg^{-1}K^{-1}$ specific heat capacity. This signified that the specific heat capacity increased with increase in moisture content and temperature. This trend of increase in specific heat capacity with moisture was also reported by Oke *et al*., (2007); Sanni *et al*., (2016) and Ikegwu *et al*., (2016). Specific heat capacity for sweet potato ranged from 1.905 ± 0.457 KJ /Kg °C to 2.0 ± 0.382 KJ /Kg °C (Oke *et al.*, 2007) while 1803.88 J/Kg °C to 1900.62J/Kg °C specific heat capacity was reported for cassava flour (Sanni *et al*., 2016) while specific heat

capacity of 670.33 JKg^{-1} K^{-1} was obtained for the optimized tigernut flour.

Diffusivity of tigernut flour varied between 1.197 × $10^{-4}m^2s^{-1}$ and 2.713 × $10^{-4}m^2s^{-1}$. Tigernut sprouted for 42 hours dried at 63.41ºC for 13 hours had the highest 2.713 × $10^{-4}m^2s^{-1}$ diffusivity, while the tigernut sprouted for 42 hours dried at 46.59 ºC for 13 hours had the lowest 1.197 × $10^{-4}m^2s^{-1}$ diffusivity. In this study it was observed that diffusivity decreased with increased in moisture content and decrease in temperature. Similar trend was reported for the thermal diffusivity of sweet potato (Oke *et al*., 2007), thermal diffusivity of cassava (Sanni *et al*., 2016) and the thermal diffusity of African yam bean (Ikegwu *et al*., 2016).The thermal diffusivity ranged from 3.89 × $10^{-7}m^2s^{-1}$ to 4.81 × $10^{-7}m^2s^{-1}$ for cassava (Sanni *et al*., 2016) while the thermal diffusivity of sweet potato ranged from 2.918 × $10^{-8}m^2s^{-1}$ to 9.203 × $10^{-8}m^2s^{-1}$ (Oke *et al.*, 2007). Thermal diffusivity of 1.605 × $10^{-4}m^2s^{-1}$ was observed for the optimized tigernut flour. The results observed in this study therefore showed that these engineering thermal properties are influenced by density, moisture content and temperature. The knowledge of the thermal properties would be of assistance in heat transfer calculations involving tigernut flour processing and handling.

CONCLUSION

The bulk density of 3.02g/cm^3 was observed to be sufficient for the maximum compression of tigernut flour granular solids. Increase in the strength of the granular of tigernut flour with decrease in moisture content was observed. Consolidation stress of the tigernut flour was higher than its corresponding shear and unconfined yield strengths in all the varied bulk densities evaluated. Flowability of bulk tigernut flour depends on its consolidation stress and unconfined yield strength. All the tigernut flour samples at the studied experimental conditions had easy flowability, with flow function that ranged from 4.01 to 4.86. Tigernut flour sprouted at 43.53 hours dried at 56.44 ºC for 12.02 hours had an excellent flowability, with flow function of 4.86, internal friction angle of 42.20º, friction factor of 1.52, wall friction angle of 47.8 and half hopper angle of 22.8º, recording Hausner ratio, Carr's index and angle of repose of 1.18, 15.34 and 29.66º respectively, with an excellent flowability. Thermal conductivity of 0.054 $Wm^{-1}K^{-1}$, specific heat capacity of 670.33$Jkg^{-1}K^{-1}$ and diffusivity of 1.605 × $10^{-4}m^2s^{-1}$ respectively were obtained for its thermal properties. This information could be useful in the industrial processing and handling of tigernut flour.

Table 4 Flow Properties of Tigernut Flour Samples

S	Ff	θ_i	θ_w	H (θ)	θ(º)
1	4.01	41.50	48.50	1.510	23.50
2	4.68	41.88	48.12	1.518	23.13
3	4.14	41.58	48.42	1.512	23.05
4	4.80	42.10	47.90	1.522	23.11
5	4.22	41.60	48.40	1.513	23.30
6	4.80	42.08	47.92	1.522	23.10
7	4.66	42.00	48.00	1.519	23.13
8	4.80	42.05	47.95	1.521	23.10
9	4.10	41.55	48.45	1.511	23.40
10	4.50	41.80	48.20	1.516	23.14
11	4.51	41.75	48.25	1.515	23.14
12	4.69	41.90	48.10	1.518	23.12
13	4.11	41.57	48.53	1.512	23.40
14	4.56	41.85	48.15	1.517	23.13
15	4.51	41.95	48.05	1.519	23.14
16	4.44	41.67	48.33	1.513	23.15
17	4.49	41.68	48.32	1.514	23.24
18	4.25	41.65	48.35	1.513	23.26
19	4.42	41.59	48.41	1.512	23.24
20	4.25	41.70	48.30	1.514	23.26
OPS	4.86	42.20	47.80	1.520	22.80

ff = flow function, θ_i = internal friction angle, θ_w = wall friction angle, H (θ) = friction factor, θ(º) = half hopper angle, s = sample

Table 3 Strength Properties of Tigernut Flour Sample

Sample	Compressive Strength (KPa)								
	Consolidation Stress (δ_c) (KPa)			Shear Stress (τ) (KPa)			Unconfined Yield Strength (δ_y) (KPa)		
	Bulk Density (ρ_b) gcm^{-3}			Bulk Density (ρ_b) gcm^{-3}			Bulk Density (ρ_b) gcm^{-3}		
	1.62	2.01	3.02	1.62	2.01	3.02	1.62	2.01	3.02
1	5.7×10^1	2.16×10^2	3.09×10^2	1.68×10^2	6.19×10^2	8.99×10^2	2.25×10^2	8.35×10^2	1.208×10^3
2	6.1×10^1	2.12×10^2	3.02×10^2	1.45×10^2	5.93×10^2	9.24×10^2	2.10×10^2	8.05×10^2	1.226×10^3
3	6.1×10^1	2.00×10^2	3.03×10^2	1.49×10^2	6.00×10^2	9.23×10^2	2.10×10^2	8.00×10^2	1.226×10^3
4	6.15×10^1	2.14×10^2	3.06×10^2	1.585×10^2	6.16×10^2	9.18×10^2	2.20×10^2	8.30×10^2	1.224×10^3
5	6.0×10^1	1.98×10^2	2.98×10^2	1.41×10^2	5.80×10^2	9.02×10^2	2.01×10^2	7.78×10^2	1.200×10^3
6	6.3×10^1	2.11×10^2	3.01×10^2	1.45×10^2	5.87×10^2	9.29×10^2	2.08×10^2	7.98×10^2	1.230×10^3
7	6.25×10^1	2.15×10^2	3.04×10^2	1.365×10^2	5.95×10^2	9.21×10^2	1.99×10^2	8.30×10^2	1.225×10^3
8	6.2×10^1	2.10×10^2	3.02×10^2	1.34×10^2	5.73×10^2	9.23×10^2	1.96×10^2	7.83×10^2	1.225×10^3
9	6.0×10^1	1.96×10^2	2.96×10^2	1.39×10^2	5.89×10^2	8.99×10^2	1.99×10^2	7.85×10^2	1.195×10^3
10	6.5×10^1	2.11×10^2	2.99×10^2	1.75×10^2	6.49×10^2	9.57×10^2	2.40×10^2	8.60×10^2	1.256×10^3
11	6.2×10^1	2.11×10^2	3.01×10^2	1.36×10^2	5.69×10^2	8.95×10^2	1.98×10^2	7.80×10^2	1.196×10^3
12	6.2×10^1	2.11×10^2	3.00×10^2	1.35×10^2	6.97×10^2	9.25×10^2	1.97×10^2	8.08×10^2	1.225×10^3
13	5.4×10^1	2.15×10^2	3.00×10^2	1.66×10^2	6.45×10^2	9.10×10^2	2.20×10^2	8.60×10^2	1.210×10^3

		10^2	10^2		10^2	10^2	10^2	10^2	
14	6.2×10^1	2.12×10^2	3.02×10^2	1.34×10^2	6.76×10^2	9.24×10^2	1.96×10^2	7.88×10^2	1.226×10^3
15	6.5×10^1	2.10×10^2	3.00×10^2	1.77×10^2	6.30×10^2	9.46×10^2	2.42×10^2	8.40×10^2	1.246×10^3
16	6.5×10^1	2.10×10^2	3.00×10^2	1.76×10^2	6.36×10^2	9.46×10^2	2.41×10^2	8.46×10^2	1.246×10^3
17	6.5×10^1	2.10×10^2	2.99×10^2	1.65×10^2	6.69×10^2	9.71×10^2	2.30×10^2	8.70×10^2	1.270×10^3
18	6.5×10^1	2.19×10^2	2.99×10^2	1.75×10^2	6.41×10^2	9.61×10^2	2.40×10^2	8.60×10^2	1260×10^3
19	6.5×10^1	2.10×10^2	3.00×10^2	1.77×10^2	6.34×10^2	9.42×10^2	2.42×10^2	8.44×10^2	1.242×10^3
20	6.5×10^1	2.19×10^2	2.99×10^2	1.75×10^2	6.41×10^2	9.61×10^2	2.40×10^2	8.60×10^2	1.260×10^3
OPS	6.5×10^1	2.15×10^2	2.99×10^2	1.65×10^2	6.55×10^2	9.79×10^2	2.30×10^2	8.70×10^2	1.278×10^3

OPS – optimized sample, values are means of three determinations.

Table 5 Scale Flowability of Tigernut Flour

Sample	ρ_b Kg/m^3	ρ_L Kg/m^3	Hausner Ratio	Carr's Index	Angle of Repose (°)	Flowability
R1	0.630	0.477	1.320	24.286	43.360	Passable
R2	0.580	0.465	1.246	19.830	32.570	Good
R3	0.610	0.481	1.268	21.150	39.810	Fair
R4	0.570	0.459	1.242	19.470	32.740	Good
R5	0.620	0.483	1.284	26.130	40.700	Fair
R6	0.565	0.458	1.232	18.940	35.340	Fair
R7	0.605	0.480	1.260	20.666	37.380	Fair
R8	0.560	0.459	1.220	18.041	35.310	Fair
R9	0.650	0.485	1.340	25.380	44.190	Passable
R10	0.500	0.427	1.170	14.600	27.820	Excellent
R11	0.600	0.477	1.258	20.500	36.870	Fair
R12	0.590	0.471	1.252	20.170	36.360	Fair
R13	0.585	0.469	1.248	19.830	33.690	Good
R14	0.550	0.453	1.214	17.640	34.780	Good
R15	0.520	0.435	1.195	16.350	30.260	Good
R16	0.530	0.444	1.197	16.230	30.370	Good
R17	0.530	0.444	1.197	16.230	30.370	Good
R18	0.530	0.444	1.197	16.320	30.370	Good
R19	0.540	0.450	1.199	16.660	30.550	Good
R20	0.530	0.444	1.197	16.230	30.370	Good
OPS	0.502	0.425	1.180	15.340	29.660	Excellent

OPS = optimized sample, ρ_b = packed bulk density, ρ_L = loose bulk density Values are means of three determinations

Table 6 Thermal Conductivity, Specific Heat Capacity and Diffusivity of Tigernut Flour

Sample	$\frac{Q}{4\pi}$	$\left[\frac{dT}{d(Lin\ t)}\right]^{-1}$	K $Wm^{-1}{}_{K}{}^{-1}$	C_p $J\ kg^{-1}\ K^{-1}$	ρ_b Kg/m^3	α m^2s^{-1}
R1	79.548	1.018×10^{-3}	0.0809	970.69	0.630	1.323×10^{-4}
R2	79.548	7.473×10^{-4}	0.0594	739.92	0.580	1.384×10^{-4}
R3	79.548	9.634×10^{-4}	0.0767	923.08	0.610	1.362×10^{-4}
R4	79.548	7.326×10^{-4}	0.0583	732.60	0.570	1.396×10^{-4}
R5	79.548	9.890×10^{-4}	0.0788	952.38	0.620	1.335×10^{-4}
R6	79.548	8.132×10^{-4}	0.0648	849.82	0.565	1.350×10^{-4}
R7	79.548	9.378×10^{-4}	0.0729	897.44	0.605	1.343×10^{-4}
R8	79.548	7.949×10^{-4}	0.0633	830.33	0.560	1.361×10^{-4}
R9	79.548	1.048×10^{-3}	0.0832	1069.6	0.650	1.197×10^{-4}
R10	79.548	6.557×10^{-4}	0.0530	390.73	0.500	2.713×10^{-4}
R11	79.548	9.158×10^{-4}	0.0728	881.61	0.600	1.376×10^{-4}
R12	79.548	8.498×10^{-4}	0.0678	852.31	0.590	1.348×10^{-4}
R13	79.548	7.619×10^{-4}	0.0607	769.23	0.585	1.349×10^{-4}
R14	79.548	7.802×10^{-4}	0.0620	827.84	0.550	1.362×10^{-4}
R15	79.548	6.923×10^{-4}	0.0550	661.54	0.520	1.599×10^{-4}
R16	79.548	7.032×10^{-4}	0.0560	677.65	0.530	1.559×10^{-4}
R17	79.548	7.032×10^{-4}	0.0560	679.00	0.530	1.583×10^{-4}
R18	79.548	7.032×10^{-4}	0.0560	674.00	0.530	1.583×10^{-4}
R19	79.548	7.179×10^{-4}	0.0571	681.32	0.540	1.552×10^{-4}
R20	79.548	7.032×10^{-4}	0.0560	676.19	0.530	1.563×10^{-4}
OPS	79.548	6.777×10^{-4}	0.0540	670.33	0.502	1.605×10^{-4}

K is thermal conductivity, C_p is specific heat capacity, ρ_b is bulk density, α is diffusivity.

Values are means of three determinations

REFERENCES

Abano E.E. and K.K. Amoah. 2011. *Effects of Moisture content on the Physical properties of Tigernut (cyperus esculentus).* Asian Journal of Agricultural Research, 5,56-60.

Abu-hardan M., S.E. and Hil. 2010. *Handling properties of cereal materials in the presence of moisture and oil.* Powder Technology 198, 26-24.

Ade – Omowaye, B.I.O., Akinwande B.A., Bolarinwa, I.F., and Adebiyi A.O. 2008. *Evaluation of Tiger nut (cyperus esculentus) wheat composite flour and bread.* African Journal of Food science, 2, 87-91.

Ali Nokhodchi. 2005 January *the effects of moisture on the flow properties, tensile strength, heckle plot (particle rearrangement, yield pressure, energies involved in compaction*, Pp 46-66.

Aviara, N.A., and M.A. Haque. 2001. *Moisture dependence of thermal properties of shearnut*

kernel. Journal of Food Engineering 47,109 – 113.

Aviara, N.A., M.A. Haque, and L.A.O. Ogunjimi, 2008. *Thermal properties of guna seed.* International Agrophysics 22, 291 – 297.

Balami A.A., M. Birma, S. M. Dauda and S. E. Adebayo. 2015. *Engineering Properties of Tigrnut Seeds Relevant to the Design of Cleaning and Sorting Machine.* International Journal of Manufacturing and Industrial Engineering – IJME., 2(1) , 29-31.

Belewu, M.A and Belewu, K.Y. 2007. *Comparative Physico – Chemical] Evaluation of Tigernut, Soybean and Coconut Milk Sources.* Int. J. Agric. Biol.,9, 785-787.

Bozikova, M. 2008. *Selected thermophysical characteristics of milk and milk products.* Acta Technological Agriculturae, 11 (1), 15 – 19.

Bullimer, M., Carson J., and Prescott J., 2012. *A preliminary Investigation Concerning the Effect of Particle Shape on Powders Flow properties*. Malvern Instruments, Inc. and jenike and Johansen Inc. Publication, pp. 1-10.

Carvalho, O.T., Avérous, L., and Tadini, C. C. 2011. *Mechanical properties of cassava starch-based nano-biocomposites*, 11th International Congress on Engineering and Food, Athens, Greece. Pp. 111 – 112.

Chase, G.G. 2012. *Solids notes on hopper design*. The University of Akron Buletin pp. 10 – 26.

Chinma, C. E., J. O Abu. and Y. A. Abubakar. 2010. *Effect of Tiger Nut Flour Addition on the Quality of Wheat-Based Cake.* Int. Journal of Food Seirand Tech., 45(8),1746-1752.

Chinma, C.E., O. Adewuyi. and J.O Abu. 2009. *Effect of germination on the chemical function and pasting properties of flour from brown and yellow varieties of tiger nut (cyperus esculentus).* Food research international, 42 (2009), 1004-1009.

Chou, S.K. and K.J. Chua. 2001. *New Hybrid Drying Technologies for Heat Sensitive Food Stuffs*. Trends Food Science and Technol. 12 (10), 359 – 369.

Elena, S., F. Juana, and A.P Jose. 2012. *Tigernut (Cyperus esculentus) Commercialization: Health Aspects, composition, properties and food applications*. Comprehensive Reviews in Food Science and Food Safety, 11,366-377.

Ertekin C., and O. Yaldiz. 2004. *Air Drying and Rehydration Characteristics of Date Palm (Phoenix Deotyliferal C.) Fruits*. Journal of Food Engineering, 63, 349-359.

Fadeyibi A., Z.D. Osunde, G. Agidi and E.C. Evans. 2014. *Flow and Strength properties of Cassava and Yam Starch. Glycerol Composites essential in the Design of Handling Equipment for Granular solids.* Journal of Food Engineering, 129, 38-46.

Fitzpatrick, J., S.A. Barringer and T. Igbal. 2004. *Flow property measurements of Food powders are sensitivity of Jenike's hoper Design methodology to the measured values.* Journal of Food Engineering, 61, 399-405.

Gambo, A. and A. Da'u. 2014. *Tigernut (cyperus esculentus). Composition, Products, uses and Health Benefits. A Review: Bayero* Journal of Pure and Applied Sciences, 7(1),56-51.

Gani A. Hussain A, Ahmad M. baba W.N., GaniA. Masoodi F.A., Wani S.M., Shah A., Wani [A Maqsood S. 2015. *Engineering and functional properties of four varieties of pulses and their correlative study*. Food Measure, DOI 10.100/S/j1694-015-9242-7.

Igathianathane C. Jaya S.T., Sokhansanj S., Bi X, Lim C.J. Melin S. Mohammad E. 2010. *Simple and inexpensive method of wood pellets macro-porosity measurement.* Bioresource Technology, 101 (16), 6528-6537.

Ikegwu, O.J., I.C. Emenalum, and V.N. Nwobasi. 2016. *Thermal properties of African Yam Bean Seeds as influenced by moisture content and temperature.* Nigerian Food Journal, 34 (1), 133 – 139.

Jenike, A.W. 1964. *Storage and Flow of Solids* Bull. 123, Engineering Expt. Sta. Uteh State University.

Kara, M., I. Ozturk, S. Bastaban and F. Kalkan. 2011. *Thermal conductivity of safflower*

(*Carthamus tinctorius l.*) *seeds.* Spanish Journal of Agricultural Research, 9(3), 687- 692.

Komolafe G.O., Inuwa I.M., and Osunde Z.D. 2012. *Physicochemical Evaluation and Acceptability Studies of tiger nut (Cyperus esculentus) Beverage.* Proceeding of 14th National Conference, National Science and Technology Forum Kaduna Polytechnic.

Lumay G., F. Boschini, K. Traina, S. Bontempi, J. C. Remy, R. Cloots and N. Vandewalle. 2012. Measuring the Flowing properties of powders and grain powder technology 224. 19-27.

Molenda, M. and M. Stasiak. 2002. *Determination of elastic constants of Cereal Grain in uniaxial compression.* int. Agrophys., 16 (1), 61-65

Muhammad N.O, Bamishaiye E.I, Bamishaiye O.M, Usman L.A, Salewu M.O, Nafiu M.O & Oloyede O.B .2011. *Physicochemical properties and fatty acid composition of cyperus esculentus (tiger nut) tuber oil.* Bioresearch bulletin, 5,51-54.

Myers, R.H. and D.C. Montgomery. 2002. Response Surface Methodology: Process and Product Optimization Using Designed Experiments,2nd Edition. John Wiley, New York.

Oke, M.O., S.O. Awonorin, L.O. Sanni, C.T. Akanbi and A.O. Abioye. 2007. *Determination of Some Selected Engineering Properties of Sweet Potato Cuts as Function of Temperature*. Journal of Food Technology, 5(1), 66 – 70.

Sanni, L.A., Oke, O.O., Oladimeji, F.M., and Ogbozomivaze, K.F. 2016. *Thermal Properties and Energy Utilization of Cassava Meal in Conductive Rotary Drying*. American Journal of Food Science and Technology, 4(6), 160 – 167. http://pubs.sciepub.com/ajfsc/4/6/1 Doi:10.12691/ajfst.4.6.1

Schulze, D. 2011. *Flow properties of powders and bulk solids. Ostfelia university of Applied Science publication Wolfer buttel, Germany* pp. 1-24. http://www.dietmarschulze.de.

Shikhou V.N., V.V. Velichko, T.V. Nesterenko and A.A Titchomino. 2011. *Ontogenetic Approach of Assessment of Chufa response to culture conditions by the method of chlorophyll fluorescence Induction* Russ. J. Plant Physl., 58(2), 359-363.

Shumaila, J., I.R. Syed, and D.C. Saxena. 2015. *Effect of Physical Properties on Flowability of Commercial Rice Flour/Powder for Effective Bulk Handling* International Journal of Computer Applications. International Conference on Advancement in Engineering and Technology (ICAET-2015) Retrived on 7th November, 2017 from http://research.ijconline.org/icaet2015/number11/icaet4151pdf

Schwedes, J. 2002. *Consolidation and flow of cohesive bulk solids*. Chem. Eng. Sci. 57, 287-294.

Thalberg, K., D. Lindholm and A. Axelsson. 2004. Comparison of different flowability tests for powders for inhalation powerder Technol. 146, 206-213.

Soysal, A., Oztekin, S. and O. Eren. 2006. *Microwave Drying of Parsley: Modelling, Kinetics and Energy aspects.* Biosystem Engineering, 93(4), 403 - 413.

Therdthai, N. and W. Zhou. 2009. *Characteristics of Microwave Vacuum Drying and Hot air Drying of Mint Leaves (Mentha cordifolia Opizex Fresn).* Journalof Food Engineering 91, 482 – 489.

Tomasi J. 2004. Fundamentals of cohersive powder consolitaiton and flow Granular matter 6.75 – 86 http://dx.doi.org/1o.1007/S100035-004-0167-9.

Oko C.O. C., E.O. Diemuodeke, and D. Edet. 2015. *Conical Hopper Design Parameters for Selected Food Powders Using M.Sc. Excell Add-in* Internationla Journal of Computer Applications 113 (11), 29-33.

Peleg M., C.H. Man-Heim and N. Passy. 1973. *Flow property of some food powders.* Journal of Food Science 38 (6) 959-964. DOI 10.111/J.1365-2621. 1973.TBO2124.

PERSONAL COMPUTER-BASED CONTROL AND MONITORIBG SYSTEM FOR BIODIESEL ALGAE PHOTOBIOREACTOR

Ondimu[1], S.; Raude[2], J.M.; Wanjala[3], G

[1, 2, 3] Jomo Kenyatta University of Agriculture and Technology, Nairob Kenya

ABSTRACT

Growing of Algae for biodiesel production has gained popularity in recent times. This is because biodiesel from algae has an economic advantage over other oil crops. The oil content that can be extracted from microalgae biomass depends on the culture conditions and microalgae species. This means that besides selecting the best microalgae species, it is also necessary to ensure and maintain the best culture conditions for optimal biodiesel production. Optimum algae growth conditions can be best be provided by a Controlled Environment Bioproduction System (CEBS) for the algae called as photo-bioreactor (PBR). This paper reports design and fabrication of a PC based control system for a PBR production system for algae being developed at the School of Biosystems and Environmental Engineering (SoBEE) in Jomo Kenyatta University of Agriculture and Technology (JKUAT) in Kenya. The control system is intended to ensure that optimum PH, temperature, nutrients content; light intensity/duration and salinity of growth medium for algae are maintained. The paper covers the design and fabrication of the PC control and monitoring system. The control and monitoring system consists of a computer program and a microcontroller connected to sensors and actuators. The computer program (master) provides the graphical user interface (GUI) consisting of control buttons and means for real time data logging and analysis as well as real-time simulation of PBR activities. It is available in executable file that can be run in any windows OS computer. The microcontroller program (slave) provides the means for connecting sensors and is used to measure as well as monitor the conditions in the PBR tanks. Communication between the computer program and the microcontroller is achieved through the universal serial bus (USB). The control system consists of both open and closed loop systems. The open loop system is used to control the light duration at predetermined intervals of time. The closed loop system is used to control the nutrient concentration, light intensity, PH and oxygen: carbon dioxide ratio.

Keywords: Control and Monitoring system, Graphical User Interface, Microcontroller, Microalgae, Photo-Bioreactor, Response time

INTRODUCTION

The three most important global challenges in the 21st century is food shortage, energy deficiency and environmental degradation. These three challenges are such that they should be mitigated simultaneously. Any attempt to mitigate any one of them in isolation will lead to escalation of the other two resulting in what has come to be known as the global 'trilemma'. Biodiesel can be a potential alternative to fossil fuels as a source of renewable and environmentally friendly source of energy. This fuel releases less greenhouse gases to the environment and has the potential of reducing air pollution and cancer by up to 90% and 95%

respectfully (Huang *et al.*, 2010). Of the current biodiesel sources, Algae biomass has the greatest potential for biodiesel production (Mata *et al.*, 2010, Oilgael, 2013; Rodolfi *et al.*, 2008). In addition, it does not compete with food crops. Thus, biodiesel production from algae is an attempt to mitigate the three global challenges simultaneously. For that reason, growing of algae for the purpose of biodiesel production has gained popularity over the past few years.

The oil content that can be extracted from microalgae biomass depends on the culture conditions as well as the microalgae species (Hu, 2004). Therefore, after selecting the microalgae species with the highest oil content (exceeding 80% of the dry biomass weight) production conditions should be optimum. This requires a Controlled Environment Bioproduction System (CEBS). The most suitable CEBS for algae production is a Photobioreactor (PBR). A PBR should ensure that the following requirements for algae growth (Sierra et. al., 2008; Trendici, 2004 and Zittelli *et al.*, 2013) are optimum: - Co_2 supply, water, temperature, efficient light exposure, culture density, PH level, air supply rate and mixing regime. This requires control of CO_2, Nutrient content, light duration/intensity, Salinity, PH content and temperature (Anderson, 2003; Chen *et al.*, 1994). There are different types of PBR systems namely: tubular reactors, horizontal reactors, vertical-flat panel reactors, vertical column reactors, bubble column reactors, airlift reactors, stirred tank reactors and immobilized reactors (CathCart, 2011; Merchuk, 2003; Molina, 2008; Richmond and Zhang, 2001 and Tredicci, 2004). Vertical column reactors are the most convenient for PBR (Molina, 2008 and Richmond and Zhang, 2001).

PBR systems comprise of the lighting system (Light source, optical transmission system); air handling and gas exchange system; mixing system (reaction area); instrumentation and control system; nutrient system; filtration system and electrical system. The instrument and control system play the most important role in ensuring that optimum algae growth conditions are maintained (Davis *et al.*, 2011; Dormido et al., 2014 and Trendici, 2004). This paper reports development of a control and monitoring system for a flat plate PBR system being developed at School of Biosystems and Environmental Engineering, Jomo Kenyatta Univeristy of Agriculture and Technology. Figure 4.1 is an illustration of the algae PBR system when completed.

The objective of this paper is to present the design and fabrication of a personal Computer (PC) based control and monitoring system biodiesel algae PBR.

The paper is divided into four sections. Section 1 is the introduction in which the contents of the paper are introduced. Sections two and three presents discuss the design and fabrication of a PC based control and monitoring system for an algae production PBR. Section four explains how the fabricated system works and presents some simulation testing results.

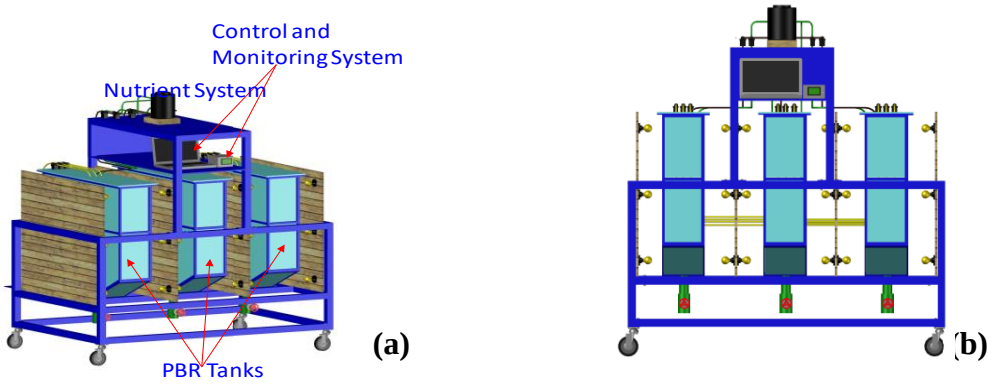

Figure 4.1: Illustration of the complete PBR system (a: pictorial view; b: front view)

1. Design Of The Pc Control System

The PBR control and monitoring system was designed using the master-slave approach. The circuitry layout of the system is shown in Figure 2.1. It comprises of two programs that can interact with each other: the computer program and the microcontroller program. The computer program is higher in hierarch (master) than the microcontroller program (slave) and is the decision maker. The microcontroller is the implementer of the controller decision. The master-slave approach has a number of advantages: - it reduces microcontroller overload; ensures consistency of the system; reduces time losses; provides an interactive Graphical User Interface (GUI); and ensures effective real time simulation, data logging and data analysis. However, with this approach the control function cannot be take place when the computer is off. This is because the microcontroller cannot make the decisions on its own. There is an effort to improve the microcontroller program so that it can be in a position to perform the control decision in case the computer program is off.

The procedure used to design the control system for the photo-bioreactor was divided into three parts: selection of components, design of the computer program and design of microcontroller unit.

i. Section of components

The components for PBR control and monitoring system included hardware and software components. Factors considered in the selection of these components included accuracy, availability, speed of response and cost among others.

After consideration of different combinations of these factors the following components were selected for development of the PBR control and monitoring system.

a. HP Laptop
   - Processor: Intel (R) Pentium (R) CPU N3710 @ 1.60 GHz
   - RAM: 4.00 GB (3.85GB usable)
   - System type: 64-bit operating system, x64 based processor
   - Operating System: Windows 10
b. Micro-controller: Arduino Mega 2560
c. Solenoid valves
d. Bread board
e. Sensors (temperature sensors, PH sensor)
f. Visual studio 2015 professional
g. Visual basic programming language
h. Proteus 8 Professional Software

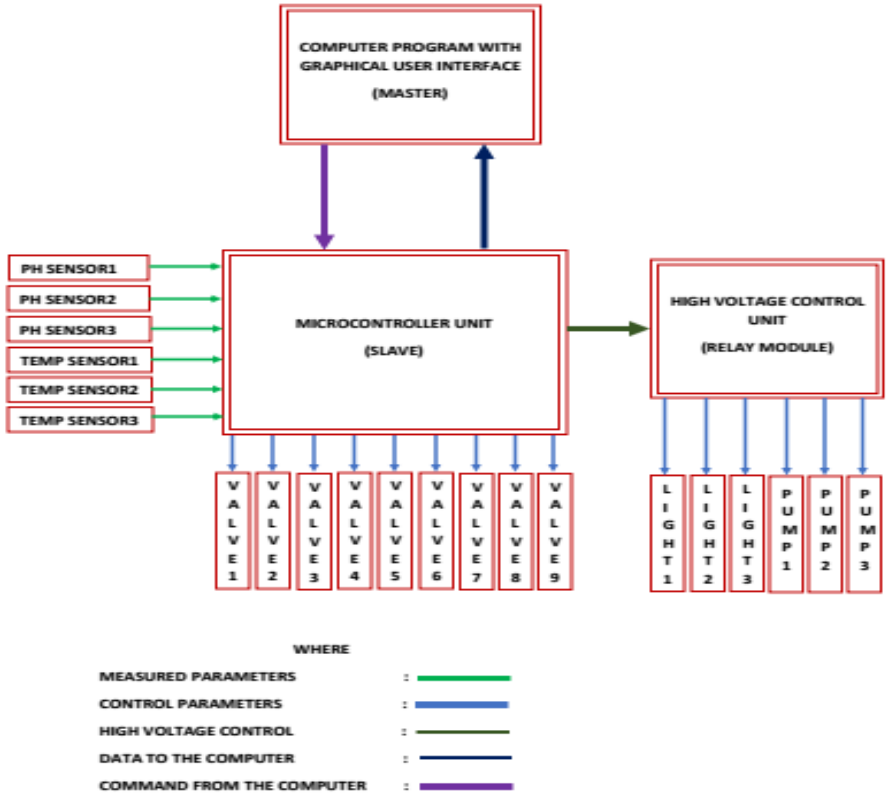

Figure 2.1: Circuitry layout of the PBR control system

ii. Design of Computer program

The computer control program contains the graphical user interface (GUI) which allows for interaction and simulation of the control system. The GUI was designed in visual studio 2015 with visual basic as the programming language using HP laptop.

iii. Design of the microcontroller unit

The mictroller unit comprises of a box casing, micro-controller and system circuitry and micro-controller program. The micro-controller box casing was the last component to be sized. The circuit diagram for the system was designed and tested in proteus8 professional software on a HP laptop. Figure 2.2 shows a circuit diagram that controls opening and closing of solenoid valves through transistor switching. Similarly, circuits for temperature, PH and light intensity control and monitoring were designed for the complete the control system. The microcontroller selected was the Arduino Me 2560.

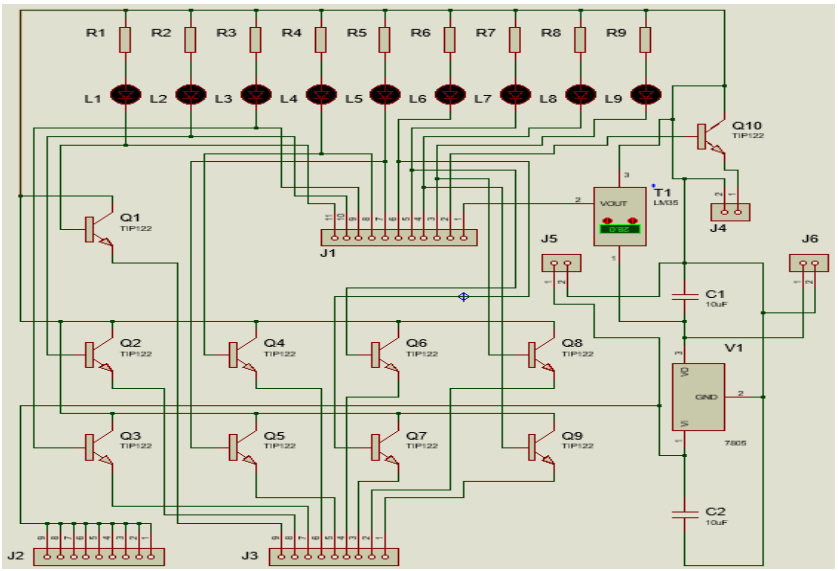

Figure 2.2: Circuit diagram for the power regulation and solenoid valves control

3.0 Fabrication of Control System

Fabrication of the PBR control system involved fabrication of system hardware and development of system software. The hardware component comprises of the HP laptop, control circuit boards and microcontroller box. The software component comprises of the computer and the microcontroller programs.

i. Fabrication of the system hardware

Prototype control circuits were assembled on bread boards as per the corresponding circuit designs to test actual operation of the control system using the components shown in Table 3.1. After ensuring that the prototype circuits were working as required, various electronic components were soldered to their respective positions in the circuits to form corresponding circuit's boards. Figure 3.1 shows the bread board assembly of the circuit in Figure 2.1.

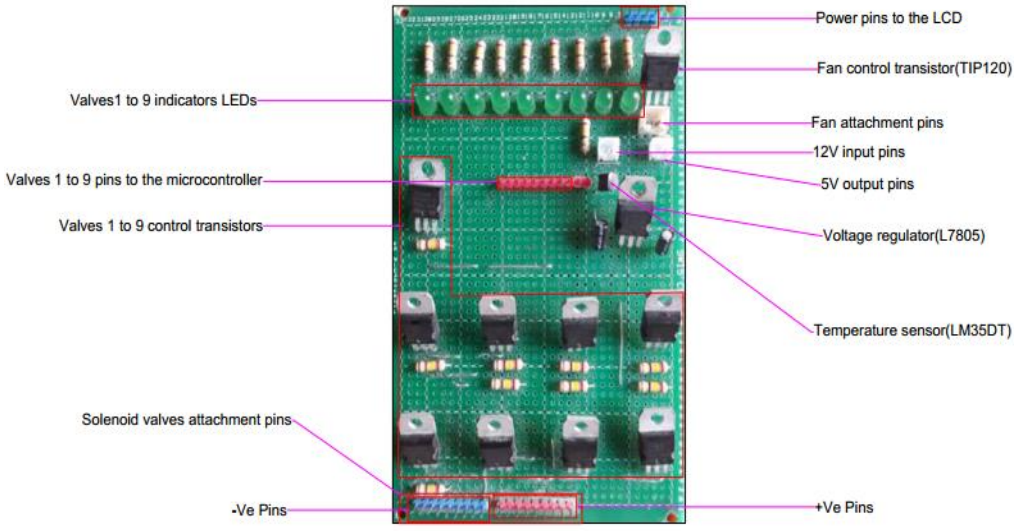

Figure 3.1: Power regulation and solenoid valves control unit

Table 3.1 Components used to develop the power regulation and solenoid valves control circuit

Value	Component/Description
C1, C2	Capacitors, 10uf Radial
J1, J2, J3	Header pins, male straight
J4, J5, J6	JST connectors, two pin male
L1, L2, L3, L4, L5, L6, L7, L8, L9	LEDs, 5mm green diffused
Q1, Q2, Q3, Q4, Q5, Q6, Q7, Q8, Q9	Transistors, TIP120 NPN
R1, R2, R3, R4, R5, R6, R7, R8, R9	Resistors, 240Ω 1/4W 5%
T1	Temperature Sensor, LM35DT
V1	Voltage regulator, L7805

After developing circuit board assembly units for all components of the control system, they were assembled in a metallic housing to form the microcontroller box unit shown in Figure in 3.2.

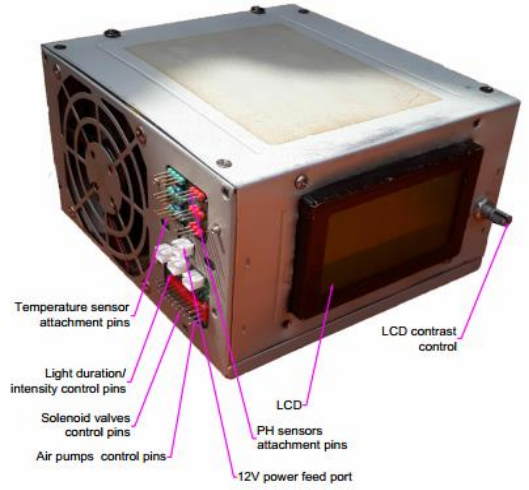

Figure 3.2: Microcontroller Box Unit

The components of the microcontroller unit box: Arduino mega 2560 board; Power regulation and solenoid valves control unit (switching on and off solenoid valves); Fan; Liquid Crystal Display; LCD contrast adjustment Potentiometer (10KΩ0; Temperature and PH sensors attachment ports; Light bulb attachment ports; Air pumps control Port and Solenoid valves attachment port

ii. Fabrication of the system Software

The control system for the photo-bioreactor is composed of two major units; a computer program and the microcontroller unit. The computer program provides the graphical user interface while the microcontroller measures the control parameters. The computer program is higher in hierarch than the microcontroller program and acts as a master to the microcontroller. All the decisions to control the actuators are made by the computer program.

a. The Computer graphical User Interface

The graphical user interface (GUI) for the control systems was developed in visual studio with visual basic as the programming language. The materials and tools used for the development of the GUI were: HP Laptop, visual studio 2015 professional and visual basic programming language

The GUI was developed using visual basic as the programming language. The interface provides the platform for real time data logging and analysis as well as buttons to perform control operations. It consists of data cells for real time data viewing. The buttons provides the means for controlling the control parameters as shown in Figure 3.3. The interface also provides a visual simulation of the activities that are happening in the tanks as shown in Figure 3.4.

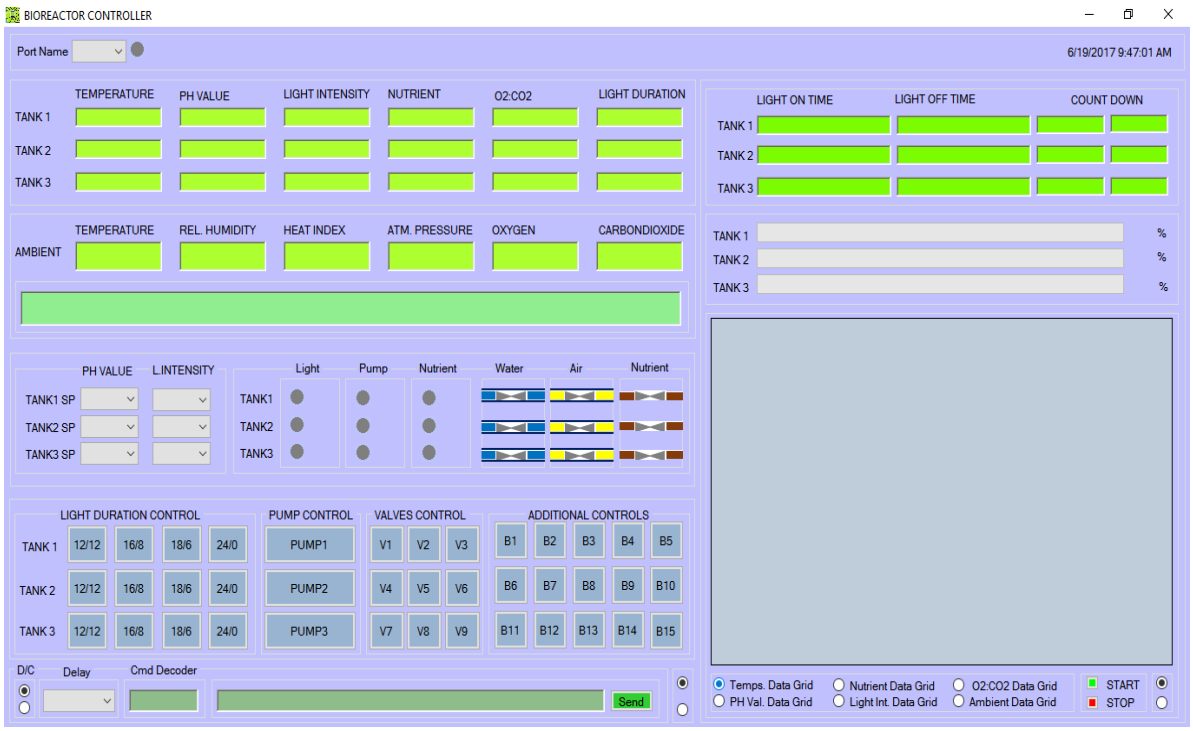

Figure 3.3: Graphical User Interface (GUI)

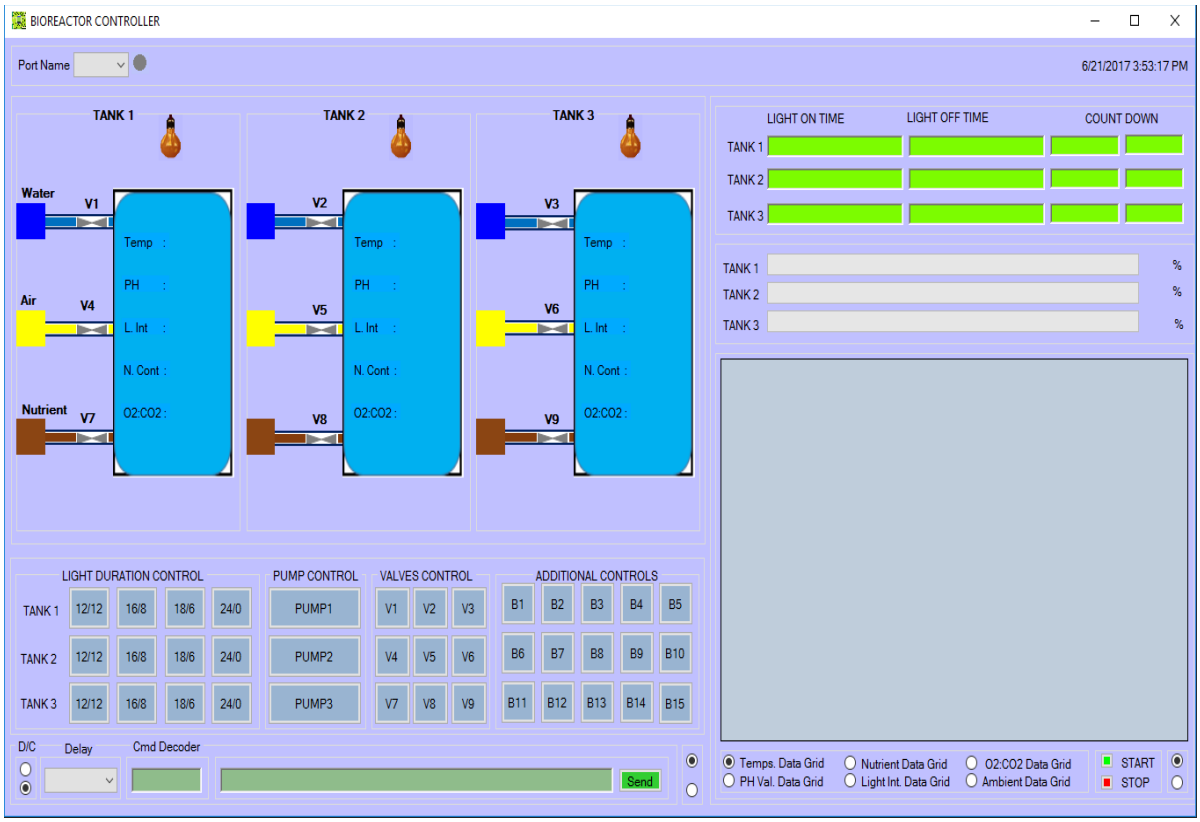

Figure 3.4: Graphical User Interface switched to photo-bioreactor tanks simulation mode

iii. The development of the microcontroller program

This was the last stage in the design and development of the microcontroller box unit. It involved the development of the microcontroller code that can interact with the computer GUI. The code was developed in the Arduino Internal Development Environment (Arduino IDE 1.6.9) and a number of libraries were incorporated within the program: GLCD library, PH sensor library and One wire library.

4.0 Preliminary Performance Tests

Figure 4.1 is a picture of the PC based control and monitoring system developed in this study. Figure 4.2 is a schematic summary of the components of the system.

How the system works

The computer program is higher in hierarchy than the microcontroller program and acts as a master to the microcontroller. All the decisions to control the actuators are made by the computer program. The microcontroller does the measurement of the control parameters such as temperature, PH, Nutrients content, light intensity/duration and oxygen carbon dioxide ratios. The measurements obtained are then shared to the computer program through the serial communication. The computer program then checks the parameters and compares them with the desired set points to see if they are within the acceptable limits. If the parameters are within the accepted limits the computer program bothers no the microcontroller. In case the parameters are outside the acceptable limits then the computer program will order the microcontroller to perform the necessary action in order to control the parameters. This may be to tell the microcontroller to turn on the solenoid valve for more nutrients to enter a tank or to tell the microcontroller to turn off the light because eighteen hours of lighting are over.

Preliminary tests

Preliminary tests were conducted to determine the response time of the control and monitoring system. The response time between the time a command is sent by the computer program to the actual time that the microcontroller performs the command is dependent on the delay time in the microcontroller program and the write-timeout value for the serial port in the computer program.

Microcontroller time delay is the time interval between two consecutive readings of measurements from a sensor by the microcontroller. It is the time rest taken by the microcontroller after taking a reading or a set of readings from a given sensor before it can take another reading or a set of readings from the same sensor. The microcontroller time delay is included in the microcontroller program and is equal to 1000 milliseconds. Serial port write-timeout is the number of milliseconds before a time-out occurs when a write operation does not finish. The average serial port time was found to be 500 ms

Response time = Microcontroller time delay + Serial port write-timeout

Thus; Response time = 1000 + 500 =1500 milliseconds

5. CONCLUSION

This paper reports the design and fabrication of a Personal Computer (PC) based Control and monitoring system for biodiesel algae photobioreactor (PBR). Preliminary tests showed that the system has a response time of 1.5 seconds. However more tests are required to characterize its performance. This will be done once the whole PBR system is completed. Once completed the PBR system will be used to optimise conditions for biodiesel algae production. This will contribute greatly towards promoting production of microalgae as a commercial venture. It will also promote the utilization of biodiesel from algae as a viable clean fuel thus mitigating energy deficiency and environmental degradation without negatively affecting food production.

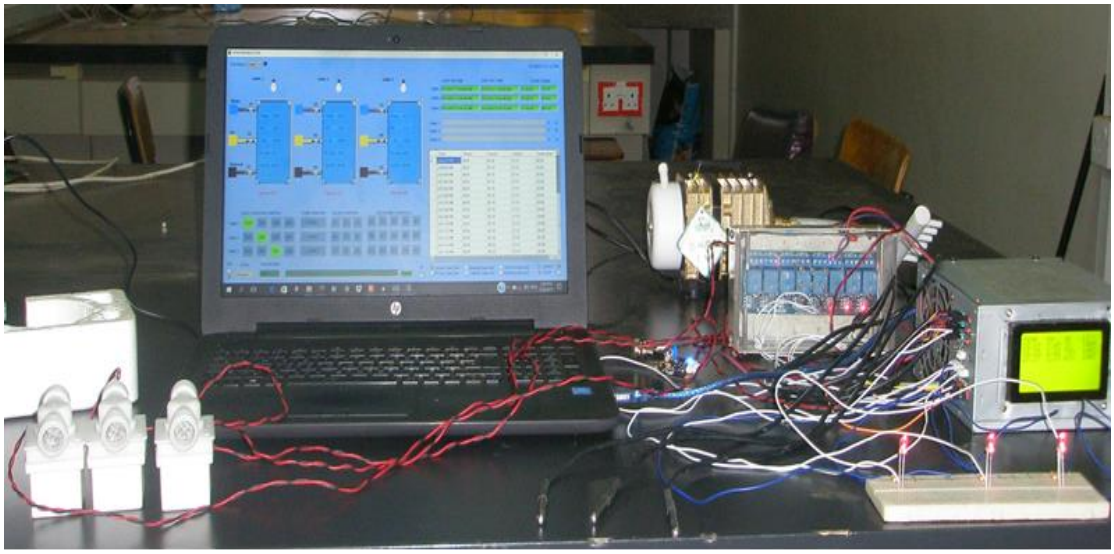

Figure 4.1: PBR Control and Monitoring system

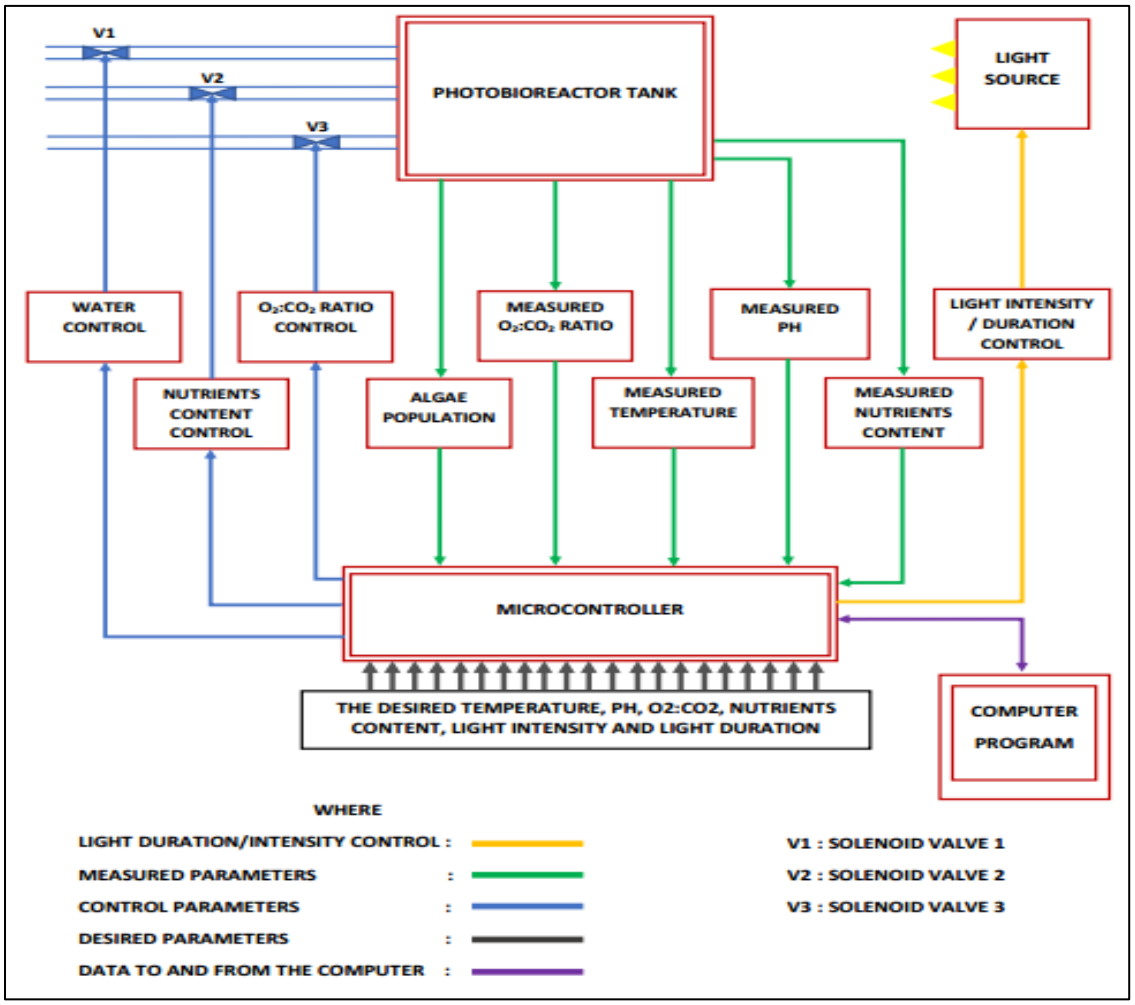

Figure 4.2: The flow diagram of the system

Acknowledgement

We acknowledge the Research, Production and Extension (RPE) Division of Jomo Kenyatta University of Agriculture and Technology (JKUAT) who are funding the Project.

REFFERENCES

Anderson, J., and P. Katja. 2003. *Does Excessive Phosphorus Necessarily Cause Increasing Biomass of Diazo-trophic Cyanobacteria?* Proceedings of the Estonian Academy Sciences, Biology, Ecology, 52(3) p.205—217.

Cathcart, P. 2011. *Inexpensive, vertical production photobioreactor.* U.S. Patent Application US2011/0027875 A1 (3 February 2011).

Davis, R., A. Aden and P.T. Pienkos 2011. *Techno-economic analysis of autotrophic microalgae for fuel production.* Applied Energy, 88, 3524-3531. DOI: 10.1016/j.apenergy.2011.04.018

Dormido, R., J. Sanchez, N. Duro, S. Dormido-Canto, M. Guinaldo and S. Dormido. 2014. *An Interactive Tool for Outdoor Computer Controlled Cultivation of Microalgae in a Tubular Photobioreactor System.* Sensors, 14: 4466-4483.

Hu, Q. 2004. *Environmental effects on cell composition*. In: Richmond, A. (Ed.), Handbook of Microalgal Culture. Blackwell Science Ltd., Oxford OX2 0EL, UK, Pg.83–93.

Huang, G., F. Chen, D. Wei, X. Zhang and G. Chen. 2010. *Biodiesel Production by Micro-algal Biotechnology.* Applied Energy, 87 Pg. 38–46

Mata, T.M., A.A. Martins and N.S. Caetano. 2010. *Microalgae for biodiesel production and other applications: a review*. *Renew. Sust. Energ. Rev.*, 14, 217-232.

Merchuk, J.C and M. Gluz. 2003. *Bioreactors, Air-lift Reactors.* Encyclopedia of Bioprocess Technology. 320-352. DOI: 10.1002/0471250589.ebt029

Molina, G.E.., E. Sierra, J.M. Acien, J.L. Fernendez and G.C. Gonzalez. 2008. *Characterization of a flat plate photobioreactor for the production of microalgae*. Chemical Engineering Journal, 138, 136-147. DOI:10.1016/j.cej.2007.06.004

Oilgae 2013. Energy from Algae: Products, Market, Processes & Strategies. Comprehensive Report. Retrieved from http://www.oilgae.com/ref/report/oilgae_reports.html

Richmond, A. and Z. Zhang. 2001. *Optimization of a flat plate glass reactor for mass production of Nannochloropsis sp. outdoors.* J. Biotechnol., 85, 259–69.

Rodolfi, L., Z.G. Chini, N. Bassi, G. Padovani, N. Biondi, G. Bonini and M.R. Tredici. 2008. *Microalgae for oil: strain selection, induction of lipid synthesis and outdoor mass cultivation in a low-cost photobioreactor*. Biotechnol. Bioeng. 102: 100–112.

Sierra, E., F.G. Acien, J.M. Fernandez, J.L. Garcia, C. Gonzales and E. Molina. 2008. *Characterization of a flat plate photobioreactor for the production of microalgae*. Chem. Eng. J. 138: 136–147.

Tredici, M.R. 2004. *Mass production of microalgae: Photobioreactors. In: Richmond A., editor. Handbook of microalgal culture: biotechnology and applied phycology*. Oxford: Blackwell Publishing, p 178–214.

Zittelli, G.C., N. Biondi, L. Rodolfi and M.R. Tredici. 2013. *Photobioreactors for mass production of microalgae. In: Richmond, A. & Hu, Q., editors. Handbook of microalgal culture: applied phycology and biotechnology*. Oxford: Blackwell Publishing, p 225-266.

THE TEK MECHANICAL CASSAVA HARVESTER DEVELOPMENT IN GHANA – CHALLENGES, OPPORTUNITIES AND PROSPECTS FOR CASSAVA PRODUCTION IN AFRICA

Bobobee[1], E.Y.H.; Yakanu[2], P.N.; Marenya[3], M.O.; Ochanda[4], J.P.O

[1] Kwame Nkrumah University of Science and Technology, Kumasi. Ghana

[2, 3, 4] University of Venda, South Africa.

ABSTRACT

The low level of engineering technology inputs into agriculture is a major constraint hindering the modernization of agriculture and food production in many parts of Africa. Cassava (Manihot esculenta Crantz), is a climate resilient crop grown by smallholder farmers in most sub-Saharan Africa countries. Cassava provides dietary carbohydrates for over 800 million people globally. It is also a bio-fuel source that can replace fossil fuels. Africa is not visible in the cassava industrialisation and export market because it depends on over-aged farmers, who use manual tools and traditional production methods that do not attract the youth. One major challenge to all year-round cassava production for industry and export in Africa is the time consuming, labour intensive and expensive manual harvesting method. Manual cassava harvesting is full of drudgery and takes 5 to 10 minutes to uproot a plant, depending on soil condition. The main objective of this paper is to demonstrate and popularise an innovative mechanical cassava harvester developed in Ghana (OAPI patent No. 17219), to mechanise and modernise cassava production in Africa. The device harvests at a rate of one plant per second or less especially when the ground is hard. For the innovation to be disseminated successfully, tractor operators and smallholder farmers must be trained to acquire mechanised production methods. Cassava farmers need to change from planting in the traditional haphazard manner to adopt row and ridge planting to comply with mechanical harvesting at plant maturity. The device is to up-scale and increase cassava production for food security, industrial use and export in Africa.

Keywords: Cassava, mechanical harvester, drudgery, aging farmers.

INTRODUCTION

Cassava (*Manihot esculenta* Crantz) is an important food security crop in the tropical and sub-tropical areas of the world, with its roots providing dietary carbohydrates for over 800 million people (FAO, 2013). Global cassava production for 2016 was estimated at 288.4 million tonnes, with 54% 157.2 (million tonnes) by Africa, 32% by Asia, and 14% produced in South America (FAO, 2016). Unlike Africa, Asia encourages the development of cassava crops for industrial and energy purposes (UNCTAD. 2013). In China, cassava has been listed as one of the main raw materials that can be used for ethanol production and animal feed in future (Chengyu *et al*., 2010, Zhiguo *et al* 2008, DFAO, 2016). In Africa, cassava is the second most important food staple after maize in terms of calories consumed (FAOSTAT, 2012). Today the four leading cassava producing countries in Africa are Nigeria, Democratic Republic of Congo, Ghana and Angola (FAO. 2012, Nweke, 2004). In southern

Africa the crop is cultivated in Namibia, the northern and eastern provinces of South Africa, Mozambique, Angola, Swaziland, Botswana and Zimbabwe. In Tanzania, Malawi, Zambia, Angola and Mozambique, cassava is a very important crop and to a lesser extent in other South African Development Community (SADC) countries. In the cassava growing regions of Sub-Saharan Africa, the crop is for household food security. While cassava has a long history in sub-Saharan Africa, its production in South Africa is insignificant, except by small holder farmers, who cultivate local landraces in Lowveld areas in Bushbuckridge in Limpopo, Nkomazi and Nelspruit in Mpumalanga and KwaZulu Natal provinces. Given that cassava represents a valuable subsistence and cash crop in many countries, Ogola and Mathews (2013) have evaluated its adaptation and agronomic performance in the dry environments of Limpopo province.

Cassava production in Africa is mainly by smallholder farmers, who depend on manual tools for their field operations. However, a lot of challenges such as small farm holdings that are fragmented and dispersed prevent the development and use of modern equipment for its production (Kolawole *et al*., 2010). The most difficult and time-consuming operation in cassava production is cassava harvesting (Yulan, *et al.,* 2012, Agbetoye 2005, Nweke *et al*., 2002). Cassava is mostly harvested manually by lifting the lower part of the stem and pulling the roots out of the ground, then removing the tubers from the base of the plant by hand. The upper parts of the stems with the leaves are removed before harvest. Manual harvesting tools such as levers, cutlasses, hoes, mattocks and ropes can be used to assist in uprooting the tubers. The appropriate manual harvesting method under the current practice depends on soil texture and moisture regimes (Adjei-Nsiah, S. 2012, Peipp and Maehnert. 1992). Harvesting cassava roots by hand is easy if the soils are sandy or during the rainy season. In heavier soils or during the dry season, harvesting usually requires digging around the roots to free them and lifting the plant. To facilitate lifting, the plant is usually coppiced to about 30 to 50 cm above ground. The protruding stem is used to lift the roots out of the ground. While lifting, care should be taken not to break the roots, as this will lead to losses if broken roots are not retrieved from the soil and to contamination that may accelerate spoilage. Manual harvesting of cassava consumes a lot of energy and time and the operation is not mechanised in most countries in Africa (Amponsah *et al.,* 2014; Bobobee *et al.,* 2013; Agbetoye and Ileybare, 2012; Agbetoye, 2005). However, if large-scale tuber production and harvesting is envisaged, development of a mechanical harvesting device is desirable. According to Agbetoye and Ileybare, (2012), several researchers are working extensively in an attempt to come up with effective manual, semi-mechanized/mechanized methods of harvesting cassava. After clearing the land, harvesting is the most labour-intensive operation, and agricultural engineers have sought to mechanise it. Mechanical harvesting of cassava is difficult because of the non-uniform geometry of the roots in the ground. Methods of mechanical cassava harvesting have some advantages, such as high efficiency, low tuber damage and low cost (Xue *et al.,* 2010 and Wang *et al.,* 2011). Nevertheless a few cassava harvesters have been designed and some are in operation, mostly by large-scale farmers in Asia and Latin American countries (FAO, 2013,). Cassava roots can be harvested at any time of the year. Some farmers harvest as early as six months after planting while others may leave the crop for 18 to 24 months after planting (MAP). The food quality of roots, particularly the starch content, increases with time up to an optimal period of 12 to 15 MAP, after which there is a loss of quality, mainly due to increased lignification (IFAD/FAO, 2004, Aye, 2012). Planting of cassava is traditionally done on the flat in a random manner, but recently, Bobobee *et al.,* (2013) are recommending planting cassava in rows and preferably on ridges to aid mechanical weeding and harvesting to support industrial use of the crop. According to Philippine Root Crops Information Service (2005), harvesting cassava during relatively dry soil is the best since the soil does not stick to the harvesting implement or roots easily. This is the time when manual harvesting is also very difficult. During the harvesting process, the cuttings for the next crop are selected and kept in a protected location to prevent desiccation.

Today with the interest to use cassava for various industrial products such as high-quality cassava flour, starch, and other alcoholic beverages, large-scale cassava production is attracting attention on the African continent, especially in Nigeria and Ghana (FAO. 2016). It makes economic and environmental sense to produce more cassava not only for food in the future as climate change, population growth, energy and water supplies add pressure to worldwide food systems. However, cassava harvesting for large-scale industrial processing is a major constraint and presently, there is no known commercial mechanical cassava harvesters in use by many cassava producers on the continent. The present situation especially to harvest all year round demands technological interventions by agricultural engineers and technologists to make cassava an industrial commercial crop on a sustainable basis. To address the above challenges, agricultural engineers at the Kwame Nkrumah University of Science and Technology (KNUST), Kumasi, Ghana collaborated with their counterparts from the University of Leipzig in Germany developed an appropriate mechanical cassava harvesting technology, (The TEK MCH) to harvest cassava root tubers by the 'dig and expose' principle.

1.1 Objective

The main objective of this paper was to identify challenges, opportunities and prospects for cassava production in Africa through the introduction, demonstration and promotion of a novel mechanical cassava harvesting technology in sub-Saharan Africa. The specific objectives were to;

Evaluate the TEK Mechanical Cassava harvester, an innovative device to harvest cassava mechanically,

Establish mechanised cassava pilot farms on ridges and flat land to test mechanical cassava harvesting in different agro-ecological zones in Ghana and South Africa,

Evaluate the draught and other implement performance parameters in mechanical cassava production and harvesting,

Compare mechanical cassava harvesting techniques with manual harvesting methods in terms of field capacity, root damage and drudgery.

2.0 MATERIALS AND METHODS

2.1 Project Sites (Ghana)

Pilot study sites at Anwomaso and Akatsi in Ghana were selected to demonstrate mechanical cassava production and harvesting. The locations were selected based on their potential for higher cassava production levels on commercial basis. In Ghana, Anwomaso (KNUST) arable farms (6°41'56.75"N, 1°31'25.85"W) and 274m above sea level (a.s.l), is in the tropical rain forest zone. Anwomaso experiences bi-modal tropical rainfall pattern and wet semi-equatorial climate. It is characterized by double maxima rainfall lasting from March to July and again from September to November. The mean annual rainfall is 1200 mm, which is ideal for minor season cropping. Temperatures range between 20°C in August and 32°C in March. Relative humidity is fairly moderate but quite high during rainy seasons and early mornings. Soils in Anwomaso are mainly Forest Acrisols (FAO/UNESCO, 1998). The climate in Akatsi is characterized by high temperatures (21° C- 34.5° C), high relative humidity (85%) and moderate to low rainfall regime (1,084 mm) with distinct wet and dry seasons of about equal lengths. Akatsi has Savanna Cambisols (FAO/UNESCO, 1998) soil types characterized as moderate to well-drained, deep red to brown loamy sand to sandy loam topsoil over coarse sandy loam to clay loam sub-soils

2.2 Project Sites in South Africa

Two project sites were selected in Limpopo and Mpumalanga provinces of South Africa. The Limpopo field was located at the University of Venda Experimental farm, Thohoyandou in the sub-tropical Vhembe district (22º 58' 57" S, 30º 26' 25" E), at an elevation of 595 m asl. The climate at Thohoyandou is characterized by moderate temperatures (15° C- 24.5° C), high relative humidity (52.3 -81.1%) and moderate to high rainfall regime (1069.3 mm). The

Limpopo field has *Shordlands* soil form with high clay content and classified as Nitisols (FAO/UNESCO, 1998). The Nelspruit site (25º 27' 21" S, 30º 59' 49" E) in Mpumalanga is characterised by deep, well-drained loamy sand soils of the *Glenrosa* series and classified as Cambisols (FAO/UNESCO, 1998). The Nelspruit site is located on the Agricultural Research Council's Institute for Tropical and Sub-tropical Crops (ARC-ITSC) orchards. Both areas (Univen and Nelspruit) are dominated by a Savannah biome with vegetation type of sour lowveld bushveld.

2.3 Seedbed preparation field layout and crop establishment

The fields (one ha minimum) at all sites were ploughed with disc ploughs in Ghana and mouldboard ploughs in South Africa. All fields were deep ploughed to be free from hidden obstructions and harrowed with disc harrows to produce smaller clod sizes, before ridging. Both the Ghanaian and the South African fields were ridge landforms according to Bobobee *et al*., (2013). Ridges were constructed with an average height of 0.3m and spaced 1.2m apart (crest to crest) to accommodate the tractor track width. Intra-row spacing was varied for optimum plant population density of 10,000 plants/ha. Cassava stakes were cut into 20-25 cm length with 8-10 nodes and planted at an inclined angle of about 30-60º with half of the length buried in the soil.

2.4 Soil mechanical analysis

Soils were sampled at random locations at the corners and mid-sections of the fields to measure soil penetration resistance, bulk density and moisture contents in the 0-40 cm layer at 10 cm intervals. Composite samples were taken at depths of 0-20, 20-40 and 40-60cm using the soil auger for soil physico-chemical analysis and particle–size distribution and texture (USDA textural triangle). These soils were chemically analysed to test for their pH-levels (1:1H_2O), Organic Carbon content (%), total Nitrogen (%), Exchangeable cations in me/100g (Ca, K, Mg and Na), Base sat (%), T.E.M, C.E.C (me/100g), Exchangeable A (Al + H) and Available Brays (ppmP and ppmK)

2.5 Crop care and farm sanitation

All the fields planted were on long fallow lands and no organic or inorganic fertilisers were applied to the cassava in both countries. In addition to the pre-emergence chemical weed control in the Ghanaian fields, weeding was mainly by manual methods using hoe and machete every two–three months after planting (MAP) depending on weed infestation levels. Farm boundaries and access roads were occasionally sprayed with herbicides. Fields were maintained clean close to harvesting time to minimise residues clogging the harvester.

2.6 The mechanical harvester

The fully-mounted mechanical cassava harvester with a slatted conical mouldboard without any transport system (Fig 1) was adapted from a Leipzig model and developed to operate on the "dig and expose" principle.

Figure 1: Cassava harvester according to the "dig and pull principle" being commissioned in South Africa

The harvester mass is 300 kg, and it requires 47-60 kW pusher-type motive power. The cutting width is 1000 mm with a depth of cut of 240-400 mm. At a working speed of 2.1-6.7km/h and depending on soil condition, operator experience and skill, the implement can harvest 0.5 – 0.7 ha/h at a fuel consumption of 15-23 l/ha. The detailed description and performance has been discussed by Bobobee *et al*., (2013) and Amponsah *et al*., (2014).

2.7 Draught, speed and slip measurements

In Ghana the draughts developed by the ploughs, harrows and harvester as they operate to prepare seedbed and excavate the cassava root cluster were measured using a 10 tonne commercial electronic dynamometer (RON 2125S®, Israel) with a digital data logger (Fig. 2). In operation, the dynamometer was attached between a pulling tractor and the instrumented tractor that hitches the implement. Draught forces were measured for the implements in the transport position (no load) and when engaged in the soil during work and harvesting (load). Load conditions and draught force measurements were taken after the implement has stabilized in the soil at the operating depth. Average speed of operation was derived from the time taken for the tractor implement assembly to traverse a fixed distance marked on the field. To measure implement slip, the distance covered by 10 rear tyre revolutions when working and in no-load positions were used. Figure 2 shows the implement draught measurement procedure with one tractor pulling the instrumented one hitching a harvester. The RON 2125S dynamometer logs the force measurements, which were later transferred to a computer and analysed with popular spreadsheet programmes.

Figure 2: Implement draft determination by RON 2125S electronic dynamometer

In South Africa, the three-point hitch dynamometer and data logging instrumentation (Figure 3) developed by the ARC-IAE was used to determine, speed, fuel consumption, slip drawbar force, and engine power required by the implements tested. The dynamometer measures forces on every hitch point i.e. vertically, horizontally as well as laterally. The resultant pulling force is measured by using the data from all three measuring points. The correct setting of the 3-point hitch dynamometer is important to be able to sense the forces and other parameters generated by the implement and the tractor. Calibration of all the bridge channels on the data logger was performed by lowering the implement to a stable position on the ground. The data logging process and the test runs were performed at the same constant working speed and depth. During the test run all the instrumented data were logged at 100 Hz onto the data logger memory bank. After operating the implements, the disturbed soils created by the implements were excavated to expose the width and depth of work and to measure the profile created. The data was then downloaded to the computer on the base station using popular spreadsheet programmes to process and to generate reports for each implement.

Figure 3: Three-point hitch dynamometer

2.8 Soil Profile measurement

The profile of the soil disturbed soil by each implement was measured using laser measuring units on a steady beam to profile both the horizontal width of cut and the vertical depth of the cut soil (Figure 4). The profiled area is then calculated.

Figure 4: Soil profile measurement using the laser beam technology

2.9. Heart rate and drudgery estimation

In this study, heart rate is used as proxy for the intensity of physical activity or manual work in agriculture. Heart beats of manual workers and tractor operators were measured at rest before work, during work and after work (recovery). This is to estimate the energy expenditure and stress or drudgery induced in cassava production. In Fig. 5, heart rate data were collected simultaneously at a sampling rate of 5s interval using the POLAR® RS800CX Accurex instrumentation (Polar Electro, Oy, Finland). The mounting, installation and performance of the heart rate sensor and monitor is described in greater detail, by Bobobee and Girma (2007). Data from the receiver is downloaded to a computer for visualisation and processing by popular spreadsheets. Drudgery was estimated for manual planting, weeding and harvesting and mechanical land preparation and harvesting activities of operators by evaluating the heart beats of the workers during work. In this paper, only harvesting drudgery has been reported. Corresponding energy consumption values were used to calculate the mandatory rest periods required for each operation.

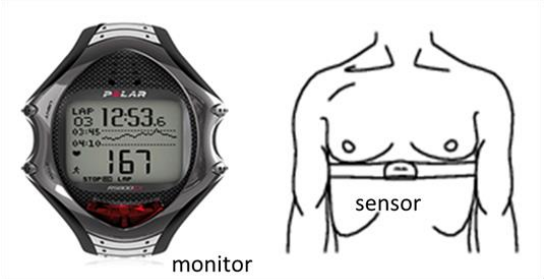

Figure 5: The polar (RS800CX) heart rate monitor and chest strap sensor

Figure 6: Manual cassava harvesting, with the workers instrumented with the Polar heart rate monitors

The mandatory rest period in minutes per hour required by workers when performing physical harvesting activity (Figure 6) depends on the gross energy consumed in carrying out that activity. Mathematically, rest period is as expressed in Equation (1).

$$T_r = 60 \times \left(1 - \frac{250 or 300}{P}\right) \text{min/ } h \quad (1).$$

Where, T_r = Total rest period (min/h)

P = Gross energy consumption (Watts)

250 W is used as numerator in the hot tropics of sub-Saharan Africa, while 300 W is used for the cool temperate and sub-tropical areas of South Africa.

Using the average working heart rates obtained for a particular field activity the corresponding gross energy consumption (Watts) was determined and used to compute the mandatory rest period required to enable the duration a worker can recuperate and gain lost energy. The more intense the physical activity as in the manual harvesting (Figure 6), the higher the heartbeat of the worker with a corresponding higher gross energy consumption leading to a longer rest period. Mechanical harvesting (Figure 7) on the other hand is less strenuous and does not demand longer rest periods.

Figure 7: Mechanical cassava harvesting

2.10 Root tuber damage assessment

Cassava deteriorates from 24 h after harvesting due to its high moisture content. Any bruises and damage will accelerate tuber deterioration and spoilage (Bayoumi *et al.,* 2008). Cassava root damage caused during harvesting was due to either shallow harvesting depths or relatively deeper root penetration or longer horizontal root spread beyond the harvester operating width. Quantitative methods were employed to determine root damage. Damaged and whole tubers after harvesting were separated and weighed (Figure 8). The percentage damage for each harvesting method was computed by dividing the damaged cassava weight by the total yield. Farmers, market women and processors use the qualitative (eye-balling) approach to assess damage. From farmers and processors perspectives, cassava root damage was assessed when the tubers do not come out whole after harvesting but with cuts and bruises that could render it unsuitable for long storage.

Figure 8: Cassava root tuber damage assessment in the field

3.0 RESULTS AND DISCUSSION

3.1 Soil physico-chemical properties

Table 1 shows the soil chemical and mechanical properties at land preparation at all sites and at harvest at the Ghana sites Anwomaso soils were strongly acidic up to 60 cm depth. With such acidity levels, important soil nutrients such as Potassium and Phosphorus will not be easily available for plant growth (Brady and Weil, 1996). Akatsi soils on the other hand, had moderate acidity after ploughing and at harvest.

.

With the relatively high yield obtained from the project sites 15 MAP, it means that cassava can be cultivated in soils with pH ranging from 4.4 – 6.0 without adverse yield loss, which agrees with the findings of O'Hair, (1995), Philippine Root Crops Information Service, (2005) and Okigbo, (2007) that cassava can survive in poor soils with pH ranging from 4 to 9. Even though the pH appeared to be unsuitable for crop growth, the cassava yield was not seriously affected at the Ghana locations.

Soil organic carbon was generally low (<2%) at the Ghana sites but were slightly better at Anwomaso within the topsoil (0-20 cm), with Akatsi having extremely low organic carbon (%) at ploughing and at harvest. Low C.E.C (5 - 15 me/100g) and very low (<5 me/100g) indicate low to moderate soil fertility, respectively. All the study sites generally fell within the range of moderate soil fertility and thus were suitable for plant growth after ploughing. At harvest however, the soil fertility was lower for the sites indicating that, the soil fertility had been used and this reflected in the high cassava crop yield at both places. Nitrogen contents were low to medium at planting, and very low (<0.1) for all sites at harvest. This indicated the cassava crops utilized the soil Nitrogen for their growth and development as expected. Soils at Anwomaso are predominantly sandy loam at 0-20cm and sandy clay to sandy clay loam at 20-60cm soil depth. Soils at Akatsi are mainly loamy sand from 0-60 cm soil depth. Soils at the Anwomaso had better nutrient and water holding capacity compared to that at Akatsi.

In South Africa, soil organic carbon was generally higher (<3%) at the Venda site but lower (<1%) at Nelspruit sites within all horizons (0-60 cm). Low C.E.C (1.9 - 18 me/100g) and very low (<5 me/100g) indicate low to moderate soil fertility, at the Venda and Nelspruit sites, respectively. All the study sites in Ghana and South Africa generally fell within the range of moderate soil fertility and thus were suitable for cassava growth after ploughing.

Location (Soil depth)	pH (1:1 H_2O)		O.C. (%)		C.E.C (me/100g)		N (%)		Sand %	Silt %	Clay %	Soil Texture		FAO (UNESCO) Classification (1998)
	AP	A	AP	AH	AP	AH	AP	AH				AP	AH	
Akatsi														
0-20cm	5.70	6.12	0.22	0.34	2.45	5.16	0.16	0.03	83.02	14.98	2.00	Loamy sand	Loamy sand	Cambisols
20-40cm	6.00	6.12	0.18	0.27	1.60	4.43	0.13	0.02	81.70	14.30	4.00	Loamy sand	Loamy sand	
40-60cm	5.60	5.91	0.15	0.17	1.94	4.17	0.11	0.02	80.46	15.54	4.00	Loamy sand	Loamy sand	
Anwomaso														
0-20cm	5.50	4.83	0.96	0.87	3.64	6.61	0.23	0.11	64.94	25.06	10.00	Sandy loam	Sandy loam	Forest Acrisol
20-40cm	5.00	4.78	0.52	0.47	3.72	7.02	0.13	0.05	50.70	21.30	26.00	Sandy clay loam	Sandy clay loam	
40-60cm	5.00	4.60	0.43	0.23	3.53	6.87	0.10	0.02	43.10	26.90	28.00	Clay loam	Sandy clay loam	
Venda														
0-20cm	5.83	na	2.70	na	18.161	na	na	na	22	20	58	clay	Sandy loam	Nitisols
20-40cm	5,56		1.53		13.87				11	16	73	clay	Sandy clay loam	
40-60cm	5.29		1.92		13.581				10	18	72	clay	Sandy clay loam	
Nelspruit														
0-20cm	6.42	na	0.69	na	2.328	na	na	na	80	6	14	loamy sand	loamy sand	Cambisols
20-40cm	6.42		0.69		1.799				80	6	14.00	loamy sand	loamy sand	
40-60cm	6.08		0.74		4.824				72	6	20.00	loamy sand	loamy sand	

Table 1: The soil chemical analysis results (pH, O.C., C.E.C., N and Soil Texture) at Akatsi, Anwomaso and Venda and Nelspruit during ploughing (AP) and at harvest (AH) [na = not available at reporting time]

3.2 Soil mechanical properties

The soil bulk densities, cone index and moisture contents at the Ghana sites before ploughing and at harvest are shown in Fig 9. There is a general increase in bulk density with depth for all sites before ploughing and at harvest. At harvest soil bulk density ranged from 1.56 – 1.68 g/cm^3 at Anwomaso, 1.45 – 1.57 g/cm^3 and 1.54 – 1.65 g/cm^3 at Akatsi with increasing soil depth. This trend agrees with the findings of Arshad *et al*., (1996), that bulk density increases with depth in the soil profile.

The soil bulk densities for Anwomaso site was lower at ploughing and harvest than for Akatsi. The high bulk density at ploughing at Akatsi could be attributed to the fact that the soils were more consolidated causing the clods to easily compact. The high bulk densities at harvest still made harvesting possible for the TEK mechanical cassava harvesters. Report by USDA, (1999) considered that compacted soil layers have high bulk densities. Bobobee *et al*, (1994) reported a maximum soil bulk density of 1.82 g/cm^3 at harvest for the Leipzig harvester. Soil core sizes range from 15 cm diameter by 15 cm high to rectangular cores 1 cm thick and 5 cm across. Soil bulk density as an important factor influences soil microscopic properties like large pores, hydraulic conductivity, penetration resistance, etc, which are significant in land utilisation (Koolen 1987, Gupta et al, 1989).

The mean soil penetration resistances before ploughing (BP) and at harvest (AH) for Anwomaso, and Akatsi sites increased with depth (Fig.9). Penetration resistance is one soil physical property modified by tillage. In this project, the mechanical resistance of the soil to a penetrometer is related in a poorly understood manner to clay mineralogy and to soil physical properties such as dry bulk density ($D_{b)}$, texture, structure, water content and percent organic matter, Cassel (1982). Tillage operations (ploughing, harrowing and harvesting), alter penetration resistance primarily by effecting changes in D_b, structure, and water content. Bernier et al (1989), studied the soil disturbance of a winged sub-soiler in a sandy loam and clay soil. The bulk density profiles indicated that passage of the sub-soiler compacted the top soil while loosening the subsoil. They concluded that the effects of tillage on soil physical properties could not be satisfactorily interpreted by conventional statistics. At harvest, penetration resistance ranged from 1.77 – 2.24 MPa at Anwomaso, 0.73 – 1.53 MPa and 0.92 – 3.03 MPa at Akatsi with increasing soil depth. From fig. 9, it is clear that soil penetration resistance increased with increasing bulk density. Ploughing generally reduced the penetration resistance which agrees with the findings of Reichert *et al.*, (2004).

From fig. 9, mean soil moisture content before ploughing and at harvest for Anwomaso, and Akatsi increased with increasing depth with the Akatsi soil being the driest. For the range of soil depth tested, soil moisture increased with depth and ranged from 12.06 – 15.69 % (d.b.) at Anwomaso and 1.02 – 3.71 % (d.b.) at Akatsi. The increasing moisture content down the soil profile could be due to the fact that the topsoil experienced more evaporation than lower horizons. The soil moisture content for Akatsi before ploughing decreased with increasing soil depth. This change could be attributed to the fact that it had rained the day before ploughing when the samples were taken and moisture had not infiltrated completely into lower horizons

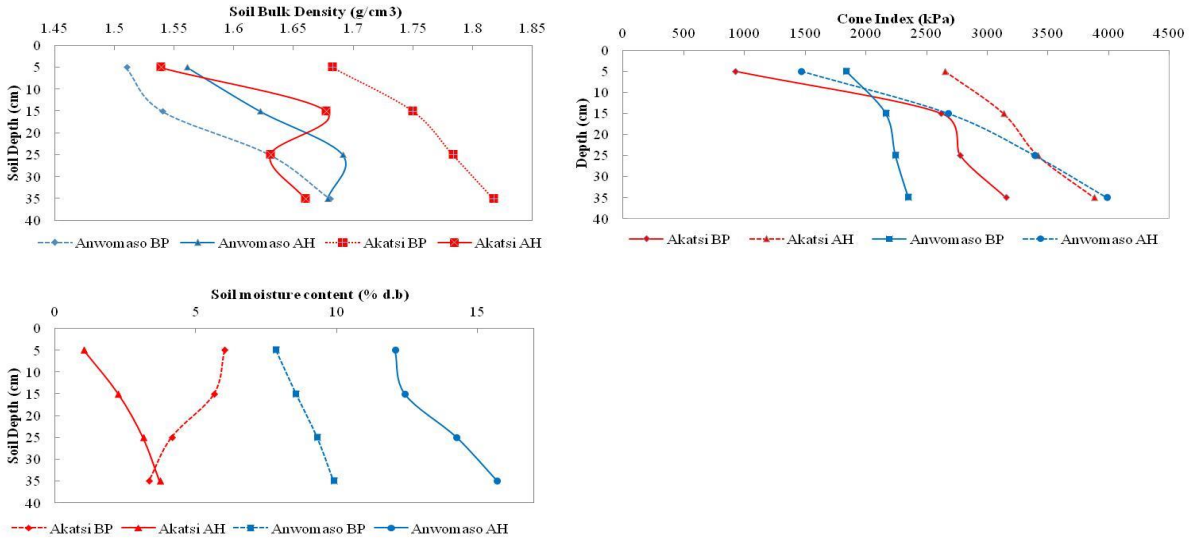

Figure 9: Graph of Mean Bulk Density (g/cm^3), Cone Index (kPa) and Moisture content (%) before ploughing (BP) and at harvest (AH) versus soil depth for the two Ghana trial sites

3.3 Depth of tuber penetration and harvester performance

Figure 10 shows the mean root tuber depth of penetration when harvesting elite cassava varieties by both manual and mechanical means at 15 MAP for Akatsi and Anwomaso. From the graph, mechanical cassava harvesting on the ridge at Anwomaso had higher mean root tuber penetration depth of 26.01 cm compared with a mean root penetration depth of 24.96 cm at Akatsi.

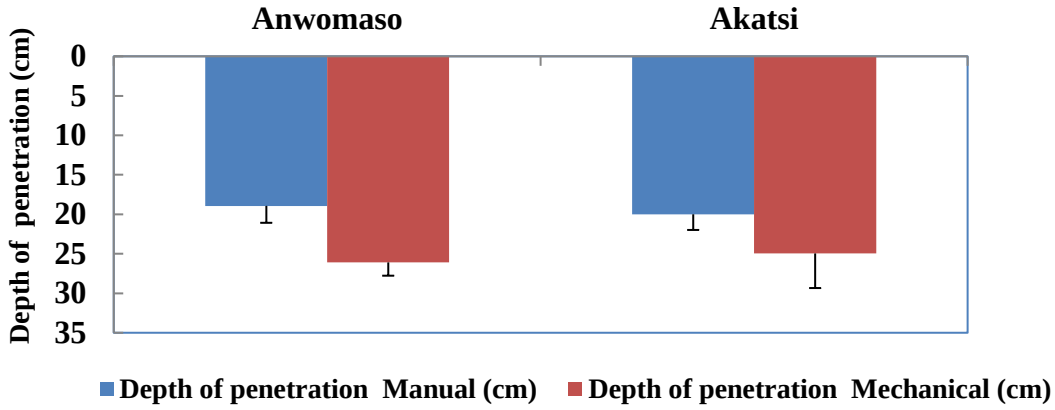

Figure 10: Mean Depth of Cassava root tuber excavation (cm) for both ridge and flat landforms at Anwomaso and Akatsi at 15 MAP

There was no significant difference ($p<0.05$) for the mean depth of root excavation for manual and mechanical harvesting at Akatsi, and Anwomaso. Mechanical harvester performance was evaluated under working depth, percentage root tuber damage, field capacity, fuel consumption, working speed, percentage wheel slip, draught force and tractor power requirement and energy consumption. The mean depth of mechanical harvester penetration at Anwomaso and Akatsi ranged from 24.00- 27.00 cm. From fig. 10, the mean depth of harvester penetration at Anwomaso was higher than at Akatsi implying eminent higher root damage during harvest at Akatsi. To minimise damage, the harvester has to go deeper beyond the depth of root penetration. Odigboh and Moreira, (2002) and Sam and Dapaah, (2009) reported that ridges are able to control cassava roots tubers to reasonable depths to allow for optimum mechanical harvesting. Another reason could be due to the ease with which ridges were easily pulverized. The harvester cutting edge goes deeper under ridges and shatters the soil better during harvesting than on the flat landform. This is in agreement with what Ennin *et al.,* (2009), reported that planting cassava on ridges had the advantage of higher cassava root yield, better and easier field management and the potential for mechanization to further decrease drudgery and increases the scale of productivity of cassava compared to planting on the flat.

3.4 Tuber Damage Assessment

From Figure 11, the mean percentage tuber damage at Anwomaso and Akatsi ranged from 9.5-10.8 and11.8-16.25% for both manual and mechanical harvesting.

The lowest mean percentage harvesting root tuberr damage was recorded for cassava varieties that developed bunchy tubers and on ridges, compared to higher tuber damage for varieties that developed laterally, did not cluster but spread both in the latitudinal and longitudinal directions along rows and on ridges. Bobobee *et al,* (1994) reported 10.7-22% average tuber damage for the Leipzig mechanical harvester while Kolawole *et al.,* (2010) reported 23.3% tuber damage for another mechanical harvester. Generally, the higher percentage root tuber damage for Akatsi could be attributed to the low moisture content, high bulk density, high penetration resistance (fig 11) and the relatively low depth of harvester penetration (fig.10) at harvest.

3.5 Field capacity for mechanical harvesting

From Figure 12, mechanical harvesting ranged from 2.2 – 2.23 (h/ha) whilst manual cassava harvesting capacities ranged from 105 - 239 (h/ha), confirming a higher amplification of efforts with the mechanical harvester. Bobobee *et al,* (1994) reported a range of 2.63 – 4.0 h/ha for the Leipzig harvester. Ospino *et al,* (2007) also, reported a mean field capacity range of 1.0 – 1.6 h/ha for the CLAYUCA Cassava Harvester Model P600, whilst Oni (2005) reported a range of 0.83 – 1.25 h/ha for the NCAM harvester. The low moisture content at Akatsi (Fig.9) compared to Anwomaso, could be responsible for the difficulty to manually harvest both on the ridge and on the flat landforms. This confirms the fact that mechanical harvesting is most suitable during the dry season while manual harvesting on the other hand is preferred during the wet season as reported by Bobobee *et al.,* 1994 and Ospino *et al.,* 2007. Nweke *et al.,* (2002) reported a labour requirement of 22-63 man-days per hectare for manual harvesting of cassava. Comparing the capacities obtained for mechanical and manual harvesting methods in Fig 10, it confirms that manual cassava harvesting is more time consuming and could be full of drudgery than mechanical harvesting. The high man-hours required to manually harvest at Akatsi strongly correlates with the low soil moisture content, high soil bulk density and penetration resistance and drudgery level, confirming that the harder the soil, the more difficult to harvest manually.

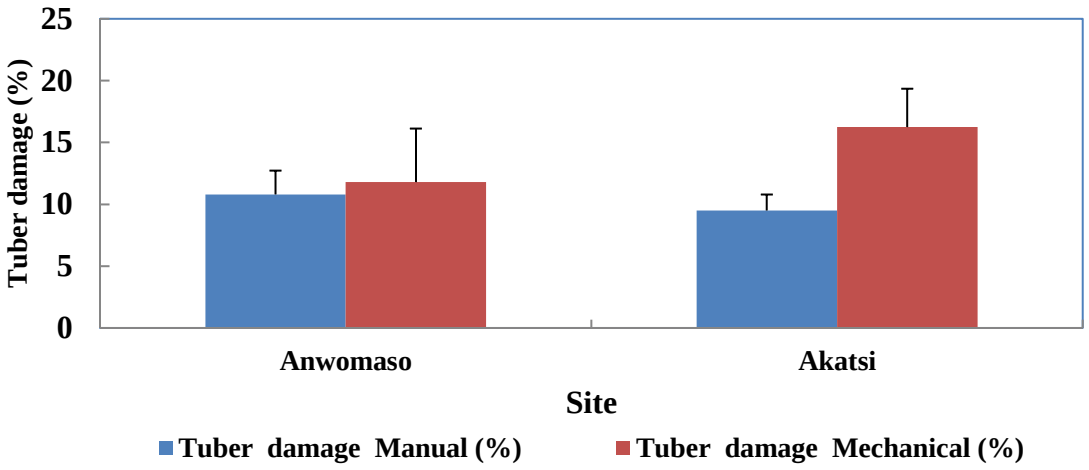

Figure 11: Cassava tuber damage (%) for the Ghana sites

The results for the two sites show the above soils conditions do not adversely affect mechanical harvesting

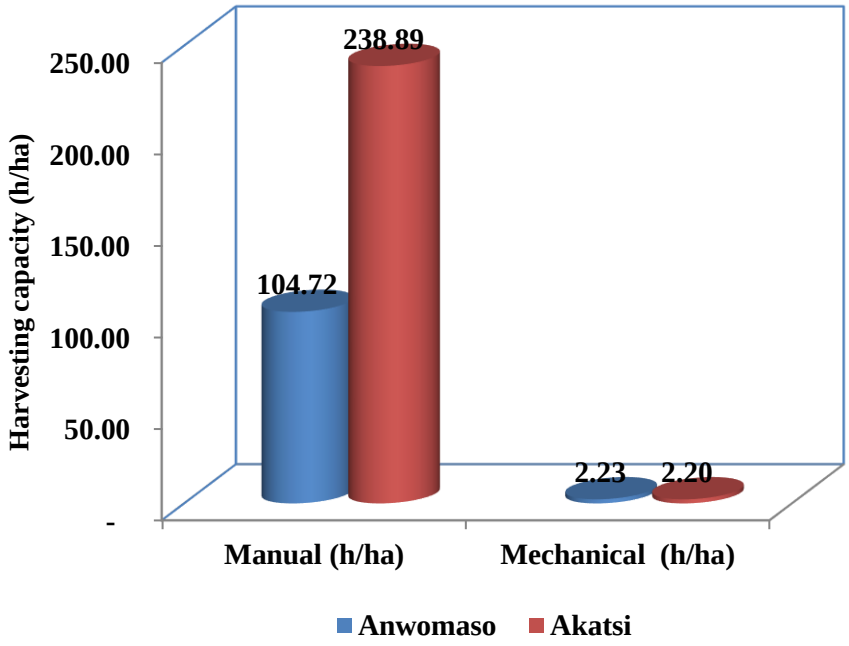

Figure 12: Field capacity for manual and mechanical cassava harvesting for the Ghana sites

3.6 Fuel consumption, wheel sip and travel speed

Table 2 depicts the mean fuel consumption, wheelslip and travel speeds for mechanical cassava harvesting at Akatsi and Anwomaso. The harvester recorded the highest mean fuel consumption of 22.26 l/ha at Akatsi compared with 20.44 l/ha at Anwomaso. During the tests, it was observed harvesting on the flat has higher fuel consumption than harvesting on the ridges.

Table 2 Mean tractor wheel-slip (%), fuel consumption and travel speed for mnechaical cassava harvester at Akatsi and, Anwomaso

Parameter	Akatsi	Anwomaso
Fuel consumption (l/ha)	22.26	20.44
Wheel slip (%)	12.92-14.93	8.19 – 14.80
Travel speed (km/h)	4.98	5.49

In Table 2 above, the mean harvesting tractor wheel-slip recorded for Akatsi and Anwomaso ranged from 12.92 – 14.93% are all within acceptable ranges for a deep soil engaging implement like the cassava harvester. Akatsi recorded the higher mean wheel-slip than Anwomaso. The sandy soils at Akatsi had the lowest moisture content and more likely to fail under the tires thus impeding soil grip and movement relative to the other sites.

The highest mean working speed of 5.49 km/h was obtained at Anwomaso, whilst the lowest speed of 4. 98 occurred at Akatsi. However, no statistical difference ($p<0.05$) existed between the two sites. The above speeds are higher than the 2.4 – 4.1 km/h Bobobee *et al.,* (1994) reported for the Leipzig mechanical harvester but lower than the values Ospino *et al.,* (2007) reported for the CLAYUCA Cassava harvester prototype, which had an operational speed of 7.0 km/h. Several factors such as wheel slip, moisture content, depth of penetration, operator experience and skill etc. could have caused these differences in mean fuel consumption for mechanical harvest. The higher fuel consumption values at Akatsi could be due to the relatively dryer soil coupled with a higher soil bulk density and higher penetration resistance.

Figure 13, shows the typical profiles of the working speed, fuel consumption, engine and drawbar power for the harvester performance using the three-point hitch dynamometer and data logger instrumentation while working in South Africa. The values obtained fall within the acceptable limits as those recorded under Ghanaian conditions. The results are in agreement with Owen (1989), who investigated the effect of travel speed on draught forces and soil disturbances associated with sub-soiling and found that the draught force was significantly correlated with the square of travel speed.

3.7 Draught force and tractor power requirement

The draught force and other parameters of ploughs, harrows and harvester in Ghana and South Africa are summarised in Tables 3&4, respectively. Table 3, shows the mean draught force, average working speed, depth of harvester penetration, soil specific resistance (SSR), drawbar power and brake horse power (Brake Hp) observed for the harvester at the Ghana sites during harvest. The draught force values ranged between 9.214 kN to 14.52 kN for both sites. Taking drawbar power to Brake Horse Power (Brake Hp) ratio of 19% and knowing the width of cut for the harvester to be 1 metre, the SSR (kN/m^2), Drawbar Power and Axle Power (Tractor Engine Power required) are calculated (Hunt, 1977).

In Table 4, the performance of the mouldboard plough, disc harrow and the harvester using the three-point hitch dynamometer and data logger in South Africa are shown. The speed, specific fuel consumption, engine power, wheel slip and work rate results agree with those obtained in Ghana for the harvester. The specific fuel consumption for the disc harrow is nearly 50% lower than the mouldboard plough and harvester.

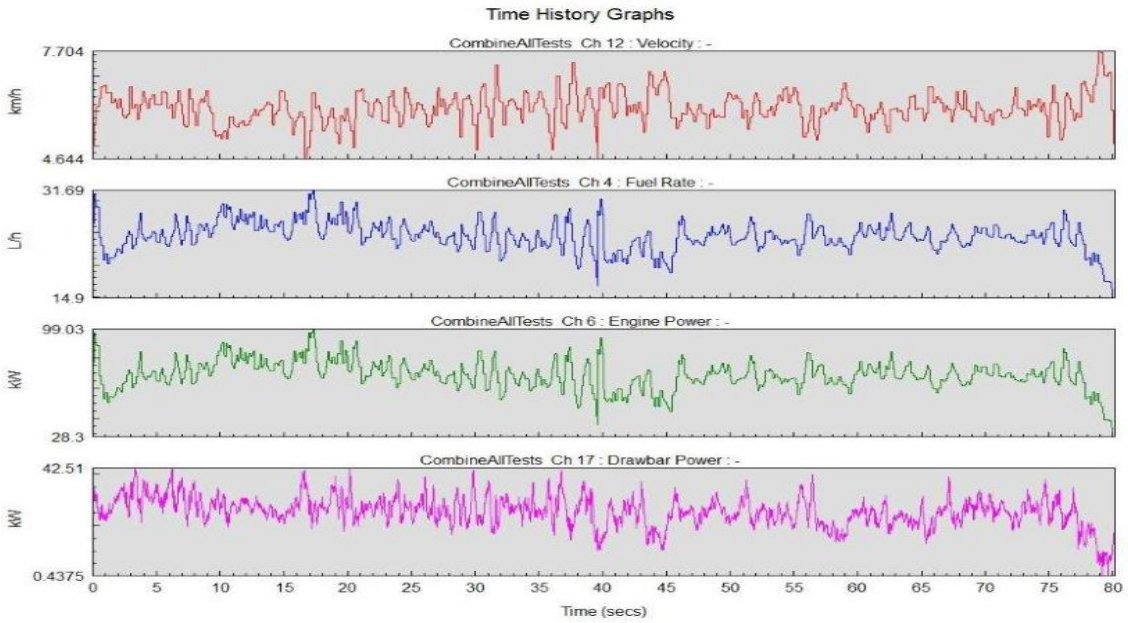

Figure 13: Combined travel speed, fuel consumption and power profiles when using the harvester to plough in South Africa

Table 3: Draught forces of harvester used to calculate the tractor engine power requirement at Anwomaso and Akatsi.

Site	Draught force (kN)	Travel speed (km/h)	Depth (m)	SSR (kN/m^2)	Drawbar power (kW)	Engine power (kW)
Anwomaso	9.214-11.03	1.22-1.32	0.24-0.266	34.82-46.03	11.24-14.56	59.48-76.75
Akatsi	13.2-14.52	1.11-1.22	0.24-0.3	48.4-54.10	16.10-16.12	84.76-84.83

Table 4 Plough, harrow and harvester performance in South Africa

Parameter	**Mouldboard plough**	**Disc harrow**	**Harvester**
Speed (km/h)	5.35	9.05	5.01
Fuel rate (l/h)	21.94	20.85	18.49
Specific fuel consumption (l/ha)	22.92	13.00	20.56
Work rate (ha/day)	9.56	16.29	9.01
Engine power (kW)	57.96	53.39	43.42
Drawbar power (kW)	26.02	20.32	26.75
Wheelship (%)	9.1	11.62	16.12
Implement efficiency (kN/m2)	31.59		91.72
Area (m2)	0.58		0.22
Working depth (mm)	250	140	200
Width of cut (m)	1.8	3.3	1.0
MC (%)	15	15	15
Clay (%)	12	12	12

The area (depth and width) of cut of the three furrow mouldboard plough and the harvester after they work soil and the pulverized soil excavated has been profiled by the laser beam technology for measuring the depth and width of cut (figure 14). The profiles of the plough and the harvester confirmed the true depth and width of cut and the soil excavated. These parameters also affect the speed, slip, wheel slip and the drawbar force and power generated by the implements. As reported by Gill and Vandem Berg, (1975), quantitative evaluation of tillage implement performance requires a measurement of induced forces from the soil-tool interactions and a measure of soil conditions to determine when and how much change occurred in the soil. Forces applied to a tillage implements (plough, harrow and harvester) produce effects on the soil that were readily measured by the instrumentation used. In this study, tillage operations of the plough, harrow and harvester alter the soil that has been loosened, crushed, inverted, sheared, shattered etc. Several of these effects may occur simultaneously and logged by the instrumentation employed.

3.8 Drudgery Calibration

Figure 15 shows the profiles of the manual worker and tractor operator when engaged in cassava harvesting. The heart rate profiles for the manual harvesting were 60% higher than for mechanical harvesting. From the figure, the highest heart rate for the tractor operator corresponds to the average resting heart rate profiles for the tractor operator, confirming the higher drudgery levels in manual harvesting. Drudgery was calibrated using the harvesting energy consumption. The higher the heart rate, the higher the energy consumption and to protect the worker, there is need for longer rest periods to recuperate and gain lost energy.

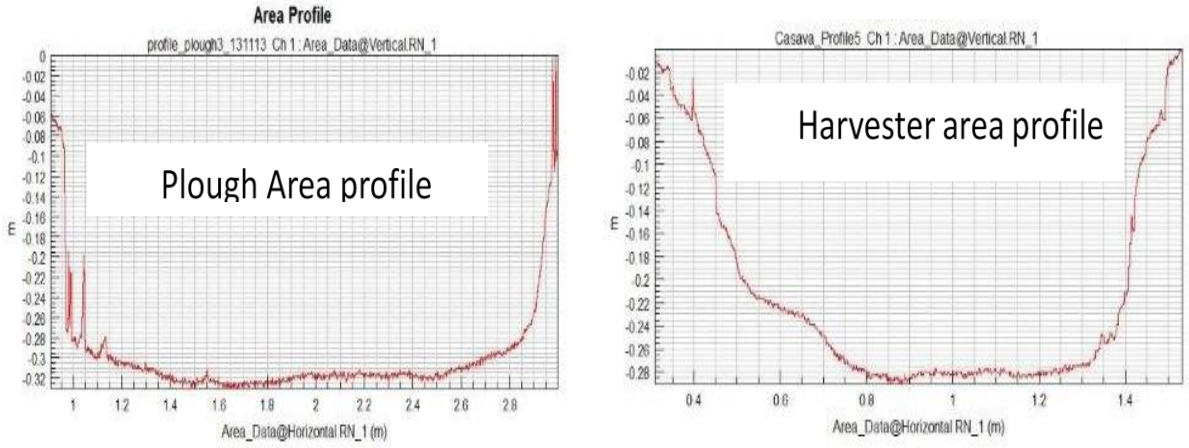

Figure 14: Area (depth and width of cut) profiles for the 3-bottom mouldboard and mechanical harvester

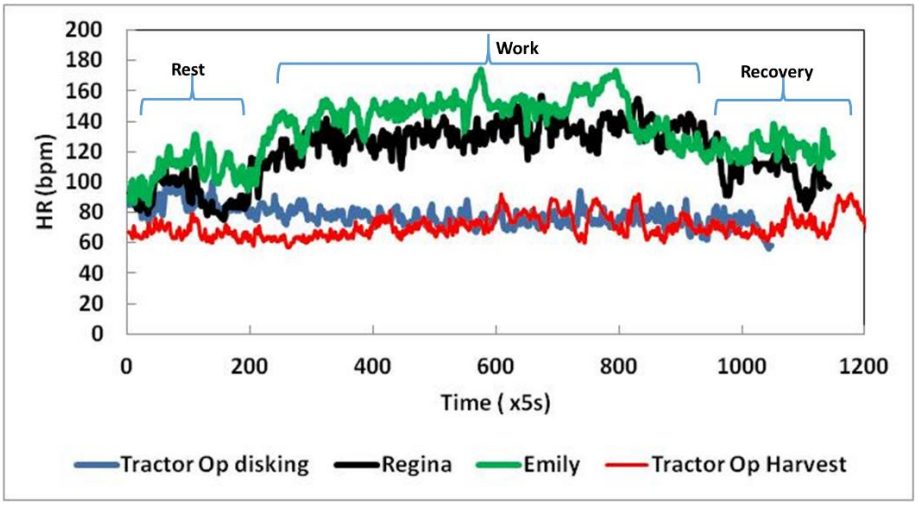

Figure.15:. Heart rate profiles to assess drudgery for manual workers and tractor operator

3.9 Mean heart rate, gross energy consumption and mandatory rest period

Table 4 shows the mean heart rate (bpm), gross energy consumption (Watt) and total mandatory rest periods (mins/h) required by manual workers and tractor operators at Anwomaso, and Akatsi during cassava harvesting. Table 4 depicts a generally higher mean heart rate for manual cassava harvesting compared with mechanical harvesting at all sites.

Rest period for manual harvesting was observed to be low when soil moisture content was high and it was easy for manual harvesting compared with harvesting when the soil is dry. According to Ospino *et al.,* (2007), in terms of energy expenditure manual harvesting was generally easier during the wet season compared to mechanical harvesting, because tractor experience higher wheel slip in softer soils. Knowledge of the total mandatory rest period required after every harvesting activity is important in order to determine the effective working hours for a field worker. For an eight (8) hour man-day, a tractor operator at Anwomaso would require a rest period of three (3) hours and twenty-one (21) minutes, making him to effectively work for only 4 hours and thirty-eight (38) minutes.

Table 5: Mean heart rate, gross energy consumption and rest period for manual workers and tractor operators at Anwomaso and Akatsi during cassava harvesting.

Study site	Mean heart rate (bpm)		Energy Consumption (W)		Rest periods (min/h)	
	Manual	Tractor operator	Manual	Tractor operator	Manual	Tractor operator
Akatsi	119.65	96.86	746.27	487.90.	39.90	29.26
Anwomaso	112.42	91.58	664.91	426.65	37.44	24.84
Lsd	Ns	ns	ns	ns	ns	ns

From Table 5, gross energy consumption is directly proportional to the total rest period required, confirming that the more the energy consumed during an activity, the more the rest period required to recuperate and to compensate for the lost energy.

CONCLUSIONS

The mechanical harvester was developed and evaluated in comparison with manual harvesting and found to have performed soil pulverization and tuber uprooting best during the peak of the dry season when the soil was dry and hard. After harvesting the field was left ploughed for subsequent harrow and planting, thus saving time, fuel and cost. The depth of penetration and width of cut of the harvester affected the draught, speed, slip, fuel consumption of the tractor, and the capacity of the tractor to pull it. The harvester did not affect the drudgery of the operator since the heart rate profile of the harvester was similar to the heart rate profile of a disc harrowing. The study revealed that several factors are critical for successful mechanised harvesting of fully matured cassava crop. These include ridging, tractor speed, wheel slip, soil moisture content, cone index, depth of penetration of digging share, depth and spread of root cluster as it affects damage to roots.

The cassava harvester developed a capacity of 2.2-2.3 h/ha, and it can harvest in two hours what 60-114 people can do in a day. The drudgery involved in manual and mechanical harvesting is evaluated using the average heart beats of workers and tractor operators to determine the energy consumption and the mandatory rest periods required. The heart rate profiles for manual harvesting were 80% higher than for mechanical harvesting. The ease of mechanical harvesting is explained by the low heart beat profiles, energy consumption and rest periods of the tractor operator compared to those of the manual harvester.

Soil water content depletion during the dry season prior to seedbed preparation and at harvest resulted in increased soil resistance to penetration. In addition, draught, power, wheel slip, and fuel consumption were increased. Draught developed by the harvester was equal to that recorded for the three-furrow mouldboard plough. Drawbar power required to pull this harvester at a depth of 25-30 cm and at a field forward travel speed of 1.11 - 1.32 m/s was a low 16-17 kW.

Fuel consumption of the harvester was equal to that of mouldboard ploughing and almost double that of harrowing. The high fuel consumption noticed with the harvester might be due to the high slip, which also depended on the low soil moisture content at the time of harvesting, the high soil penetration resistance, and the depth of penetration of the lifter, the width of cut and the area and weight of excavated soil.

Root damage of 11-17 % was caused by the harvester is within acceptable limits when compared to other harvesting methods.

RECOMMENDATIONS

- Mechanical cassava harvesting, far from being perceived as grandiose technology push academic exercise, the field test results generated new ideas that would lead to modern practices in cassava production. This calls for strategic thinking, sustained research programme development, sound human resource management and prudent financial mobilisation.

- Instead of waiting for users to reach the level of the requirements of a technology, mechanical cassava harvesting technology that is new on the African continent and at the level of users' needs and resources should be introduced, demonstrated and promoted. Over the medium and long term, the harvester project will need the constant support of committed research and development systems. Creation, strengthening and integration of this technology research and development system within the continent's

cassava project should be contemplated in the continent's cassava promotion strategy.

- Since majority of farmers on the continent plant cassava on the flat and as a mixed crop using conventional tillage practices, it will be necessary to evaluate harvesting on the flat and with conservation agricultural practices to compare performance and economic analysis of the harvester.Social impact of any large scale industrial use of cassava in producing communities and its effect on the dietary habits of the farmers.

ACKNOWLEDGEMENTS

The authors wish to acknowledge the financial support from the Ghana Government through the MOFA/WAAPP Project on No. NCRG 007, the BSU II project of the Kwame Nkrumah University of Science and Technology (KNUST), Kumasi, the technical staff of the Department of Agricultural Engineering (KNUST), GAMBOPAT Engineering Limited, the Agricultural Research Council of South Africa and numerous small holder cassava farmers in Ghana and South Africa for supporting the project in both countries.

REFERENCES

Adjei-Nsiah, S. 2012. *Evaluating l cropping sequences with cassava and three grain crops: Effects on soil fertility and maize yields in the semi-deciduous forest zone of the Ghana*. J. Sci.Environ. Manage. 3(2): 49-55.

Agbetoye, L.A.S. 2005. *Engineering Challenges in Developing Indigenous Machinery for Cassava Production and Processing*. *In:* Proceedings of the Annual Conference of the Nigerian Society of Engineers (Lagelu 2003), Ibadan, Nigeria, 8–12 December 2003; pp. 80-86.

Agbetoye, L.A.S., and I. Ilevbare. 2012. *Evaluation of L-tines for soil disturbance during mechanised cassava harvesting.* American Society of Agricultural and Biological Engineers publication. 121340884. (doi:10.13031/2013.41993).

Amponsah, S.K; E.Y.H. Bobobee, W.A. Agyare, J.B. Okyere, J. Aveyire, S.R. King and J. Sarkodie-Addo. 2014. *Mechanical Cassava harvesting as influenced by seedbed preparation and cassava variety*. Applied Engineering in Agriculture. 30(3):391-403. Doi 10.13031/aea.30.10495

Arshad, M.A., B. Lowery and B. Grossman. 1996. *Physical tests for monitoring soil quality. p.123-142. In: J.W. Doran and A.J. Jones (eds.) Methods for assessing soil quality.* Soil Sci. Soc. Am. Spec. Publ. 49. SSSA, Madison, WI.

Aye, T.M. 2012. *Cassava agronomy: Land preparation, time and method of planting and harvest, plant spacing and weed control. InR.H. Howler, ed.* The cassava handbook – A reference manual basd on the Asian regional cassava training course, held in Thailand. Cali, Colombia, CIAT. Pp 588-612.

Bayoumi, S.A.L., M.G. Rowan, I.S. Blagbrough, and J.R. Beeching. 2008. *Biosynthesis of Scopoletin and Scopolin in Cassava Roots during Post-Harvest Physiological Deterioration: The E-Z-Isomerisation Stage.* Journal of Phytochemistry, 69 : 2928–2936

Bobobee, E.Y.H., J.B. Okyere, W.A. Agyare, S.K. Amponsah, S.R. King, J. Aveyire and J. Sarkodie-Addo. 2013. *Performance evaluation of prototype mechanical cassava harvester in three agro-ecological zones in Ghana*. Ghana Journal of Agricultural Sciences, **48**: xx-xx**.**

Bobobee, E.Y.H., J.B Okyere, A. Twum, R.H. Neumann, and H. Knechtges. 1994. *Performance Evaluation of a Mechanical Cassava Harvester*. Proceedings of the International Commission of Agricultural Engineering (CIGR) XII World Congress, Ag. Eng' 94, Milano 94. Report No. 94-D-066.

Brady, N.C., R. Ray and R.R. Weil. 1996. *The Nature and Properties of Soils.* 11th edition Prentice Hall, Inc., Upper Saddle River, NJ 07458. 740 pp

Chengyu, Y., L. Dong and L. Yulan. 2010. *Discussion China's cassava planting and harvesting mechanization technology.* Journal

of Modern Agricultural Equipment. Supp. 1: 79-81.

Crouter, S.E., C. Albright, and D.R. Bassett. 2004. *Accuracy of Polar S410 Heart Rate Monitor to Estimate Energy Cost of Exercise*. Med. Sci. Sports Exercise. Vol. 36, No. 8, pp. 1433–1439

DeAngelis, K.M. 2007. *Measurement of Soil Moisture Content by Gravimetric Method.* Available online: http://www.cnr.berkeley.edu/soilmicro/methods/Soil moisturcontent.pdf. Date accessed: 28th October, 2013.

Ekanayake, I.J., D.S.O. Osiru, and M.C.M. Porto (1997). *Agronomy of Cassava. IITA Research Guide 60. Available online: http://betuco.be/manioc/Agronomy of cassava IITA nr 60.pdf. Date Accessed: 22-06-2014*

Ennin, S.A., E. Otoo and F.M. Tetteh 2009. *Ridging, a Mechanized Alternative to Mounding for Yam and Cassava Production.* West African Journal of Applied Ecology, vol. 15, pp 1-8

Ericsson, F., U. Dalarna and G. Björklund. 2006. *The Relationship between Heart rate and Power output during cycling competitions.* Available online: http://www.toppfysik.nu/userfiles/file/ pdf. Date accessed: 12-07-2014

FAO. 2012. *Food outlook. Global market analysis* November 2012.Rome. Accessed: 12-07-2014.

FAO. 2013. *Cassava, a 21st century crop.* FAOSTAT ststistical data base (http://faostat.fao.org). Acessed: 20/07/2013.

FAO. 2013. *Save and Grow. Cassava A guide to sustainable production intensification.* Rome Accessed: 14-07-2014

FAO. 2016. *Food Outlook. Biannual Report on Global Food Markets* (http://f http://www.fao.org/3/a-i6198e.pdf . Accessed: 10-07-2017.

Freedson, P.S. and K. Miller. 2000. *Objective Monitoring of Physical Activity using Motion sensors and Heart rate*. Res Q Exerc Sport. Vol 71, S21-S29.

Gill, W.R and G.E.B. Vandem. 1968. *Soil dynamics in tillage and traction. Agriculture*. Handbook No. 316. Agricultural Research Service. USDA

Gupta, P.D., C.P. Gupta and K.P. Pandey. 1989. An analytical models for predicting performance of narrow tillage tool. Trans. ASAE 28(4):1062-1067.

Hunt, D. 1977. *Farm Power and Machinery Management. Laboratory Manual and Workbook.* 7th ed. Iowa State University Press, Ames, Iowa.

FAD/FAO. 2004. The world cassava economy. Facts, trends and outlook. Rome

Kolawole, P.O., L.A.S. Agbetoye and S.A. Ogunlowo. 2010. *Sustaining World Food Security with improved Cassava processing Technology: The Nigerian experience.* http://www.mdpi.com/2071/1050/2/12/3681/pdf. . Accessed: 10 May, 2014.

Kuiper, L., B. Ekmekci, C. Hamelinck, W. Hettinga, S. Meyer and K. Koop. 2007. *Bio-ethanol from Cassava*. Ecofys Netherlands BV, pp 1 – 38. Netherlands. Available online: http://www.probos.net/biomassa-upstream/pdf/FinalmeetingEcofys.pdf. Date Accessed: 24-06-2011.

Nweke, F.I., S.C.S. Dunstan and J.K. Lynam. 2002. *The Cassava Transformation: Africa's Best Kept Secret.* Lansing, Mich., USA: Michigan State University Press.

Nweke, F.I. 2004. *New Challenges in the Cassava Transformation in Nigeria and Ghana. Environment and Production Technology Division (EPTD).* Discussion Paper No. 118. Publication of the International Food Policy Research Institute (IFPRI), Washington, D.C. U.S.A.

Odigboh, E.U and C.A. Moreira. 2002. *Development of a Complete Cassava Harvester 1 – Conceptualisation.* Journal of Agricultural Mechanisation in Asia, Africa and Latin America 4 (33): 1-7.

Ogola, J.B.O and C. Mathews. 2013. *Adaptation of cassava (Manihot esculenta) to the dry*

environments of Limpopo, South Africa: growth, yield and yield components. African Journal of Agricultural Research. 6(28): 6082-608.

O'Hair, S.K. 1995. *New Crop Factsheet: Cassava.* Tropical Research and Education Center, University of Florida. Available online: http://www.hort.purdue.edu/newcrop/cropfacts heets/cassava.html. Date accessed: 24-06-2014.

Okigbo, B.N. 1980. *Nutritional Implications of Projects giving High Priority to the Production of Staples of Low Nutritive Quality: The Case for Cassava (Manihot esculenta, Crantz) in the Humid Tropics of West Africa.* International Institute of Tropical Agriculture (IITA), Ibadan, Nigeria. In: Food and Nutrition Bulletin (UNU).2(4) p. 1-10.

Oni, K.C. 2005. *Cassava Processing as a Tool for Employment Generation and Rural Development.* Workshop on Cassava Research and Development, Raw Materials Research and Development Council (RMRDC), Abuja, Nigeria.

Ospino, B., L.F. Cadavid, M. Garcia and C. Alcalde. 2007. *Mechanisation of Cassava Production in Columbia*. Latin American and Caribbean Consortium to Support Cassava Research and Development (CLAYUCA), CIAT, Apartado Aereo 67-13, Cali, Columbia.

Owen, T. 1989. Subsoiling forces and tool speed in compact soils. Can Agric. Eng. 31(1):23-50.

Peipp, L and E. Maehnert. 1992. *Development of a technical solution to cassava harvesting problem.* Agricultural Mechanisation in Asia, Africa and Latin America. 23(1): 33-36

Philippine Root Crops Information Service. 2005. *Cassava, VISCA, baybay, Leyte*. Available online: http://www.da.gov.ph/tips/Cassava.pdf. Date Accessed: 23-06-2014.

Reichert, J.M., V.R. da Silva and D.J. Reinert. 2004. *Soil Moisture, Penetration Resistance, and least Limiting Water Range for three Soil Management Systems and black Beans Yield. In*: 13th International Soil Conservation Organisation Conference – Brisbane, July 2004. Paper No. 721, pp. 1-4. Available online: http://www.tucson.ars.ag.gov/isco/isco13/PAP ERS R.../REICHERT.pdf. Date accessed: 15-07-2014.

Sam, J and H. Dapaah. 2009. *Baseline Survey Report, West African Agricultural Productivity Programme (WAAPP)*, Ghana. pp. 13-18. Available online: *http://waapp.coraf.org/documents/WAAPP/Rapports/Final WAAPP Baseline Survey Report Ghana.pdf.* Date accessed: 23-06-2014.

UNCTAD. 2013. *INFOCOMM commodity profile: Cassava* (http://www.unctad.info/en/infocomm/aacp-products/commoditry-profile---cassava/). Accessed: 01-04/2014

USDA. 1999. United States Department of Agriculture. Soil Quality Test Kit Guide. Section II, pp. 57-58. Available online: *http://ocw.tufts.edu/data/32/383298.pdf*. Date accessed: 29-06-2014.

USDA and NRCS. 2003. Plant Guide – Cassava: *Manihot esculenta* Crantz. *National Plant Data Centre, Baton Rouge, Louisiana and Pacific Islands*, Mongmong, Guam. Available online: *http://plants.usda.gov/plantguide/pdf/cs_maes.pdf*. Date accessed: 24-06-2014.

Wang, Y., Y. Jian and Z. Xiaoting. 2011. *Experiment on mechanical properties of cassava.* Transactions of Chinese Society of Agricultural Engineering. 27(2): 50-54.

Xue, Z., H., Hui and L. Ming. 2010. *Study on 4UMS-390 II Cassava Harvester.* Journal of Agricultural Mechanisation Research. 8:79-82.

Yulan, L., S. Youpan, L. Shihao, C. Danping and W. Gaoping. 2012. *Development and prototype tial of digging-pulling style cassava harvester.* Transactions of the Chinese Society of Agricultural Engineering. 28 (Supp.2):29-35.

Zhiguo, J., H. Hui and L. Ming. 2006. *According to the research and development in our country the necessity of harvest cassava machinery.* Journal of China Tropical Agriculture.6:34-35.

PRODUCTION OF BIO-COMPOSITE POLYMERS WITH RICE AND COFFEE HUSKS AS REINFORCING FILLERS USING A LOW-COST COMPRESSION MOLDING MACHINE

Musinguzi[1], T.L.; Yiga[2], V.A.; Lubwama[3], M

[1, 2, 3] Makerere University, Kampala, Uganda

ABSTRACT

A compression molding machine was developed to produce bio-composite polymers using rice and coffee husks as reinforcing filler (5% weight) with high density polyethylene (95% weight) as the base polymer. Rice and coffee husks are typically disposed by open burning in fields. Their use as reinforcing fillers therefore reduces on the negative impacts of their disposal. The developed compression molding machine was constructed using mainly mild steel and stainless steel. It consisted of heating chamber, mold base, compression shaft and observation window. A temperature controller was incorporated to regulate the temperature in the heating chamber. Elongation, tensile strength and water absorption tests were carried out on the developed bio-composite polymers. Results indicated that inclusion of rice husks (5%) reduced the tensile strength and percentage elongation of the developed bio-composite polymer. Similar results were observed with coffee husk. Highest water absorption rates of 8% were observed for bio-composite polymers developed with Arabica coffee husks.

INTRODUCTION

Polymer production worldwide continues to grow but not that for synthetic fibers (Borghesi et al., 2016). Commodity polymers constitute 80% of the polymer market. Most of them are based on non-renewable petroleum, whose price is unstable, are non-biodegradable and not sustainable (Satyanarayana *et al.,* 2009). Research continues to focus on the need for polymers that have specific characteristics for specific purposes, but at the same time are non-toxic and environmentally friendly (Yang *et al.,* 2007). In order to produce fully renewable and biodegradable composites, both the polymeric matrix and the reinforcement must be derived from renewable resources, normally produced by plants in a period of less than one year (Narayan, 2006).

Various synthetic polymers are being prepared combined with various reinforcing fillers in order to improve the mechanical properties and obtain the characteristics demanded in actual application (Favaro *et al.,* 2010; Pritchard, 1998; Rozman *et al.,* 1998; Satyanarayana *et al.,* 2009; Sharma *et al.,* 2001). Studies are ongoing to find ways of using lignocellulosic fibers in place of synthetic fibers as reinforcing fillers (Angelini *et al.,* 2000; Beg & Pickering, 2008; Bullions *et al.,* 2006; Favaro *et al.,* 2010; Fuad *et al.,* 1994; George *et al.,* 1998; Hardinnawirda & SitiRabiatull, 2012; Josepn *et al.,* 1886; Pothan *et al.,* 1997; Premalal

et al., 2002; Raju *et al.*, 2012; Sgriccia & Hawley, 2007; Sgriccia *et al.*, 2008; Tsou *et al.*, 2014; Tsou *et al.*, 2015; Zhao *et al.*, 2009). These natural fillers are especially being sought because the production of composites using natural substances as reinforcing fillers will reduce and environmental pollution will be minimized (Premalal *et al.*, 2002; Yang *et al.*, 2007). Advantages of lignocellulosic materials include: (1) lightweight; (2) wear reduction of machinery used; (3) low cost; (4) biodegradability; (5) renewability and abundance; (6) low density; (7) non-abrasiveness; (8) recyclability; (9) absence of residues or toxic by-products; and, (10) high specific strength (Bledzki & Gassan, 1999; Campos *et al.*, 2015; Favaro *et al.*, 2010; Gacitua et al, 2005; Garcia *et al.*, 2007; Ismail and Nasir, 2001; Kim *et al.*, 2004; Maya & Sabu, 2008; Mohanty et al., 2000; Mohanty *et al.*, 2002; Oksman & Clemons, 1997; Panthapulakkal *et al.*, 2005; Premalal *et al.*, 2002; Raju *et al.*, 2012; Re *et al.*, 2013; Satyanarayana *et al.*, 2009; Yang *et al.*, 2005).

Two common and readily available agricultural wastes in Uganda are rice husks and coffee husks (GoU, 2007). Expected production trends for rice and coffee production are shown in Figure 1 (MAAIF, 2009; MAAIF & UCDA, 2015). The disposal method of choice for rice and coffee husks is open-burning in fields which have negative environmental consequences (Bevilaqua *et al.*, 2013). The use of Rice husks and coffee husks as a raw material for the production of bio-composite polymers can be both an environmentally and economically viable means of tackling this problem. Fiber glass is commonly used in the production of composite polymers and the use of fiber glass contributes to the high costs of production and reduces its biodegradability in the environment. Replacement of fiber glass with lignocellulosic fibers as reinforcing filler will reduce the overall production cost incurred during the manufacture of bio composite polymers (Espindola *et al.*, 2014; Zhao *et al.*, 2009)

Therefore, in this study, bio-composite polymers were produced with rice husks and coffee husks as reinforcing filler using a locally developed compression molding machine. Bio-composite polymers were developed from a combination of high density polyethylene (HDPE) as the base matrix polymer and rice husks, Arabica coffee husks and robusta coffee husks as the lignocellulosic reinforcing filler.

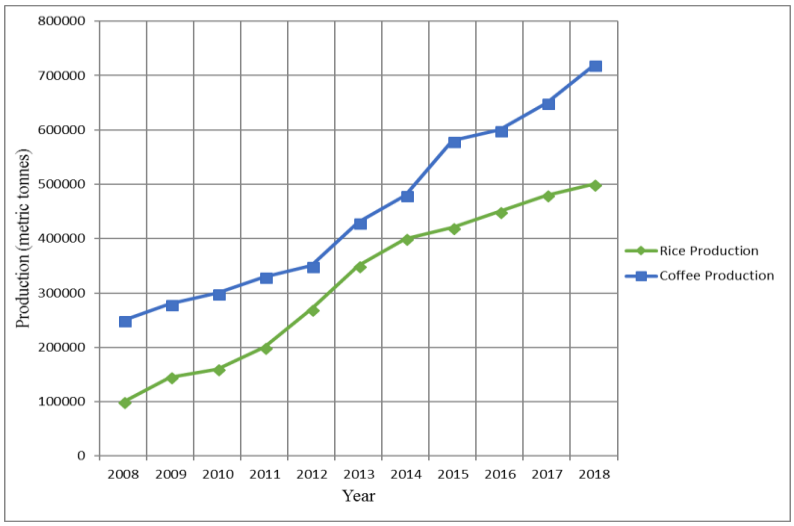

Figure 1: Projected production trends of rice and coffee in Uganda (MAAIF, 2009; MAAIF & UCDA, 2015

EXPERIMENTAL

1.1 Materials

HDPE (Marlex K606) was used as base polymer. HDPE in the form of homopolymer pellets was supplied by Ultrachemis Uganda Limited. The physical, mechanical and processing properties of the supplied HDPE are shown in Table 1. Rice husks (wita 9) were purchased from Kibimba Uganda Limited, in Bugiri District. The Arabica and Robusta coffee husks were purchased from Ugacoff Limited, in Bweyogerere. The structural morphology of the rice and coffee husks that were used in this study are shown in Figure 3.

Table 1 Physical, mechanical and processing properties of HDPE

	Property	Metric
Physical	Density	0.964 g/cm^3
	Environmental stress crack resistance	15 hr
	Melt flow	0.65 g/10 min
Mechanical	Tensile strength, yield	30.0 MPa
	Elongation at break	≥ 300%
	Flexural modulus	1.654 GPa
Processing	Processing temperature	140 – 170 °C

Figure 1: Coffee husks (A) and Rice husks (B)

1.2 Compression molding machine

A schematic of the compression molding machine that was used in the production of the bio-composite polymers is shown in Figure 3. It shows the different components of the compression molding machine including the heating chamber from which heating and compression of the bio-composite materials occurs, the support frame and the mold base in which the material is placed for compression. Mild steel with a thermal resistance of $1.333x10^{-5}$ m^2K/W was used in the construction of the frame of the compression molding machine. It was purchased from Roofings Limited, Uganda. The temperature controller, thermo-couple and

heating element were purchased from Guarantee Electricals limited, Kampala.

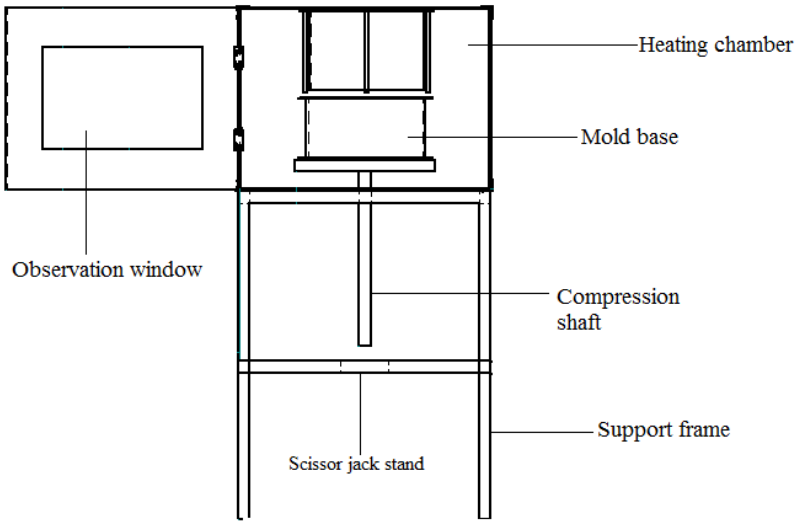

Figure 3: Schematic of the compression molding machine

In modeling of the heating systems, the following assumptions were made: (1) temperature of the ambient surroundings is constant; (2) ambient temperature is the reference temperature; and, (3) there is no heat loss to the environment. The elements that were used in the design of the heating system were, temperature controller, thermo-couple, heating coil with a 2700W power rating and a metal blade fan (see Figure 4).

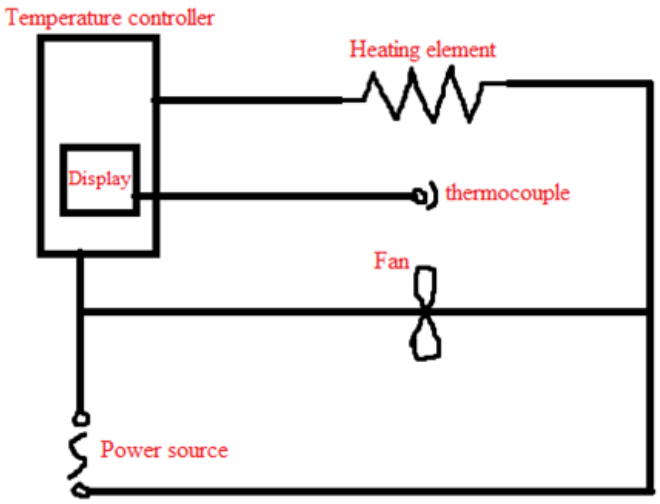

Figure 4: Schematic representation of the heating system

From the energy balance equation:

Heat in = Heat out + Heat stored

$$q_i = \frac{\theta_h - \theta_a}{R_{ha}} + C_h \frac{d\theta_h}{dt} \quad \text{...(1)}$$

Where: q_i – Heat into the chamber; C_h – Thermal capacitance of the air; Θ_h – Temperature of the cabin; Θ_a – Thermal resistance

However, using the stated assumptions, ambient temperature is zero therefore

$$q_i = \frac{\theta_h}{R_{ha}} + C_h \frac{d\theta_h}{dt} \quad \text{... (2)}$$

In order to determine the unknowns, thermal capacitance of the heating cabin is considered and it is given by the equation (3)

$$C_h = V \times \rho \times C_P \quad \text{... (3)}$$

Using the constants of specific heat of air, 1.013KJ/KgK, the density of air, 0815 Kg/m^3 and the volume of the cabin, 0.1275 m^3, the thermal capacitance is then determined. The thermal resistance of the mild steel used in the compression molding machine is calculated from:

$$R_{ha} = \frac{L}{K}$$

Where; L is the thickness of the material 1.2×10^{-5}, K is the conductivity of the material and conductivity of mild steel, K = 90W/mK

Using equation (ii), the heat equation of the compression molding machine is

$$q_i = \frac{\theta_h}{R_{ha}} + C_h \frac{d\theta_h}{dt}$$

$$\int dt \frac{(q - \frac{\theta_h}{R_{ha}})}{C_h} = \int d\theta_h \; q_i = \frac{\theta_h}{R_{ha}} + C_h \times \frac{\theta_h}{t}$$

$$q_i = \frac{\theta_h}{1.333 \times 10^{-5}} + 0.1053 \frac{\theta_h}{t} \quad \text{... (4)}$$

Equation (4) is the heat equation considered during the design and construction of the compression molding machine.

1.3 Bio-composite production

The rice and coffee husks were grinded into flour and sieved using a 1mm mesh in order to maintain a 1mm particle size. The rice and coffee husks were oven dried at a temperature of 110ºC for 4 hours to reduce the moisture content in the flour. HDPE pellets were used to produce bio-composite polymers in ratios of 95% and 100% with the remaining being filler material. Pellets were poured into the mold base of the compression molding machine and a temperature of 170ºC was set on the temperature controller and the polymer was heated for 20 minutes in order to reach its melting temperature (140ºC). The heating rate of the cabin taken at 5 minute intervals is shown in Figure 5.

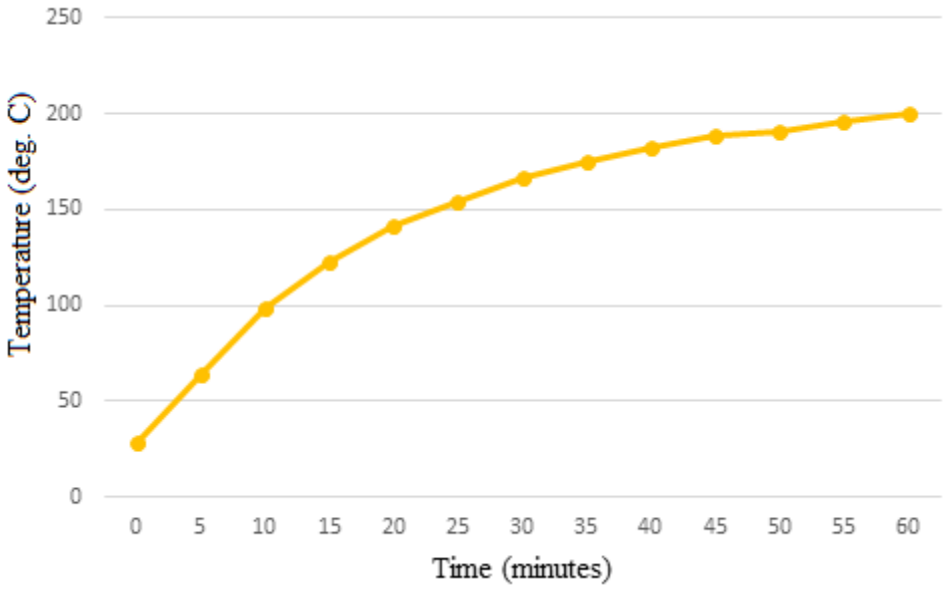

Figure 5: Heating rate of the cabin

Dried husks were then added to the molten HDPE and mixed using a fabricated metal mixer and the mold base was raised by cranking the scissor jack. The bio-composite was then compressed at 170^{o}C for 10 minutes. Cooling to room temperature was done through forced convection by the action of a metallic fan. The mixture of reinforcement/resin only becomes a composite material after the last phase of the fabrication, that is, when the matrix is hardened (Gay *et al.*, 2003).

1.4 Physical and mechanical properties

Moisture content of the rice and coffee husks were determined using thermogravimetric analysis (Lubwama & Yiga, 2017). The water absorption properties were obtained through the ASTM D570 procedure. Mass of the samples to be tested was measured prior to starting the test. The conditioned specimens were placed in a container of distilled water maintained at a temperature of about 23 °C and left for 24 hours. After 24 hours, the specimens were removed from the water one at a time, all surface water wiped off with a dry cloth, and weighed to the nearest 0.001 g immediately. The water absorption was obtained as the difference between the weights. Tensile strength measurements were obtained using ASTM D638 procedure. Elongation was determined by measuring the difference in initial and final lengths (Hattotuwa *et al.*, 2002).

RESULTS AND DISCUSSION

The developed compression molding machine is shown in Figure 6. Samples of developed bio-composite polymers are shown in Figure 7. From Figure 7 it can be observed that the distribution of the reinforcing filler material was non-uniform. This was expected because the mixing method used in this study did not enhance mobility of both the molten base polymer and reinforcing filler. Scratches were observed on all of the developed bio-composite samples because the mold plate was not smooth. Scratches also developed when removing the developed bio-composite from the mold plate after cooling.

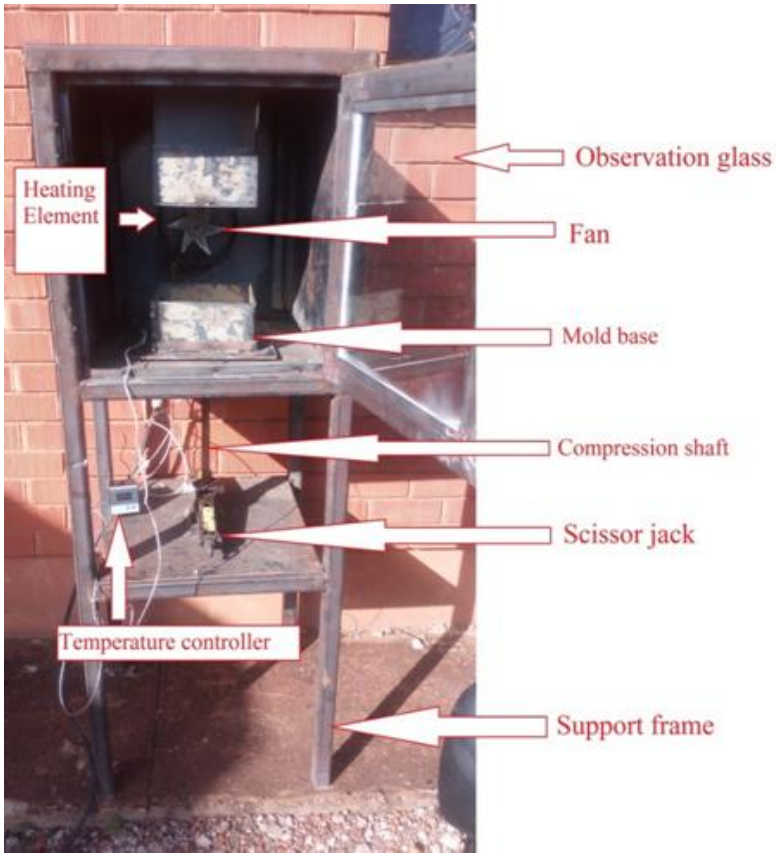

Figure 6: Developed low cost compression molding machine

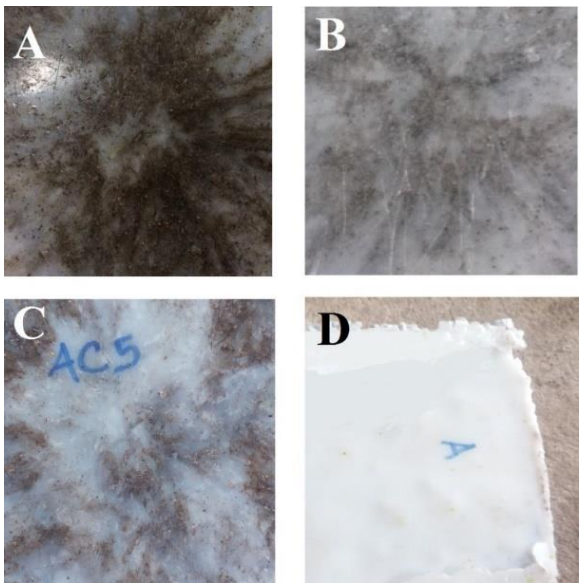

Figure 7: Developed bio-composite polymers. A (5% Robusta coffee husks); B (5% Arabica coffee husks); C (5% wita-9 rice husks); and D (100% HDPE)

The results for moisture content and water absorption rate are shown in Figure 8 and Figure 9 respectively. The bio composite polymers produced using 5% Robusta coffee husks as filler material had the highest water absorption percentage. Lignocellulosic fillers have been reported to absorb moisture even when in a plastic medium (Yang *et al.*, 2006). The low water absorption of the pure HDPE sample can be attributed to the hydrophobic nature of the polymer (HDPE). The bio composite polymers formed with 5% wita 9 rice husks had low water absorption due to the hydrophobic nature of the silica contained within the rice husks. When compared with wood-based composites however, the amount of water absorbed is so low and negligible (Yang *et al.*, 2006). Robusta coffee husks had higher moisture content than both rice husks and Arabica coffee husks (see Figure 8).

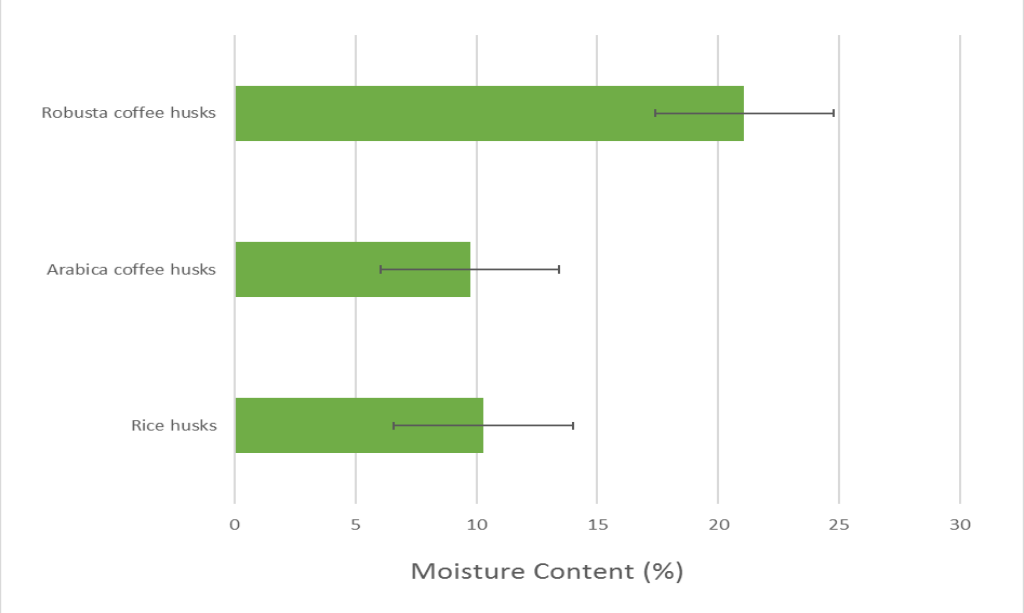

Figure 8: Percentage moisture content of the rice and coffee husks

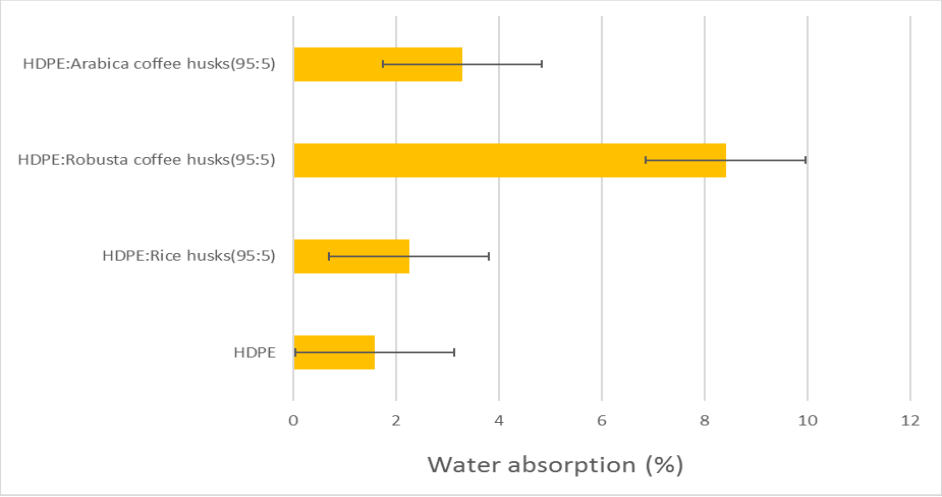

Figure 9: Water absorption percentage of the bio-composite polymers

The results for elongation at break and tensile strength are shown in Figure 10. Generally, the elongation at break and tensile strengths are lower for all of the developed bio-composite polymers. The least tensile strength of approximately 33 MPa was obtained for bio composite polymers with Robusta husks as reinforcing filler. The lower tensile strength in the developed bio-composite polymers is attributed to the irregularly shaped irregularly shaped fibers that decrease the ability of the filler to support stress transferred from the polymer matrix and the poor interfacial bonding between the filler and the matrix polymer (Yang *et al.*, 2006). The least elongation at break was in the composite formed with rice husk filler. The reduction of the elongation at break can be attributed to the induction of brittleness caused by the reinforcing filler as well as creation of voids in the composite that obstruct stress propagation in the bio composites. The low elongation at break for the composite formed with rice husks as reinforcing filler can be attributed to the brittle nature of the silica contained within the rice husks (Hattotuwa *et al.*, 2002).

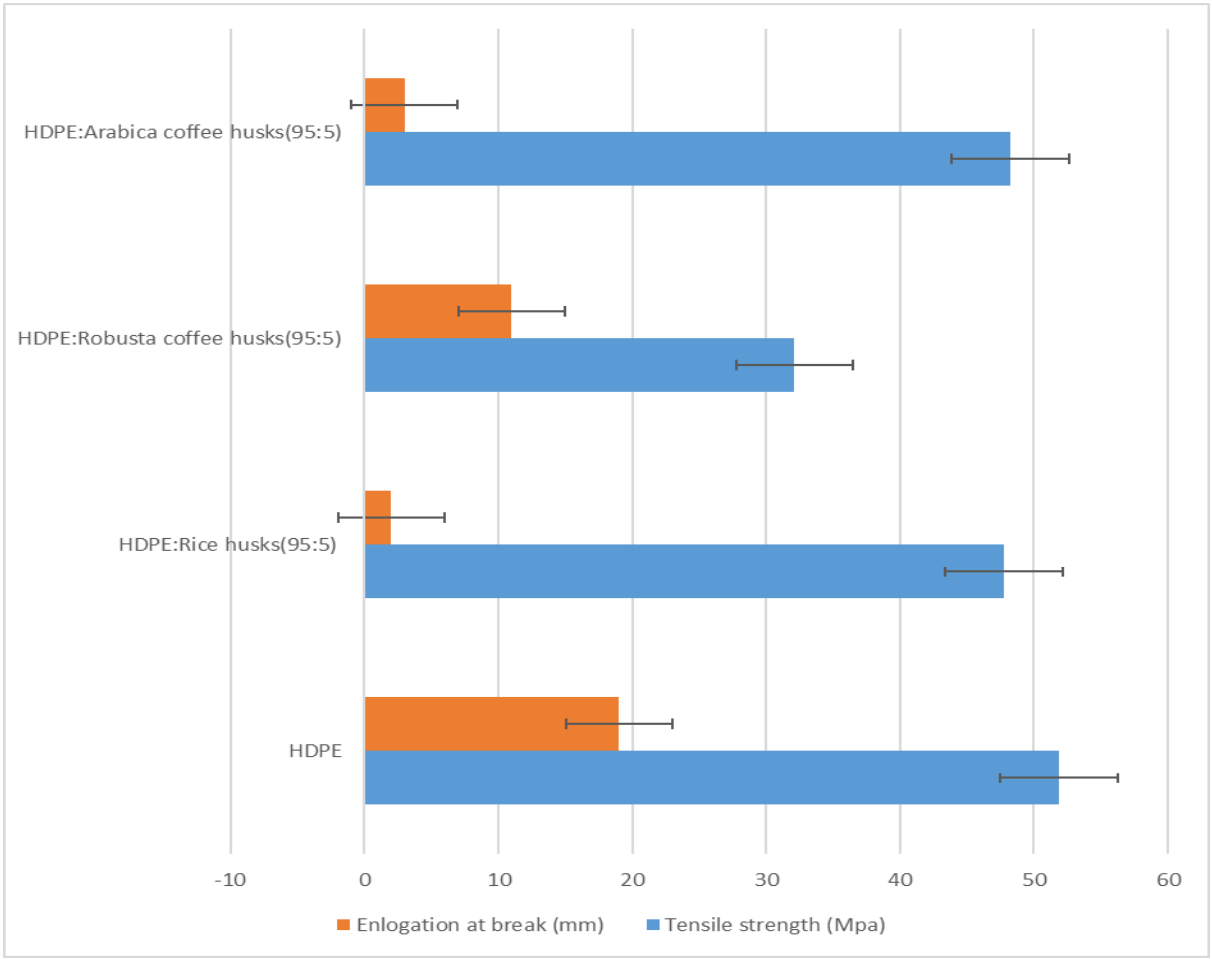

Figure 10: Mechanical properties of the developed bio-composite polymer samples

CONCLUSION

A compression molding machine was developed to produce bio-composite polymers using rice and coffee husks as reinforcing filler (5% weight) with high density polyethylene (95% weight) as the base polymer. The developed compression molding machine was constructed using mainly mild steel and stainless steel. Highest water absorption rates of 8% were observed for bio-composite polymers developed with Arabica coffee husks. Results indicated that inclusion of rice husks (5%) reduced the tensile strength and percentage elongation of the developed bio-composite polymer. Similar results were observed with coffee husk. Tensile strengths of the bio-composites decreased with inclusion of filler; however the composites retained an acceptable level of strength. When filler material was used, the poor interfacial bonding between the filler and the matrix polymer caused the tensile strength of the bio-composites to reduce. This poor interfacial bonding resulted in an increase in the number of micro voids, causing increased water absorption. The results indicate that the compression molding machine has to be modified in the following ways: (1) Incorporation of a more elaborate mixing stirrer or screw mechanism for mixing; (2) Enhancement of heating in the cabin to ensure that it is uniform; (3) modification of the mold plate to ensure that it is very smooth in order to avoid micro-cracks that become points of crack initiation and propagation.

REFERENCES

American Society for Testing and Materials. 1998. *ASTM. ASTM D570-98: standard test method for water absorption of plastics.*

American Society for Testing and Materials. 2003. ASTM. ASTM D638-03: standard test method for tensile properties of plastics.

Angelini, L.G., A. Lazzeri, G. Levita, D. Fontanelli, C. Bozzi. 2000. *Ramie (Boehmeria nivea (L.) Gaud.) and Spanish Broom (Spartium junceum L.) fibres for composite materials : agronomical aspects, morphology and mechanical properties*. Ind Crop Prod, 11:145-161.

Beg, M.D.H and K.L. Pickering. 2008. *Reprocessing of wood fibre reinforced polypropylene composites. Part II: hydrothermal ageing and its effects.* Compos: Part A - Applied Science Manufacturing; 39:1565-1571.

Bevilaqua, D.B., M.K.D. Rambo, T.M. Rizzetti, A.L. Cardoso and A.F. Martins. 2013. *Cleaner production: levulinic acid from rice husks.* Journal of Cleaner Production. 47; 96-101.

Bledzki, A.K. and J. Gassan. 1999. *Composites reinforced with cellulose based fibers.* Prog Polymer Science. 24:221-274.

Borghesi, D.C., M.F. Molina, M.A. Guerra and M.G.N Campos. 2016. *Biodegradation Study of a Novel Poly-Caprolactone-Coffee Husk Composite Film*. Materials Research, (AHEAD).

Bullions, T.A., D. Hoffman, R.A. Gillespie, J. Price-O'Brien and A.C. Loos. 2006. *Contributions of feather fibers and various cellulose fibers to the mechanical properties of polypropylene matrix composites.* Compos Sci Technol, 66:102-114.

Campos, A., G.H.D. Tonoli, J.M. Marconcini, L.H.C. Mattoso, A. Klamczynski, K.S. Gregorski. 2013. *TPS/PCL composite reinforced with treated sisal fibers: property, biodegradation and water-absorption.* Journal of Polymers and of Environment, 21(1):1-7.

Daniel G., V.H. Suong and W.T. Stephen. 2003. *Composite materials design and applications*. CRC Press Boca Raton.

Espindola, G.A., R.R. Fuentes, H.A..L Martinez, V.M. Castano and S.C. Velasco.2014. *Structural characterization of silica particles extracted from grass stenotaphrum secundatum: Biotransformation via Annelids.* Advances in Materials Science and Engineering.

Favaro, S.L., M.S. Lopes, A.G.V. Alberto Neto, R, Rogério de Santana and E. Radovanovic.2010. *Chemical, morphological, and mechanical analysis of rice husk/post-consumer polyethylene composites.* Composites: Part A 41.; 154-160.

Fuad, M.Y.A., R. Shukor, Z.A.M. Ishak and A.K.M. Omar. 1994. *Plastic Rub*. Comp. Process.; 21: 225.

Gacitua W.E, A. Ballerini and J. Zhang. 2005. *Polymer Nanocomposites: Synthetic and Natural Fillers A Review*. Maderas. Ciencia Y Tecnología. 7(3): 159-178.

Garcia D., J. Lopez, R, Balart, R.A. Ruseckaite and P.M. Stefani. 1998. *Composites based on sintering rice husk-waste tire rubber mixtures*. Mater Des 2007; 28: 2234-2238.George J, Sreekala MS, Thomas S, Journal of Reinforcing Plastic Comp. 17: 651.

Government of Uganda (GoU), 2007. *Renewable Energy Policy*, Kampala, Uganda.

Hardinnawird K and I.A. Sitirabiatull. 2012. *Effect of Rice Husks as Filler in Polymer Matrix Composites.* Journal of Mechanical Engineering and Sciences (JMES) 2: 181-6.

Hattotuwa, G.B., H.I. Premalal and A. Baharin. 2002. *Comparison of the mechanical properties of rice husk powder filled polypropylene composites with talc filled polypropylene composites*. Polymer Testing. 21 (7) 833-839.

Ismail, H and S.M. Nasir. 2001. Polymer Testing. 20: 819.

Josepn, K., S. Thomas and C. Pavithran. 1996. Polymer. 37: 5139

Kim, H.S, H.S. Yang, H.J. Kim and H.J. Park. 2004. *Thermogravimetric analysis of rice husk flour filled thermoplastic polymer composites.* Journal of Thermal Analysis and Calorimetry. 76(2):395-404.

Lubwama, M and V.A Yiga. 2017. *Development of groundnut shells and bagasse briquettes as sustainable fuel sources for domestic cooking applications in Uganda.* Renewable Energy. 111:532-542.

Ministry of Agriculture Animal Industry and Fisheries (MAAIF) 2009. Uganda National Rice Development Strategy 2009-2018, Kampala, Uganda.

Ministry of Agriculture Animal Industry and Fisheries (MAAIF) & Uganda Coffee Development Authority 2015. UCDA Database. Kampala, Uganda

Maya, J.J and T. Sabu. 2008. *Biofibers and biocomposites.* Carbohydrate polymers. 71: 343-364.

Mohanty, A.K., M. Misra and G. Hinrichsen. 2000. *Biofibers, biodegradable polymers and biocomposites: an overview*. Macromol Matererials Engineering. 276:1-24.

Mohanty, A.K., M. Misra and L.T. Drzal. 2002. *Sustainable bio-composites from renewable resources: opportunities and challenges in the green materials world.* Polymer Environment. 10:19-26.

Narayan, R. 2006. *Biobased and biodegradable polymer materials: Principles, concepts and technology exemplars.* In: World polymer congress and 41st International Symposium on macromolecules, MACRO-2006. 2006 [in CD-ROM; paper no. 2103].

Oksman, K and C. Clemons. 1997. Journal of Applied Polymer Science. 67: 1503.

Panthapulakkal, S., S. Law and M. Sain. 2005. *Enhancement of processability of rice husk filled high-density polyethylene composite profiles.* Thermoplast Compos . 18: 445-458.

Pothan, L.A., S. Thomas and N.R. Neelakantan. 1997. Journal of Reinforcing Plastic Comp. 16: 744.

Premalal, H.G.B., H. Ismail and A. Baharin. 2002. *Comparison of the mechanical properties of rice husk powder filled polypropylene composites with talc filled polypropylene composites.* Polymer Testing. 21(7): 833-839.

Pritchard, G., in: Pritchard G. (Ed.). 1998. *Plastics Additives*, Chapman and Hall, London. 241.

Raju, G.U., S. Kumarappa and V.N. Gaitonde. 2012. *Mechanical and Physical Characterization of Agricultural Waste Reinforced Polymer Composites*. J. Mater. Environ. Sci. 3(5): 907-916.

Re, L.G., M. Morreale, R. Scaffaro and F.P. La Mantia.2013. *Biodegradation paths of Mater-Bi (R)/kenaf biodegradable composites.* Applied Polymer Science. 129(6): 3198-3208.

Rozman, H.D., B.K. Kon, A. Abusamah, R.N. Kumar and Z.A.M. Ishak.1998. Journal of Applied Polymer Science. 69.

Satyanarayana, K.G., G.C.C. Arizaga and F. Wypych 2009. *Biodegradable composites based on lignocellulosic fibers-An overview.* Progress in Polymer Science. 34: 982-1021.

Sgriccia, N and M.C. Hawley. 2007. *Thermal, morphological, and electrical characterization of microwave processed natural fiber composites.* Compos Science Technology. 67:1986-1991.

Sgriccia, N., M.C., Hawley and M. Misra. 2008. *Characterization of natural fiber surfaces and natural fiber composites.* Compos: Part A – Applied Science Manufacturing. 39: 1632-1637.

Sharma, N., L.P. Chang, Y.L. Chu, H. Ismail, U.S. Ishiaku and Z.A.M. Ishak. 2001. Polymer Degradation Stab. 71: 381.

Tsou, C.H., W.S. Hung, C.S. Wu, J.C. Chen, C.Y. Huang, S.H. Chiu, C.Y. Tsou, S.M. Lin, C.K. Chu and C.C. Hu. 2014. *New composition of maleic-anhydride-grafted poly (Lactic Acid)/rice husk with methylenediphenyl diisocyanate.* Material Science. 20: 446-451.

Tsou C.Y., C.L. Wu, C.H. Tsou, S.H. Chiu, M.C. Suen and W.S. Hung. 2015. *Biodegradable Composition of Poly (lactic acid) from Renewable Wood Flour*. Polymer Science. Series B. 57: 473-480.

Uganda Bureau of Statistics (UBOS) 2010. Uganda census of agriculture 2008/2009: crop area and production report, vol. IV. Kampala Uganda.

Uganda Bureau of Statistics (UBOS) 2009. Statistical Abstract. Kampala Uganda.

USDA, 2012. *United States Department of Agriculture Foreign Agricultural Service.* Coffee: World Markets and Trade.

Yang, H.S., H.J. Kim, H.J. Park, B.J. Lee and T.S. Hwang. 2007. *Effect of compatibilizing agents on rice-husk flour reinforced polypropylene composites*. Composite Structures. 77:45-55.

Yang, H.S.; M.P. Wolcott, H.S. Kim and H.J. Kim.2005. *Thermal Properties of Lignocellulosic Filler-Thermoplastic Polymer Bio- Composites.* Journal of Thermal Analysis and Calorimetry. 82: 157-160.

Yank, A.; M. Ngadi and R. Kok. 2016. *Physical properties of rice husk and bran briquettes under low pressure densification for rural applications.* Biomass and Bioenergy.84: 22-30.

Zhao, Q.; B. Zhang, H.; Quan, R.C.M.; Yam, R.K.K. Yuen and R.K.Y. Li. 2009. *Flame retardancy of rice husk-filled high-density polyethylene Eco composites.* Composites Science and Technology. 69: 2675-2681**.**

ESTIMATION OF SOIL EVAPORATION BY SOIL HYDRAULIC FACTOR FROM BARE DUNE SAND MULCH

Dhavu[1], K.; Yasuda[2], H.; Seopa[3], J.; Senzanje[4], A

[1]Agricultural Research Council, Silverton, South Africa
[2]Arid Land Research Center, Japan
[3,4]University of KwaZulu-Natal, South Africa

ABSTRACT

A method is presented that employs soil moisture measurements and lysimetric reference evapotranspiration data to estimate a soil hydraulic factor for estimating soil evaporation. Soil evaporation is a complicated process. The soil evaporation process has two main stages. In this study, soil hydraulic factor was used to estimate soil evaporation under dune sand mulch. The soil hydraulic factor was derived from small pan evaporation data and soil evaporation data from dune sand soil columns. Dune sand soil columns were saturated and gravitational water was drained. The dune sand soil columns were then covered by dry Tottori dune sand soil of 0 cm, 2 cm and 5 cm thickness. Soil evaporation from these columns was measured gravimetrically. Potential evaporation was determined from small evaporation pans placed alongside the dune sand soil columns. Water was applied to three weighing lysimeters (for measuring actual soil evaporation) in a glasshouse to the field capacity of the dune sand soil. The weighing lysimeters were also covered by the dune sand soil of 0 cm, 2 cm and 5 cm thickness and that was dried naturally. Cumulative soil evaporation from dune sand soil columns and cumulative potential evaporation from small evaporation pans was used to determine the soil hydraulic factor under the three dune sand mulch treatments. The soil hydraulic factor was then used to estimate soil evaporation under natural drying conditions in the glasshouse. Estimated cumulative soil evaporation was compared with measured cumulative soil evaporation. The soil hydraulic factor overestimated cumulative soil evaporation during the falling rate stage of soil evaporation under 0 cm and 2 cm sand mulch. Adjusting the estimation by subtracting the difference between the estimated and the measured cumulative soil evaporation at the point where the square root of cumulative potential evaporation was equal to the soil hydraulic factor from the estimates moved the values closer to the actual measured. The soil hydraulic factor overestimated cumulative soil evaporation during the whole drying period under 5 cm dune sand soil mulch. The adjustment of the estimates did not move the values as close to the actual measured as in the 2 cm mulch. Using the soil hydraulic factor gave better estimates of cumulative soil evaporation during the constant rate stage under 0 cm and 2 cm sand mulch than under 5 cm sand mulch.

Key word: dune sand, evaporation, lysimeter, mulch, soil hydraulic factor

INTRODUCTION

Soil evaporation rates follow a three-stage process (Idso *et al.,* 1974). During stage 1 of soil evaporation, the soil evaporation rate is only limited by the amount of energy available to vaporize soil water content in the upper layer of the soil. This stage is called the constant rate stage of evaporation. Stage 1 ends when the soil water content in the upper layer of the soil decreases and the soil matric potential reaches a critical value.

During stage 2 of soil evaporation, soil evaporation rates are limited by the lack of water in the upper soil layer and by soil hydraulic properties that determine the transfer of liquid and vaporized water to the soil surface. This stage is called the falling rate stage of evaporation. Stage 2 ends when there is minimal liquid water movement. Stage 3 is determined mainly by soil physical and adsorbing characteristics. At this stage, soil evaporation rate is negligible.

Ritchie (1972) reported that during the falling rate stage of evaporation, the evaporation rate decreases as a function of the square root of time after wetting. On the other hand, and Gallardo *et al.*, (1996) found a good relationship between cumulative bare soil evaporation and cumulative potential evaporation. In the model of Ritchie (1972), soil evaporation is described as a two-stage process where a soil hydraulic factor (β) determines the point where the soil evaporation rate changes from the constant rate stage to the falling rate stage.

The soil hydraulic factor is determined using the soil evaporation (SE) by plotting cumulative soil evaporation (CSE) versus the square root of the cumulative potential evaporation (CPE).

During stage 1, the CSE is calculated as

$$CSE = CPE \quad \ldots (6.1)$$

Where, *CSE* is the cumulative soil evaporation (mm), and *CPE* is the cumulative potential evaporation (mm).

Equation (6.1) is used when $\sqrt{CPE} < \beta$ (β is the soil hydraulic factor ($mm^{1/2}$)).

During stage 2, when $\sqrt{CPE} \geq \beta$, the *CSE* is calculated as

$$CSE = \beta\sqrt{CPE} \quad \ldots 6.2)$$

to estimate soil evaporation rates with time after wetting.

Ventura *et al.,* (2006) used soil hydraulic factor to estimate soil evaporation of silty clay loam soil of Holtvile, California using sensible heat flux method and soil water content measurement method. They found that the soil evaporation estimates were similar for both methods.

Soil evaporation is, however, a complicated process. It is controlled by many factors such as soil properties, soil surface coverage and climatic conditions (Burt *et al.,* 2005; Forbes, 1995). Use of soil hydraulic factor to estimate soil evaporation under sand soil mulch has not been considered.

The objective of our study is to estimate soil evaporation under sand soil mulch using soil hydraulic factor derived from pan evaporation data and soil evaporation from sand soil columns.

MATERIALS AND METHODS

Soil evaporation from pots and potential evaporation

Wagner pots of 30 cm height and 25 cm diameter, referred to as sand soil columns, were packed with the Tottori sand dune soil to a bulk density of 1.5 Mg/m^3. Sandy soil columns were saturated and gravitational water was drained. The sand soil columns were then covered by the dry (less than 0.001 g/g water content) sand soil. Two sand soil columns were under three different treatments: 0 cm, 2 cm and 5 cm sand soil cover thickness, referred to as 0-cm mulch, 2-cm mulch and 5-cm mulch, respectively.

In April 2008, these sand soil columns were kept in temperature-controlled room at the Arid Land Research Center, Tottori University. The temperature in the room was set at 35 ^{0}C and the average relative humidity was 25 %. Evaporation from these sand soil columns was measured gravimetrically at a 12-hour interval. Cumulative soil evaporation, referred to CSE, was the cumulative sum of the soil evaporation over the period of the experiment.

Potential evaporation in both experiments was estimated by evaporation from small evaporation pans of 20 cm diameter, which was placed alongside the sand soil columns. Evaporation from the small pans was converted to class A evaporation using the Agodzo *et al.,* (1997) equation:

$$E_A = a \times E_S^b \quad \ldots (6.3)$$

Where, E_A is the class A evaporation (mm), a and b are fitting parameters, and a = 0.17, b = 1.92 and E_S is the evaporation from small evaporation pans (mm).

Class A evaporation was then converted to potential evaporation using the Doorenbos and Pruit (1977) equation:

$$ET_O = Kp \times E_A \quad \ldots 6.4)$$

Where, ET_O is the potential evaporation (mm) and Kp is the pan coefficient (dimensionless). Kp = 0.75 and was obtained from Doorenbos and Pruit (1977).

Cumulative potential evaporation, referred to CPE, was the cumulative sum of the potential evaporation over the period of the experiment.

Soil evaporation from lysimeters

The experiment was carried out in a 154 m^2 area glasshouse. The length, width and maximum height of the glasshouse were 22 m, 7 m and 4.5 m, respectively. It was unheated and naturally ventilated with single continuous roof vent. Side windows were open during daytime. The soil type of the Tottori sand dune soil was Arenosol (silicious sand, typic Udipsamment) with 96 % sand (Qiu *et al.,* 1999). The water contents at the field capacity and permanent wilting point of the Tottori sand dune soil were 0.074 cm^3/cm^3 and 0.022 cm^3/cm^3, which corresponds to the matric potential of -0.006 MPa and -1.5 MPa, respectively (Qiu *et al.,* 1999).

Three weighing lysimeters were used to measure the soil evaporation under 0-cm mulch, 2-cm and 5-cm mulch. They were filled with the same sand soil as that in the glasshouse. The soil evaporation from the weighing lysimeters was determined from the weight difference at 1-hour interval.

RESULTS AND DISCUSSIONS

Comparison of measured and estimated cumulative soil evaporation under 0 cm, 2 cm and 5 cm sand mulch are shown in Figure 1, 2 and 3 Soil hydraulic factors were used to estimate cumulative soil evaporation under 0 cm, 2 cm and 5 cm sand mulch. Actual cumulative soil evaporation was measured using lysimeters.

Soil hydraulic factor overestimated cumulative soil evaporation during the falling rate stage of soil evaporation under 0 cm sand mulch. Subtracting the difference between the estimated and measured cumulative soil evaporation at the point where square root of cumulative potential soil evaporation is equal to β from the estimates during the falling rate stage improved the estimates.

Soil hydraulic factor also overestimated cumulative soil evaporation during the falling rate stage of soil evaporation under 2 cm sand mulch. Subtracting the difference between the estimated and measured cumulative soil evaporation at the point where square root of cumulative potential soil evaporation is equal to β from the estimates during the falling rate stage also improved the estimates.

Soil hydraulic factor overestimated cumulative soil evaporation during the whole drying period under 5 cm sand mulch. Subtracting the difference between the estimated and measured cumulative soil evaporation at the point where

square root of cumulative potential soil evaporation was equal to β from the estimates during the falling rate stage did not improve the estimates.

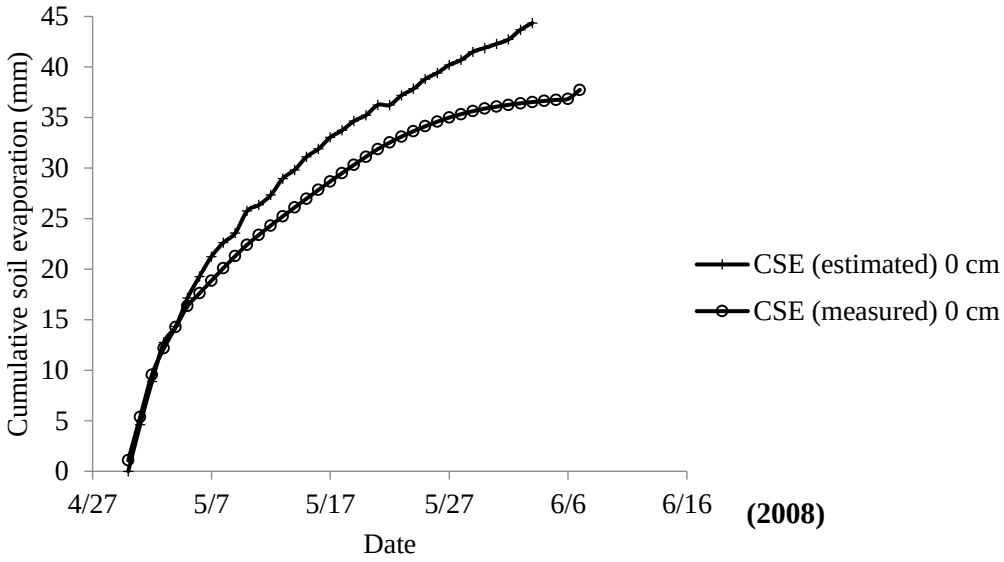

Figure 1: Measured and estimated cumulative soil evaporation for 0 cm sand mulch

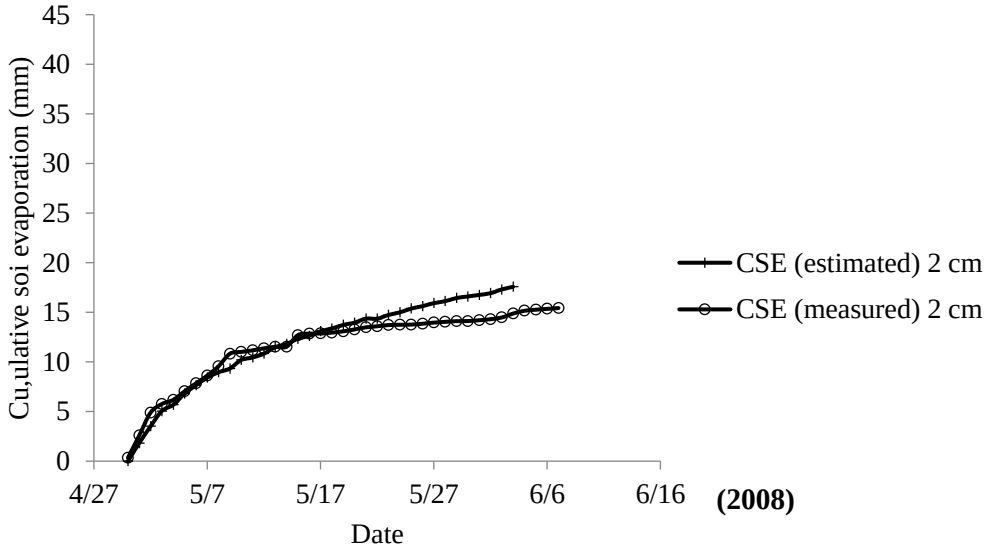

Figure 2: Measured and estimated cumulative soil evaporation for 2 cm sand mulch

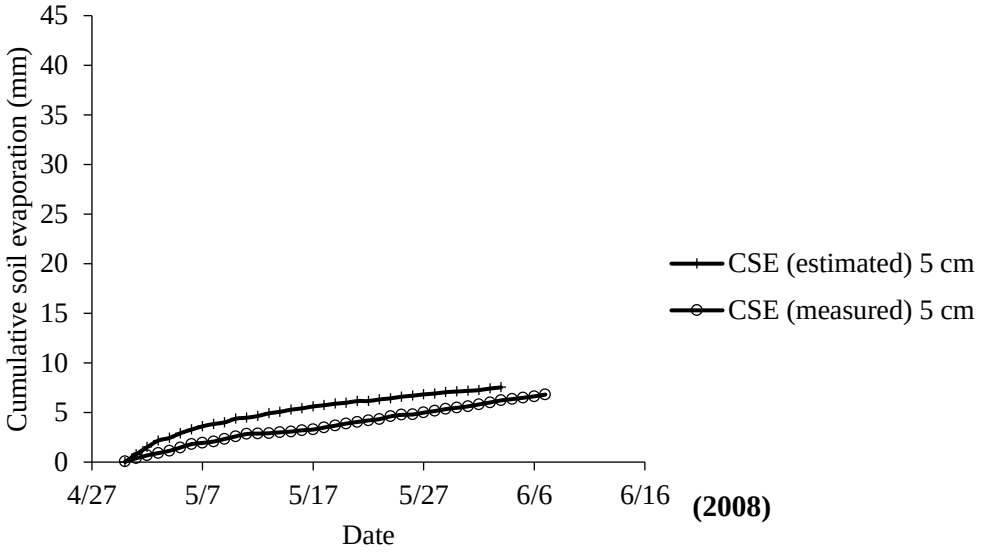

Figure 3: Measured and estimated cumulative soil evaporation for 2 cm sand mulch

These results demonstrate that soil hydraulic factor can be used to estimate soil evaporation. They also demonstrate that some adjustments can improve the estimates under 0 cm and 2 cm sand mulch, but not under 5 cm sand mulch. One explanation for these results could be that potential soil evaporation was determined using water from a free surface in the small evaporation whereas soil evaporation was restricted by the sand mulch under 2 cm and 5 cm sand mulch.

CONCLUSIONS

Using soil hydraulic factor gave better estimates of cumulative soil evaporations during the constant rate stage under 0 cm and 2 cm sand mulch than under 5 cm sand mulch. Small adjustments of the estimates improved the estimates of the cumulative soil evaporation under 0 cm and 2 cm sand mulch.

REFERENCES

Agodzo, S.K., T. Nishio and T. Yamamoto. 1997. *Trickle irrigation of okra based on small pan evaporation schedule under glasshouse condition.* Rural Env. Eng. Journal, 33, 19-36

Burt, C. M., A.J. Mutziger and R.G. Allen. 2005. *Evaporation research: review and interpretation*. J. Irrig. Drain. Eng., 131, 37-58.

Doorenbos, J and W.O. Pruit. 1977. *Crop water requirements, FAO Irrigation and Drainage Paper 24.* Food and Agriculture Organization of the United Nations, Rome, Italy, pp. 30-34.

Forbes, R.G. 1995. *Field evaporation theory: a review of basic ideas.* Applied Surface Science, 87-88, 1-11

Gallardo, M., R.L. Snyder, K., Schulbach and L.E. Jackson. 1996. *Crop growth and water use model for lettuce.* J. Irrig. Drain. Eng., 121(6), 354-359.

EFFECT OF TEMPERATURE ON DESORPTION ISOTHERMS FOR BEEF

Mewa[1], E.A.; Okoth[2], M.W.; Kunyanga[3], C.N.; Rugiri[4], M.N

[1, 2] University of Nairobi, Kenya
[3, 4] Egerton University, Kenya

ABSTRACT

Desorption isotherms of beef were determined by the standard static gravimetric technique, based on the use of saturated salt solutions with water activities from 0.05 to 0.9. Equilibrium moisture content of each sample at different temperatures and water activities were determined. The stable moisture content for meat during drying was also established. The GAB, BET and Oswin models were used to fit the experimental sorption data. Non-linear regression analysis was performed to estimate model parameters and fitting quality evaluated using the Coefficient of determination (R^2) and the standard error of estimate (SEE). The equilibrium moisture content decreased with increase in temperature at constant water activity and increased with increase in water activity at constant temperature. The critical moisture was 10-20 % (d.b). The high values of R^2 and low values of SEE for the GAB and Oswin models indicated that these models gave the best fit for the desorption data of beef.

Keywords: Beef, desorption isotherms, equilibrium moisture content, water activity.

INTRODUCTION

Moisture sorption isotherms represent the equilibrium relationship between the moisture content of foods and the water activity at constant temperature and pressure. Equilibrium moisture content (EMC) is defined as the moisture content when vapor pressure of water present in the food material has reached to the equilibrium with its surroundings. It is a thermodynamic entity and has practical significance in both drying and storage of foods. It is affected by both relative humidity and temperature of the surroundings. Water activity is defined as the ratio of vapor pressure of water in the foodstuff to the vapor pressure of pure water at the same temperature. Water activity controls microbiological growth and enzymatic activity of food products.

The knowledge and understanding of moisture sorption isotherms for food products is of great importance in design and optimization of the drying processing for instance; in assessing packaging problems, for modeling moisture changes which occur during drying, for predicting shelf life stability, for ingredient mixing predictions etc. (Spiess and Wolf, 1983; Gal, 1987). They can also be used for design and optimization of drying equipment and other engineering purposes related to dehydration (Maskan *et al.*, 1998). For food products, the sorption isotherm can be measured by means of three different measuring techniques: gravimetric, manometric or hygrometric (Iglesias and Chirife, 1978). In the gravimetric methods, the weight of the sample is measured with a balance. In the manometric methods, the vapour pressure of water is measured when it is in equilibrium with a sample at given moisture content. In the hygrometric methods, the equilibrium relative humidity with a sample at given moisture content is measured (Iglesias and Chirife, 1978).

Aiming to mathematically express the relation between the water activity of food and its moisture content, diverse models have been developed such as nonlinear, linear, regression models. In many cases, the model that is suitable for certain food product is not suitable for a different one, furthermore, the model only exhibits a suitable predictive ability for certain moisture activity ranges (Ahmat *et al.*, 2014). Several mathematical models have been proposed to describe sorption isotherms. The most common equations that are used for describing sorption in food products are the Langmuir equation, the BET equation, the Oswin model, the Smith model, the Halsey model, the Henderson model, the Iglesias-Chirife equation, the GAB model, and the Peleg model (Sahin and Gülüm, 2006).

Due to the complex composition of meat products a theoretical prediction of sorption isotherms is not possible, and sorption data must be determined experimentally (Adam *et al.*, 2000). In the literature some review papers and compilations about isotherms of different meat products can be found (Iglesias and Chirife, 1982; Lazarides, 1990, 1991). However, information on desorption isotherms of meat at temperatures found during the solar drying process is scanty. Therefore, there is a need to provide information on sorption isotherms of beef at solar drying temperatures of tropical countries in order to better understand the behavior of the product during drying. The objectives of this study were to determine and to model the desorption isotherms for beef at 30-60^{0}C.

2.1. MATERIALS AND METHODS

2.1.1. Sample collection and preparation

Meat (beef) of high microbial quality from the round of the hind quater of an inspected male carcass was purchased from Dagoretti slaughter house, Nairobi, Kenya. Excess fat was trimmed off to prevent rancidity while drying. It was then cleaned and stored in a cold room at 5°C for 48 h prior to experiments so that the storage conditions would be kept the same for all samples before drying. The meat was cooled overnight at 0°C to obtain enough consistency for cutting and cut along the direction of its fibers into thin strips of 5 cm long, 5 cm wide and 1 cm thickness. Triplicate samples were used for the determination of initial moisture content of beef using the oven method at 105°C for 3 h, (AOAC, 2000) and the average values reported as 328.69 g water/g dry matter.

2.1.3. Experimental

Desorption isotherms of fresh meat were determined using the standard static gravimetric technique. This method is based on the use of saturated salt solutions to maintain a fixed relative humidity according to the COST 90 method (Wolf *et al*., 1985). The salts used with a range of water activity from 0.05 to 0.9 (Greenspan, 1977) are shown in Table 1.

Ten empty desiccators each with an insulated lid containing different saturated salt solutions were placed in a hot air oven adjusted to a fixed temperature for 24 h so as to bring the salt solutions to a stationary temperature.

Table 1 Water activities of the saturated salt solutions at four temperatures used in the desorption experiments

		Water activity		
Salt	**30^{0}C**	**40^{0}C**	**50^{0}C**	**60^{0}C**
KOH	0.0738	0.0626	0.0572	0.0549
LiCl	0.1182	0.1125	0.1110	0.1073
CH_3COOK	0.2160	0.2012	0.1890	0.16
$Mg\ (Cl)_2.6H_2O$	0.3238	0.3159	0.3159	0.2926
K_2CO_3	0.4317	0.4320	0.4322	0.4327
NaBr	0.5602	0.5320	0.5320	0.497
$NaNO_3$	0.7312	0.7100	0.7100	0.6735
NaCl	0.7569	0.7540	0.7444	0.743
KCl	0.8362	0.8232	0.8120	0.8030
KNO_3	0.9188	0.8835	0.8521	0.8478

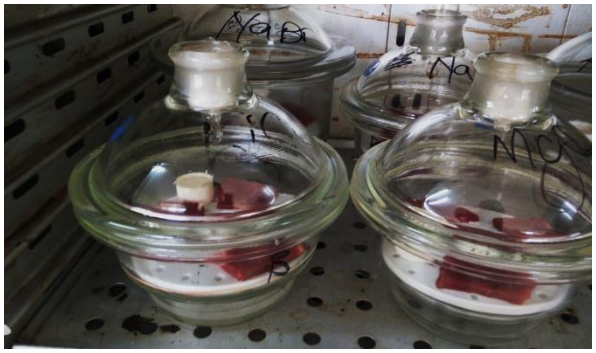

Triplicate meat samples were placed on the perforated base 5 cm above the surface of the desiccators. A small quantity of toluene was placed in each hygrostat in order to prevent fungal activity (Wolf *et al*., 1985).

Weight recording of the beef samples was done after every 4 days. This procedure was continued until the weight was constant. The equilibrium moisture content of each sample was determined by a drying oven whose temperature

Nonlinear regression analysis, using Minitab (Version 18.0, Minitab Inc., USA) software package, was used to estimate the model coefficients from the experimental sorption data for all samples. The suitability of the equations was evaluated using coefficient of determination (R^2) Eq. (4) calculated numerically by Excel and the standard error of the regression (standard error of estimate) Eq. (5) generated by Minitab. For goodness of fit of the curve to the equation, a high value of R^2 and a low value of SEE were taken.

$$R^2 = \frac{\sum_{i=1}^{N}(M_{p,i} - M_{e,avg})^2}{\sum_{i=1}^{N}(M_{e,i} - M_{e,avg})^2}) \quad \ldots(1)$$

$$\text{SEE} = \sqrt{\frac{\sum_{i=1}^{N}(M_{e,i} - M_{p,i})^2}{N}} \quad (2)$$

Where M_e is the experimental EMC value, M_p is the predicted EMC value and N is the number of experimental data.

For the purpose of this work, three models were used to fit the experimental sorption data; the GAB, BET and Oswin (Table 2).

The stable dry matter (moisture content) for meat during drying was also established from the sorption isotherms.

3.1. RESULTS AND DISCUSSION

3.1.1. Effect of temperature and water activity on the equilibrium moisture content

Equilibrium moisture content data obtained for beef at different water activities and temperatures are shown in figure 1. The mean of the equilibrium moisture content of beef ranged from 0.04 to 0.59, 0.03 to 0.42, 0.03 to 0.36 and 0.11 to 0.24 (kg water/kg dry matter) for temperature of 30, 40, 50 and 60°C respectively within the relative humidity range of 5-90%. The desorption isotherms were of sigmoid form (Type II according to the BET classification) which is common for many hygroscopic products.

Modelling equations

Table 2 Moisture sorption isotherm models

Model	Equation	References
GAB	$X_{eq} = \frac{X_M C K a_w}{(1 - K a_w)(1 - K a_w + C K a_w)}$	(Van Den Berg, 1985)
BET	$X_{eq} = \frac{X_M C a_w}{(1 - a_w)(1 + (C - 1)a_w)}$	(Brunauer *et al*., 1938)
Oswin	$X_{eq} = a\left(\frac{a_w}{1 - a_w}\right)\text{^}b$	(Oswin, 1946)

Where C, K, a and b are constants; a_w is the water activity; X_{eq} represents the equilibrium moisture content on a dry weight basis (kg water/kg dry matter) and X_M is the monolayer of water (kg water/kg dry matter)

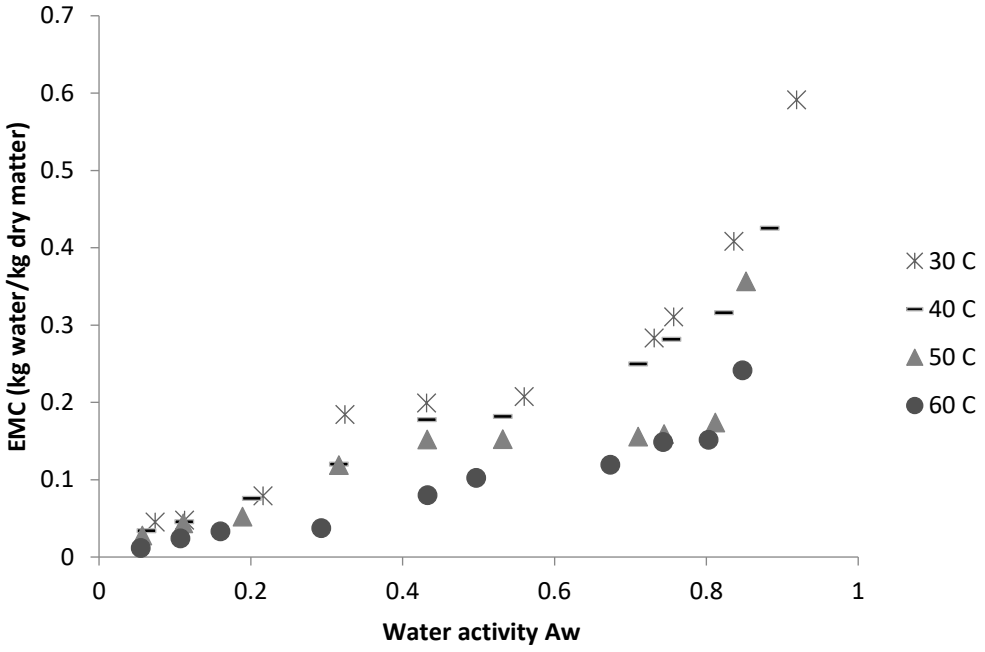

Figure 1: Desorption curves of fresh beef (experimental results): equilibrium moisture content as a function of water activity for different temperatures

Equilibrium moisture content (EMC) for beef increased with water activity at selected temperatures (Figure 1). This may be due to the fact that vapor pressure of water present in foods increases with that of the surroundings. The EMC values decreased with increased temperature at all levels of water activity. The kinetic energy associated with water molecules present in foods increases with increasing temperature. This in turn, resulted in decreasing the attractive forces and consequently, escape of water molecules. This led to a decrease in the degree of water sorption with increasing temperature at a given water activity. Several researchers (Iglesias & Chirife, 1982; Singh *et al.*, 2001) have reported similar trend for different foods.

The critical moisture content for beef (at water activity value of 0.6) within the temperature range of 30-60°C was found to be between 0.1 and 0.2 kg moisture/kg dry matter (Figure 1). Below the water activity of 0.6, microbial growth cannot occur and therefore the equilibrium moisture content found within this water activity can be considered as the stable moisture content for drying (Ahmat *et al.*, 2015).

Sorption models presented in Table 1 were tested for their effectiveness to describe the desorption isotherms for beef at different temperatures. The coefficient of determination (R^2) and standard error of estimate (SEE) values for each model are reported in Table 2. The highest values and lowest values of R^2 and SEE respectively were found for the GAB and Oswin models, therefore, these two models showed the best fit with respect to R^2 and SEE values. The coefficient of determination (R^2) for GAB and Oswin models was lower than 0.93 at 30, 40 and 60°C. These models were therefore considered as the best to describe the experimental desorption data for beef within this temperature range and water activity between 0.05 and 0.9 (Table 2. This confirms the findings obtained by some authors that the GAB model is the most appropriate for modeling agri-food products (Trujillo *et al.*, 2003; Singh *et al.*, 2006).

Table 3 Estimated parameters and model constants for GAB, BET and Oswin models

		Statistical parameters		Model constants				
Model	Temp. (°C)	R^2	SEE	X_M	C	K	a	B
GAB	30	0.9759	0.0302	0.1144	11.1308	0.8785		
	40	0.9851	0.0177	0.1175	7.6441	0.8209		
	50	0.7823	0.0499	0.0617	29.1549	0.9279		
	60	0.9473	0.0180	0.0484	8.34602	0.9930		
BET	30	0.8919	0.0815	0.0572	5.64802E+17			
	40	0.8991	0.0518	0.0577	221.0820			
	50	0.7872	0.0481	0.0473	141.9250			
	60	0.9421	0.0189	0.0366	19.1733			
Oswin	30	0.9795	0.0262				0.1897	0.4660
	40	0.9857	0.0164				0.1658	0.4586
	50	0.7805	0.0466				0.1249	0.4517
	60	0.9532	0.0167				0.0820	0.5719

Monolayer moisture (X_M) obtained from the GAB model was found to be higher than that obtained from the BET model while the energy constant for the GAB model was lower than that of the BET at the same temperatures (Table 2). The same observations have been made by (Ahmat et al., 2014). In both models, the monolayer moisture content decreases as the experimental temperature increases (Table 2) as has been obtained for most agri-food products (Singh et al., 2001; 2006).

The energy constant representing multilayer water (K) for the GAB model, which ranges from 0 to 1 (Ahmat et al., 2014), was highest at 60°C. Multilayer water is water associated with neighboring molecules by water-water or water-solid substrate hydrogen bonding. A high value indicates that water is freezable and strongly bound (Timmerman et al., 2001). The value of b in the Oswin model ranged between 0.4660 and 0.5719 and decreased as temperature increased. This indicates that the interaction between water molecules and the solid skeleton decreases with temperature increase. These results are similar to those obtained for other meat products (Singh et al., 2006).

Figure 2 and 3 show the experimental points of desorption isotherms at 40°C by GAB and Oswin models respectively. They represent a visually good fit between the experimental values and those obtained from the models.

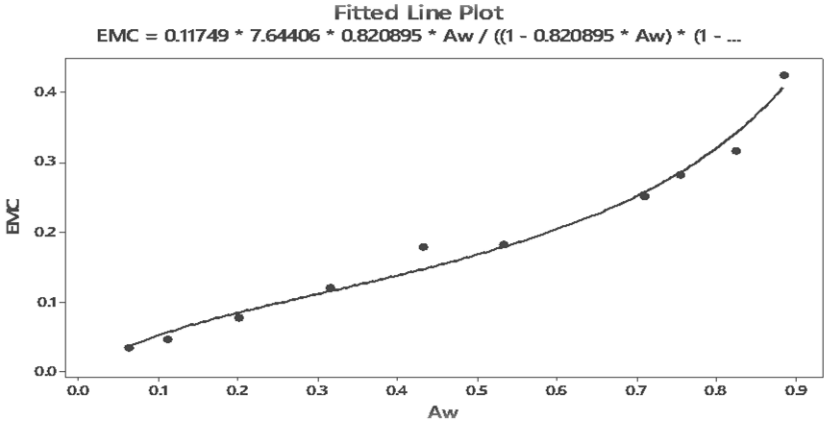

Figure 2: Experimental and predicted values of equilibrium moisture content of fresh beef at different water activities using GAB model

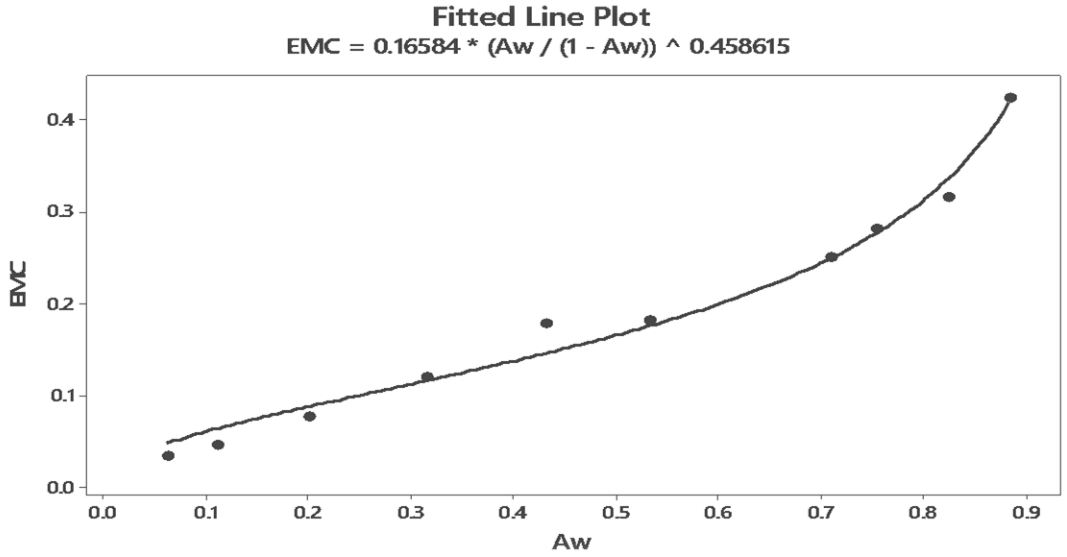

Figure 3: Experimental and predicted values of equilibrium moisture content of fresh beef at different water activities using Oswin model

4.1. CONCLUSIONS

The desorption isotherm of beef at different temperatures and water activities were determined by the standard gravimetric method using various saturated salt solutions. There was a significant effect of temperature on the equilibrium moisture sorption in the range of temperatures studied. The equilibrium moisture content increased with increasing temperature at constant water activity. The critical moisture content for safe drying of beef (at 0.6 Aw) was 10-20 % (d.b). Among the sorption models chosen to test, GAB and Oswin models are suitable for describing the relationship between the equilibrium moisture content, water activity and temperature for beef.

REFERENCES

Ahmat, T., M. Barka, A. Aregba and D. Bruneau, 2015. *Convective drying kinetics of fresh beef: An experimental and modeling approach*. Journal of Food Processing and Preservation, 39: 2501-2595.

Ahmat, T., D. Bruneau, A. Kuitche and A.W. Aregba 2015. *Desorption isotherms for fresh beef: An experimental and modeling approach*. Meat science, 96: 1417-1424.

Brunauer, S., P.H., Emmet and E.Teller. 1938. *Adsorption of gases in multimolecular layers.* Journal of the American Chemical Society, 60: 309–319.

Gal, S. 1987. *The need for, and practical applications of sorption data. In R. Jowitt, et al. (eds).* Physical Properties of Foods, 2: 13-25., London: Elsevier Applied Science.

Greenspan, L. 1977. *Humidity Fixed Points of Binary Saturated Aqueous Solutions.* Journal of Research of the National Bureau of Standards, 81a: 89-112.

Iglesias, H.A and J. Chirife. 1982. *Handbook of food isotherms. Water sorption parameters for food and food components.* New York: Academic Press.

Iglesius, H.A. and J. Chiriffe. 1978. *An empirical equation for fitting water sorption isotherms for fruits and related products.* Canadian Institute of Food Science and Technology Journal, 11: 12-15.

Lazarides, H.N. 1990. *Sorption isotherm characteristics of an intermediate moisture meat product*. Lebensmittel Wissenschaft Technologie, 23: 418–421.

Lazarides, H.N. 1991. *Application of the transformed GAB equation to delineate moisture sorption behaviour of an intermediate moisture meat product.* Lebensmittel Wissenschaft and food components. Academic press, New York

Maskan, M and F. Göğüş. 1998. *Sorption isotherms and drying characteristics of mulberry (Morus alba).* Journal of Food Engineering, 37: 437-449.

Oswin, C.R. 1946. *The kinetics of package life. The isotherm.* Journal of Chemical Industry 65: 419–421.

Sahin, S and S. Gülüm. 2006. Physical Properties of Foods, 205, 218 p. Springer; New York, United States.

Singh, R.R.B., K.H. Rao, A.S.R., Anjaneyulu and G. R. Patil. 2001. *Moisture sorption properties of smoked chicken sausages from spent hen meat.* Food Research International, 34: 143-148.

Singh, R.R.B., K.H. Rao, A.S.R. Anjaneyulu and G.R. Patil 2006. *Water desorption characteristics of raw goat meat: Effect of temperature.* Journal of food engineering, 75: 228-236.

Spiess, W.E.L. and W.R. Wolf. 1983. *The results of the COST 90 project on water activity*. In. R. Jowitt et al. (Eds.), Physical properties of foods, pp. 65-91. London: Applied Science Publishers,

Timmerman, E.D. and J. Chirife 1991. *The physical state of water sorbed at high activities in starch in terms of the GAB sorption equation.* Journal of Food Engineering, 14: 171-179.

Trujillo, F.J., P.C. Yeow and Q.T. Pham. 2003. *Moisture sorption isotherm of fresh lean beef and external beef fat.* Journal of Food Engineering, 60: 357-366.

Van Den Berg, C. 1985. *Development of B.E.T. Like Models for Sorption of Water on Foods; Theory and Relevance,* In D. Simatos and J.L. Multon (Eds), Properties of Water in Foods, pp. 119 – 135. Dordrecht: Martinus Nijhoft Publishers

Wolf, W., W.E.L. Spiess, and G. Jung. 1985. Standardisation of isotherm measurements (COST-project 90 and 90 BIS). D.Simatos, & J. L. Multon (Eds.). Properties of Water in Foods, p661. Dordrecht: Martinus Nijhoft.

EN MASSE BEHAVIOUR OF GRANULAR MATERIALS IN SILO LOAD CALCULATIONS

Gumbe[1], L.O.

[1]Department of Biosystems and Environmental Engineering, Technical University of Kenya, Kenya

ABSTRACT

Calculations of silo structure design problems, such as the evaluation of the interaction between the loads imposed on thin walled storage structures by grains and deformation of the storage structure wall or the evaluation of loads imposed on confining structures by particulate media during flow, would be greatly enhanced by accurate description of the load-deformation behaviour of stored particulate media en-masse. Early models represent situations which are extremely idealized versions of rea life counterparts. The solutions are those for various simple stress distributions of linearly elastic isotropic homogeneous media on the one hand, and certain results derived from the upper bound methods of ideally plastic analysis on the other hand. This paper discusses mechanical properties of granular materials and their impact on load distribution in silos.

Keywords: granular material; silo; pressure distribution; elastic, plastic, viscoelastic, elastoviscoplastic

INTRODUCTION

The solution to grain storage structure design problems, such as the evaluation of the interaction between the loads imposed on thin walled storage structures by grains and deformation of the storage structure wall or the evaluation of loads imposed on confining structures by particulate media during flow, would be enhance by description of the load-deformation behaviour of biological particulate media en-masse Manbeck and Nelson (1972). However, there is controversy as to whether such materials are elastic, viscoelastic, elastoplastic or elastoviscoplastic.

Granular materials, which include everything from coal to coco pops, soils and all cereal grains, are large conglomerations of discrete macroscopic particles that do not quite fit into any of the known phases of matter: solid, liquid, or gas (Heinrich *et al.*, 1996). The changing personalities of granular materials can have devastating implications, for example the disturbance of the earth following an earthquake can be enough to trigger solid ground to turn to mush with catastrophic consequences. Tordesillas (2004) asserts that, *"Even a fractional advance in our understanding of how granular media behave can have a profound impact on the economic and general well-being of nations worldwide."* Yet, despite being second only to water on the scale of priorities of human activities and believed to account for ten per cent of all energy consumed on earth, the physics behind granular materials remain largely unknown. Scientists have generally turned to the continuum theory for predicting the behaviours of solids, liquids and granular media (Harris, 2009) – it looks at an object as a whole rather than the sum of its parts. The alternative of modeling every single grain, as in the discrete element method (DEM), is computationally intensive and extremely costly.

Knowledge of constitutive relations in granular agricultural materials is of utmost importance in transportation, processing and in the design of processing and storage structures such as silos and bins. Jansen's theory, for example, is

commonly used in most international standards for silo design (Moya *et al.,* 2002). This theory, as well as many others such as Airy's theory or Reimbert's theory considers some material properties such as the angle of internal friction, the grain wall friction coefficient and the specific weight. Hence, it is possible to find values for all these properties in literature to apply in design (Mohsenin, 1980). However, to accurately model silo loads, it is necessary to consider additional material properties not taken into account in the traditional methods (Moya *et al.,* 2002; Vanel *et al.,* 2000). Constitutive models continue to rely on the theory of elasticity to predict the load-deformation behaviour of granular materials (Harris, 2009).

In an attempt to understand this behaviour, previous studies of rheology and strength of agricultural materials have focused on loading specimens to failure at a constant deflection rate or applying impact loading (Mohsenin, 1980). It is however well known that loading below the yield stress in metals and other composite engineering materials can eventually result in failure (Stinchcomb, 1989). Mclaughlin and Pitt (1984) showed that apple tissue could fail under cyclic or static loadings of magnitudes insufficient to cause failure initially. The question that arises is whether these small, repeated loads (cyclic loading) applied to bulk shelled maize can cause eventual damage as occurs in metal fatigue.

1.1 Classification of Granular Materials

Based on ISO classification (I S O 3 5 3 5, 1977), the Mechanical Handling Engineers' Association (MHEA), UK divided the granular material according to the dimension of particles (*D*) into ten categories; however Chattopadhyay et al. (1994) proposed the five following groups:

- dust $D \leq 0.42$ mm
- grain $D \leq 3.35$ mm
- lump $D \leq 40$ mm
- clump $D \leq 200$ mm
- block $D > 200$ mm

The classification of granular materials according to bulk density (ρ) is as follows:

- light $\rho < 600$ kg m $^{-3}$
- medium 600 kg m $^{-3} < \rho \leq 1\,100$ kg m^{-3}
- heavy 1 100 kg m$^{-3} < \rho \leq 2000$ kg m $^{-3}$
- very heavy $\rho > 2000$ kg m $^{-3}$

The flowability defined as a motion of particles with reference to neighbouring particles or along surfaces is the next parameter describing granular materials (Peleg, 1985). It has a huge influence on processes occurring during storage and handling of materials in industry and agriculture. The conventional classifications of materials according to flowability are derived from the classification based on the flow function (*FF*) proposed by Jenike (1961). Chattopadhyay *et al.,* (1994) extended Jenike's (1961) classification adding two extreme classes:

- fluidlike flooding
- very free flowing FF > 10
- free flowing 10 > FF > 4
- average flowing 4 > FF > 2
- poor flowing 2 > FF
- sluggish/interlocked

In the case of agricultural and food raw materials and products, apart from the classifications mentioned above, attention should be paid also to a number of additional features, such as:

- possibility of freezing,
- hygroscopicity,
- toxic properties,
- properties conducive to spontaneous combustion and
- explosive properties

Stress- Strain Models

Studies of the responses of cereal grains to mechanical stresses have progressed from analyses based on simple Hookean models to viscoelastic models using generalized Kelvin and Maxwell models, used singly or jointly Herum *et al.,* (1979). More recently elastoplastic models have been used Zhang *et* al., (1986). Upon repeated uniaxial loading, Shapolyanskaya (1952) found that

the load-deformation behavior of wheat kernels approached that of an elastic body.
Thus, applying the Hertz theory of contact stresses, he evaluated a modulus of elasticity for wheat kernels. In his study of core samples of wheat kernels, Zoerb (1960) noted the same strain hardening tendencies but concluded that plastic rather than elastic behavior characterized the mechanical properties of wheat.

Shelef and Mohsenin (1967) supported Zoerb's observations, as did Arnold and Roberts (1969) by means of a variety of parallel-plate and indenter uniaxial compression tests.
Manbeck, H.B and Nelson, G.L. (1972) and Manbeck, H.B., and Nelson, G.L. (1975), Schott, and Britton (1984), Mensah, *et al.*, (1981) and Herum *et al.*, (1979). are among the researchers who categorized various grains as beirig viscoelastic. Zhang *et al.*, (1985), categorize wheat as being elastoplastic. Briassou and Curtis, (1985) categorizes grains as being non-time dependent in behavior.

While some earlier researchers treated the materials as elastic materials are very complex and may be defined as being elastoviscoplastic, Li *et al.*, (1989).

2.1 Elastoplastic Models

The elastoplastic theory developed by Lade (1977) for cohesionless sand and verified for wheat *en masse* by Zhang *et al.*, (1986) has the following form;

$$d\varepsilon_{ij} = d\varepsilon_{ij}^{e} + d\varepsilon_{ij}^{p} + d\varepsilon_{ij}^{c} \quad \ldots (2.1)$$

Where:
$d\varepsilon_{ij}$ is the total strain increment tensor, and superscripts e, p, and c, refer to the elastic, plastic and plastic collapse strain increment components respectively. The complete elastoplastic constitutive relationship includes an elastic component and two work hardening plastic components. Figure 2.1 show basic elastoplastic components as described by Lade's model.

$d\varepsilon_{ij}$ Is the volumetric strain increment

Lade and Nelson developed a procedure to construct an incremental elastoplastic model with multi-intersecting yield surfaces. By using this Lade-Nelson method Chi and Kushwaha (1990) derived the complete elastoplastic model as presented below;

2.1.1. Lade's complete Elastoplastic Constitutive Equation

The complete elastoplastic stress-strain equation developed by Lade (1977) may be written in incremental form as;

$$d\{\sigma\} = [E_{ep}]d\{\varepsilon\} \quad \ldots (2.2)$$

$$[E_{ep}] = [E] - \frac{[E]}{A}\left[\left\{\frac{\partial g_c}{\partial \sigma}\right\}\cdot(b_c)^t + \left\{\frac{\partial g_p}{\partial \sigma}\right\}\cdot(bp)^t[E]\right] \quad (2.3)$$

The terms in equation (3.3) are defined below;

$$A = \begin{vmatrix} L_{11} & L_{12} \\ L_{21} & L_{22} \end{vmatrix} \quad \ldots (2.4)$$

$$b_c = L_{22}\left\{\frac{\partial f_C}{\partial \sigma}\right\} - L_{12}\left\{\frac{\partial f_P}{\partial \sigma}\right\} \quad \ldots (2.5)$$

$$b_P = L_{11}\left\{\frac{\partial f_P}{\partial \sigma}\right\} - L_{21}\left\{\frac{\partial f_C}{\partial \sigma}\right\} \quad \ldots (2.6)$$

$$L_{11} = \left\{\frac{\partial f_C}{\partial \sigma}\right\}^t \cdot [E]\cdot\left\{\frac{\partial g_C}{\partial \sigma}\right\} + \left\{\frac{\partial K_C}{\partial W_P^P}\right\}\cdot\{\sigma\}^t\cdot\left\{\frac{\partial g_C}{\partial \sigma}\right\} \quad \ldots (2.7)$$

$$L_{22} = \left\{\frac{\partial f_P}{\partial \sigma}\right\}^t \cdot [E]\cdot\left\{\frac{\partial g_P}{\partial \sigma}\right\} + \left\{\frac{\partial K_P}{\partial W_P^P}\right\}\cdot\{\sigma\}^t\cdot\left\{\frac{\partial g_P}{\partial \sigma}\right\} \quad \ldots (2.8)$$

Alternatively,

$$L_{11} = \left\{\frac{\partial f_C}{\partial \sigma}\right\}^t \cdot [E]\cdot\left\{\frac{\partial g_C}{\partial \sigma}\right\} \quad \ldots (2.9)$$

$$L_{22} = \left\{\frac{\partial f_P}{\partial \sigma}\right\}^t \cdot [E]\cdot\left\{\frac{\partial g_P}{\partial \sigma}\right\} \quad \ldots (2.10)$$

All factors have their usual meaning.

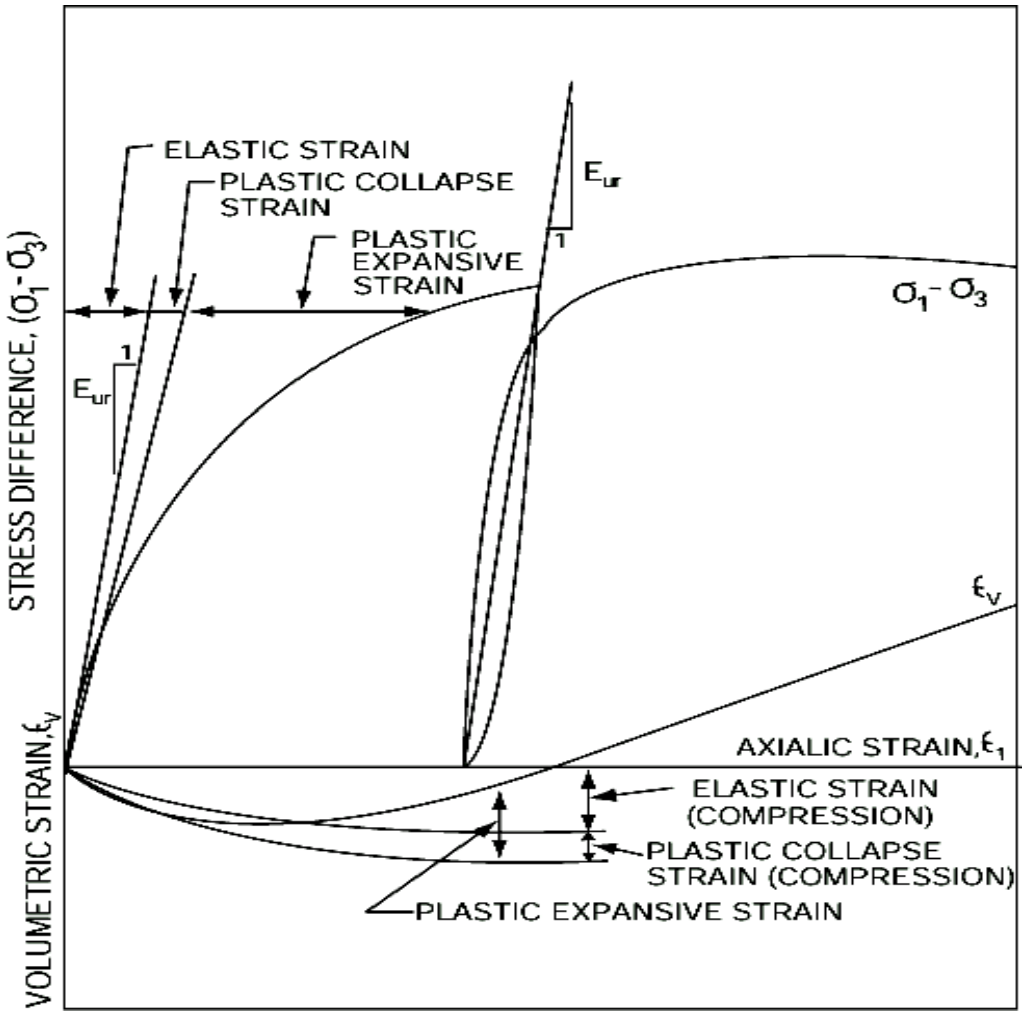

Figure 2.1: A schematic representation of elastic, plastic collapse and plastic expansive strain components determined in triaxial tests (Lade, 1977).

The elastoplastic constitutive matrix (2.2) can readily be determined if the stress state is known.

The Mohr-Coulomb failure criterion finds many applications in engineering practice (Ti, 2009; Dartevelle, 2003). Analysis of stress data from triaxial cell tests on granular materials often involves the Mohr Circle construction to graphically determine strength parameters (Stafford *et al.*, 1986). The Mohr circle construction helps to determine the stresses on any given plane.

From a series of tests, the minor (σ_3) and major (σ_1) principal stresses may be derived. On a graph with shear stress along the y-axis and normal stress along the x-axis, a circle centered on x = $(\sigma_1+\sigma_2)/2$ of radius $(\sigma_1-\sigma_2)/2$ is drawn for each test. A smooth curve, tangent to these circles defines the equation for the failure characteristic of the material in question. The ideal Mohr-Coulomb failure plot is shown in Figure 2.2.

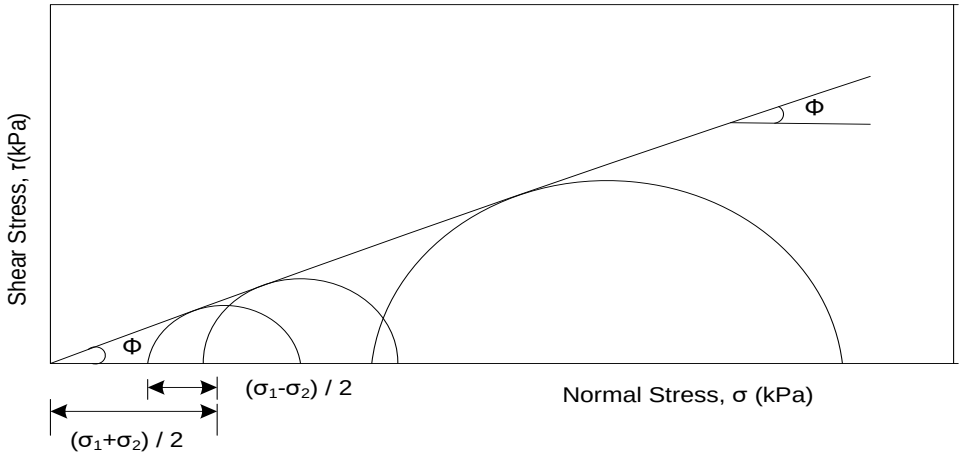

Figure 2.2: Ideal Mohr-Coulomb failure envelop for cohesionless granular materials (Dartevelle, 2003)

The basic equation if of the form,

$$\tau = c + \sigma \tan \varphi \qquad \ldots (2.11)$$

Where:

σ is normal (principal) stress
τ is shear stress
c is cohesion
ϕ is angle of internal friction,

all measured at failure.

The alternative to the above method of plotting circles is to directly plot $(\sigma_1-\sigma_2)/2$ against $(\sigma_1+\sigma_2)/2$ for each test and draw a best-fit straight line through the points. From this so-called K_f line, *c* and φ may be derived (Stafford *et al.*, 1986). For cohesionless granular materials such as shelled maize, the cohesion, c, is usually assumed to be negligible (Zhang *et al.*, 1994).

Horabik and Molenda (2014) presented an analysis based on the e Discrete Element Method (DEM) proposed by Cundal (1979) based on elementary interactions between the grains. The method consists in a simplified solution of the equation of motion for each grain of the material.

The calculation procedure is based on the assumption that during a very short time step Δt acceleration and speed are constant, and the disturbance of motion of a single grain does not reach further than to the nearest neighbours. DEM provides new possibilities of deeper insight into the micro-scale behaviour of bulk solids, which are not available with traditional or even modern approach of continuum mechanics where gradients of displacement and stress are extremely high like during flow around inserts (K o b y ł k a, M o l e n d a, 2013).

The rapid development of computer calculation techniques permitted the realization of computer simulations of a variety of processes occurring in granular materials, such as: dynamic effects in silos, mixing, segregation, gravitational discharge from silos (Z h a n g *et al.*, 1993; M a s s o n, M a r t i n e z, 2000; K o u *et al.*, 2002; Paraf i n u k *et al.*, 2013; K o b ył ka and M o l e n d a (2014).

DEM simulations generally produce a huge scatter of inter-particle forces which after averaging provide useful information. An example of the horizontal forces acting on a vertical wall in quasi-static assemblies (6000 particles in two dimensions) is presented in Figure 2.3. Analysis of the distribution of horizontal forces averaged for 10 particle–wall contacts indicated a moderately smooth increase in the force with increase in particle bedding depth (S y k u t et al., 2008). The DEM values are considerably larger as compared to J a n s s e n's (1895) solution. Similarly, B a l e v i č i u s *et al.*, (2011) obtained good agreement of lateral pressure distribution vs material depth with experimental data which were significantly larger than J a n s s e n 's (1895) solution and E u r o c o d e 1 (2003) recommendations. González-Montellano et al. (2012) obtained the pressure distribution of particles similar to maize grains along the vertical direction of the wall reaching its maximum at the silo-hopper transition using DEM. M a s s o n , Ma r t i n e z (2000) reported on the impact of anisotropy of contact orientations on the pressure distribution.

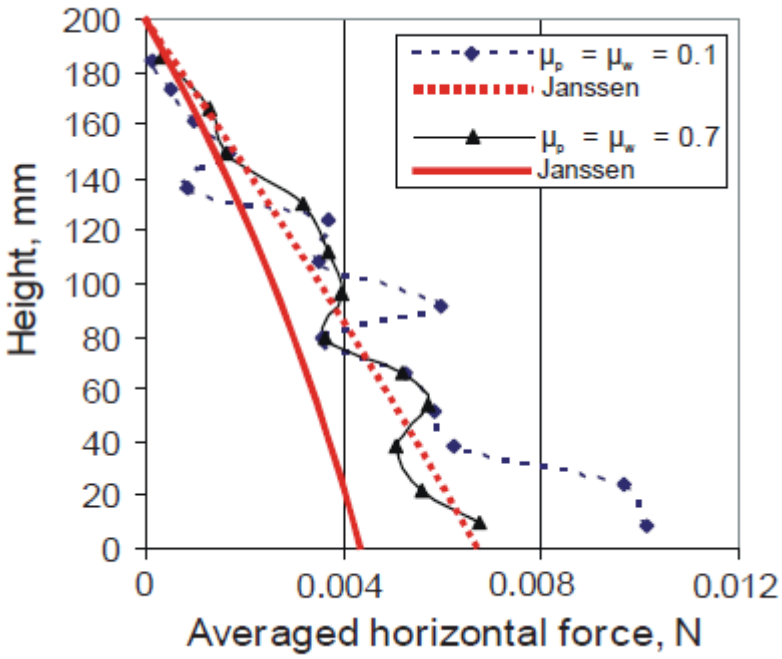

Figure 2.3: Wall horizontal force averaged for 10 particles -wall contacts compared to Janssen's (1895) solution.

Horabik and Moleda (2014) concluded that granular solids constitute a very wide group of materials of specific mechanical, physical, and chemical properties. In that group granular materials of biological origin represent a very important source of products of agriculture and food processing industry. Precisely determined parameters of mechanical properties of granular materials and properly chosen constitutive models are fundamental for proper design and control of storage, handling, and processing of those materials. There have still been a lot of particular and specific operations not fully understood or precisely described yet. A few examples of such processes discussed in the paper indicate that further development of tools for modelling the mechanics of granular solids is necessary. One of the most promising tools is the DEM. All these actions are necessary to ensure that the equipment used for storage and processing of granular materials meets two basic demands: predictable and safe operations and high quality of processed materials.

Viscoelastic Models

The linear and non-linear viscoelastic models have been predominantly used to model material behaviour (Gumbe, 1995). These models incorporate time in stress-strain equations. Such equations are specifically important in the design of storage structures such as silos and foundations both of which are exposed to rapidly declining or changing periodic ambient temperatures, moisture content, among others (Gumbe, 1995).

For linearly viscoelastic material, the following criteria hold (Findley et al., 1976).

1. For any step input in strain (ε_0) the relation between the stress $\sigma(t)$ and strain is;

$$\frac{\sigma(t)}{\varepsilon_0} = E(t) \qquad \ldots (2.12)$$

For a step input of stress, σ_0, the relation between strain, $\varepsilon(t)$ and stress is;

$$\frac{\varepsilon(t)}{\sigma_0} = J(t) \quad \ldots (2.13)$$

Where $E(t)$ and $J(t)$ are the stress relaxation modulus and creep compliance respectively.

2. The Boltzman's superposition principle holds, that is, the stress at any time *t* depends on the strain history of the material;

$$\sigma(t) = \int_0^t E(t-\tau)\frac{\delta\varepsilon}{\delta\tau}\delta\tau + \sum_{i=1}^{n}\Delta\varepsilon_i E(t-t_i) \quad \ldots (2.14)$$

Where

$\varepsilon(t)$ Is the applied strain

$\Delta\varepsilon_i$ Is the jump in the applied strain occurring at time, t_i

Most viscoelastic models are built on the spring-dashpot arrangement as the basic building blocks. The two basic models are the Kelvin solid model and the Maxwell fluid model (Chung, 1988). Figure 2.4 a show the Kelvin model with the spring and dashpot arranged in parallel while Figure 2.4 b shows the Maxwell model where the spring and dashpot are arranged in series.

The two basic equations governing the stress-relaxation behaviour of the Kelvin and Maxwell models at constant strain are given in (2.15) and (2.16) respectively;

$$E(t) = E \quad \ldots (2.15)$$

$$E(t) = Ee^{-t/\tau} \quad \ldots (2.16)$$

Where;

$E(t)$ Are the relaxation modulus and E the spring constants

The Maxwell and Kelvin models have been noted to have several deficiencies in predicting the behaviour of viscoelastic materials (Chung, 1988; Gumbe, 1993). These deficiencies include,

- Neither the Maxwell nor Kelvin model represents the behaviour of most viscoelastic materials in actual systems.
- The Maxwell model shows no time-dependent recovery nor does it show the decreasing strain rate under constant stress, a characteristic of primary creep.
- The Kelvin model does not exhibit time-independent strain on loading, nor does it describe a permanent strain after unloading.
- Both models show a finite initial strain rate where the initial strain rate for many materials is very rapid.

Due to the above limitations of the simplified models, several other viscoelastic models have been adopted to help make more accurate predictions of viscoelastic behaviour of engineering materials (Chung, 1988; Aklonis and MacKnight, 1983; Gumbe, 1993). One such model, which has been found to be fairly accurate, is the generalized Maxwell-Weichert model (Aklonis and MacKnight, 1983) that consists of an arbitrary number of Maxwell elements connected in parallel as shown in Figure 2.5.

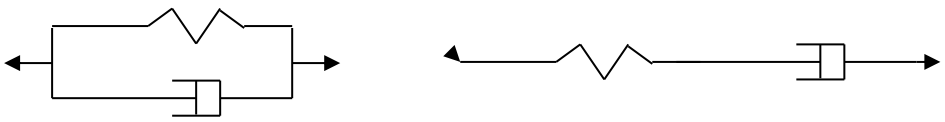

a) Kelvin model

b): Maxwell model

Figure 2.4: Basic Viscoelastic models

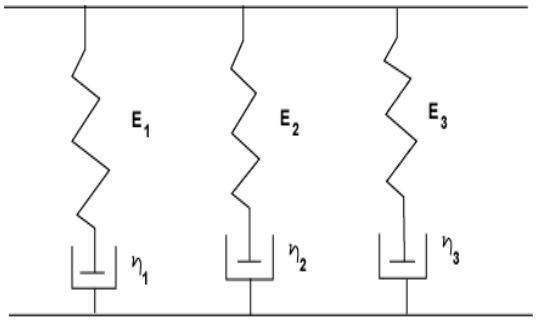

Figure 2.5: Generalised Maxwell-Weichert model (Aklonis and MacKnight, 1983)

The generalized stress-relaxation equation for the Maxwell Weichert model is of the form;

$$E(t) = \sum_{i=1}^{z} E_i e^{-k_i t} \quad \ldots (2.17)$$

Where

E (t) is the relaxation modulus (MPa)
t is the time of relaxation (minutes)
k is the exponent (1/minute)

For practical purposes however, equation (2.17) has to be presented to finite levels. Equation (2.18) therefore is the representation of (2.17) at two levels (Herum, 1979);

$$E(t) = E_1 e^{-k_1 t} + E_2 e^{-k_2 t} \quad \ldots (2.18)$$

The two equations, (2.17) and (2.18), describe the Maxwell-Weichert linear viscoelastic model as long as the constants E_1, E_2, k_1 and k_2 are determined.

Oranga (2005) conducted test to evaluate relaxation parameters which included the stress-relaxation moduli, E_1, E_2 and the stress-relaxation exponents' k_1, k_2.
Figures 2.6-2.8 show the stress relaxation curves for the three maize varieties, at an initial bulk density of 800 kg/m^3 (three replications) and the fitted curves according to the given regression equations indicated.

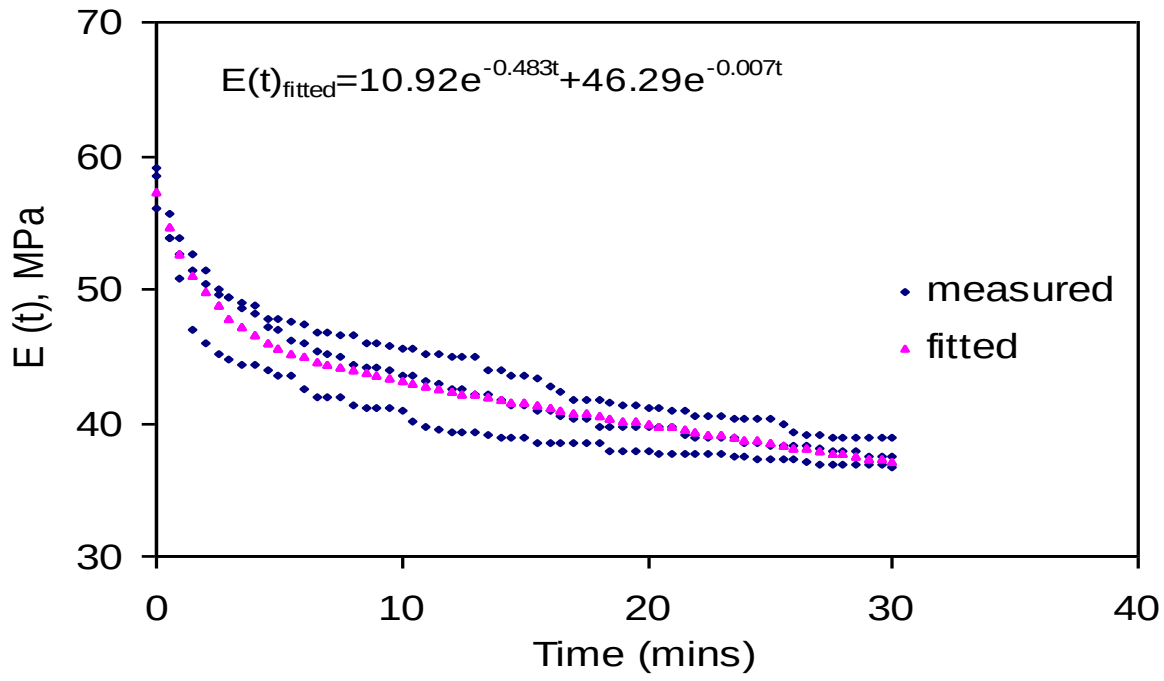

Figure 2.6: Stress-relaxation curve for variety V1

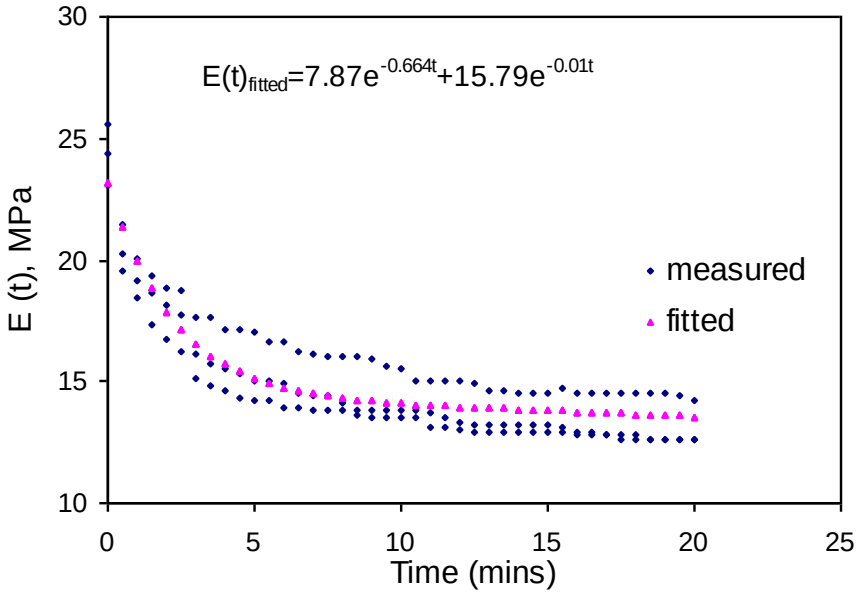

Figure 2.7: Stress-relaxation curve for variety V2

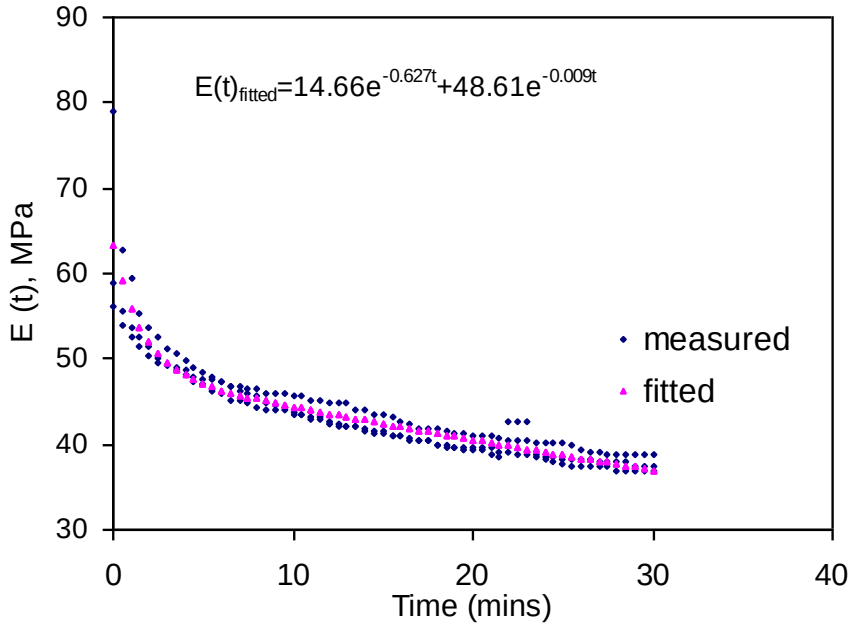

Figure 2.8: Stress-relaxation curve for variety V3

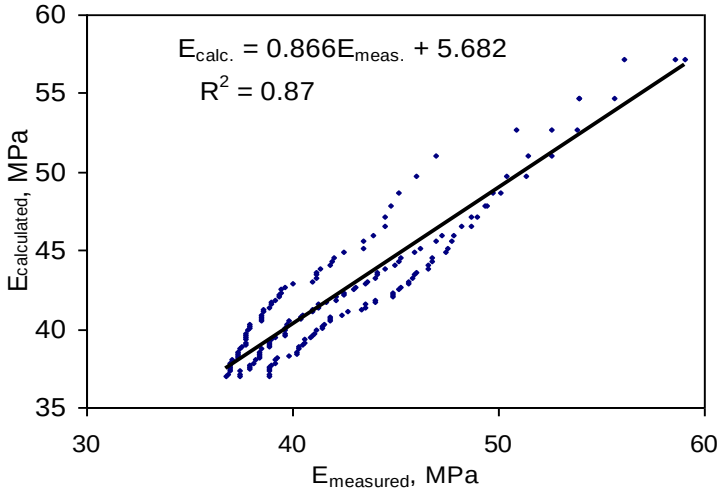

Figure 2.9: Coefficient of determination, R^2, for E(t), variety V1

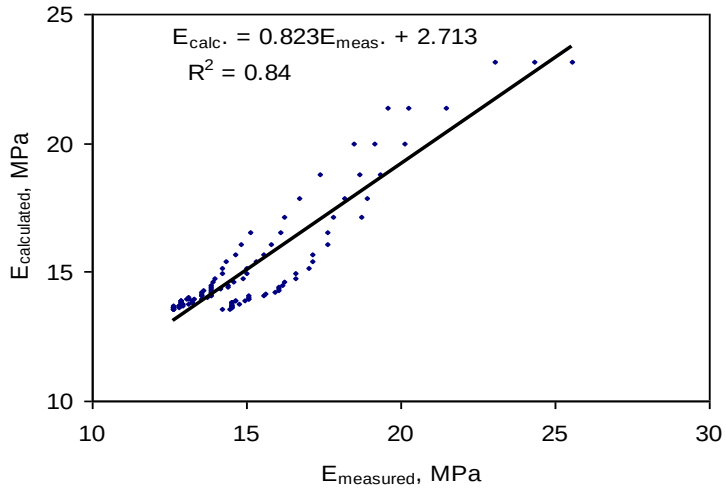

Figure 2.10: Coefficient of determination, R^2, for E(t), variety V2

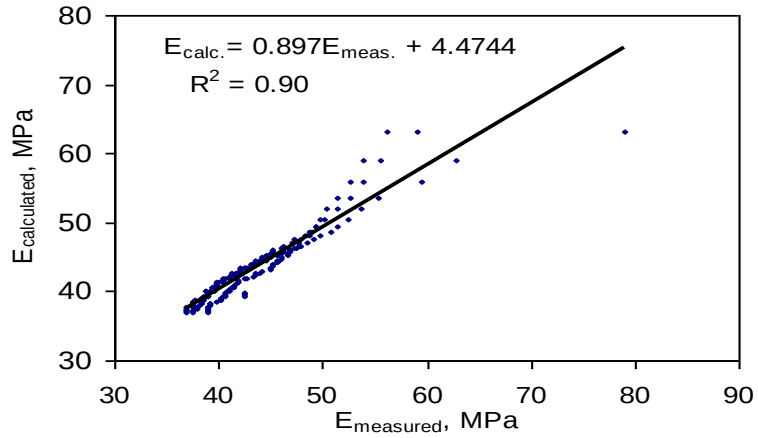

Figure 2.11: Coefficient of determination, R^2, for E(t), variety V3

The standard error on the residuals for each of the varieties V1, V2 and V3 were found to be 1.17, 0.95 and 1.82 MPa respectively. Similarly, the coefficient of determination between the measured values and the fitted values were obtained as 0.87, 0.84 and 0.90 for V1, V2 and V3 respectively as shown in Figures 2.9-2.11. These were indicators that the measured data and the regressed values fitted quite closely statistically.

The flexibility of the Maxwell-Weichert model in reproducing the viscoelastic behaviour of shelled maize *en masse* was further demonstrated by plotting the above results on a log-log scale as shown in Figure 2.12.

Figure 2.12, taken from one of the replications for V1, shows the application of the generalized form of Maxwell-Weichert model described in equation 2.17 with an almost infinite number of parameters (observed on the step-decline of the curve). Such behaviour, which was observed for all the varieties, has been reported for polymer viscoelastic materials by Aklonis and MacKnight (1983).

Elastoviscoplastic Models

Li *et al.*, (1989) presented a study based on the constitutive equation based on the elastic-viscoplastic (EVP) theory for cohesionless sands (Youngs, 1982) to model the stress-strain behaviour of wheat en masse under monotonic and cyclic loading conditions. This EVP model considers:

I. The effect of confining pressure or hydrostatic pressure on the deformation and strength characteristic of the particulates;
II. The development of large inelastic shear deformations during the loading process; and
III. The coupling between inelastic shear and volumetric deformation with changing stress state.

The three-dimensional constitutive formulation incorporates the effect of the evolution of intergranular structure on both stress-strain response and inelastic volume change induced by shear deformation. Stress-strain behaviour predicted by the Youngs' EVP model is based on an associated plasticity formulation for deviatoric strains and a separate constitutive equation for coupled volumetric strains. The parameters of the constitutive equations are assumed to be a function of void ratio, or bulk density, and the mean stress both of which reflect the effects of loading history. The parameter calculation technique used in the study was similar to that described by Youngs (1982).

2.2.1. One Dimensional Constitutive Equation

The key features of the elastic-viscoplastic (EVP) constitutive equation developed by Youngs (1982) are explained through the one-dimensional formulation.

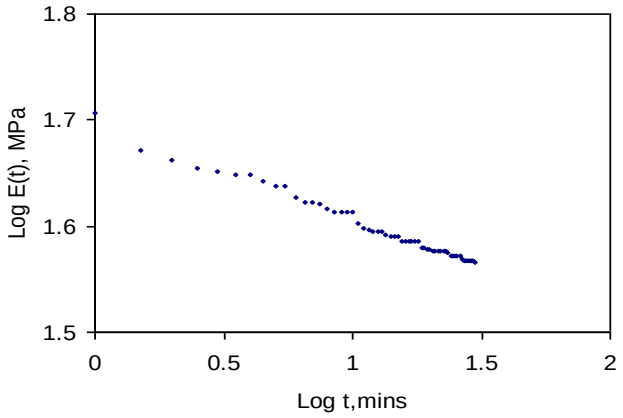

Figure 2.12: Behaviour of Maxwell-Weichert model in stress-relaxation for V1

For further in-depth understanding of the stress transfer and displacement mechanisms involved in elastic viscoplastic constitutive models the reader may consult these references (Chen and Baladi, 1985; Feda, 1982; and Youngs, 1982). The one-dimensional, stress-strain model is used as the stepping stone for presenting the three-dimensional model.

In the one-dimensional model, two strain rate equations (based on particulate theory) one for shear strain and one for volumetric strain, are used to characterize the grain en masse behaviour. The shear strain rate ($\dot{\gamma}$) equation consists of two components: 1) elastic shear strain rate ($\dot{\gamma}_e$) and 2) viscoplastic shear strain rate ($\dot{\gamma}_{vp}$). The elastic shear strain rate is the recoverable component of strain; whereas, the viscoplastic component is the irrecoverable (permanent) component of strain. The following shear strain rate equation was derived by Youngs (1982):

$$\dot{\gamma}_e = \dot{\gamma}_e + \dot{\gamma}_e = \frac{\dot{\tau}}{G} + |\dot{\gamma}|\left(\frac{\tau - \tau^r}{\frac{\dot{\tau}}{|\dot{\tau}|}\tau^y - \tau^r}\right)^m \frac{\dot{\tau}}{|\dot{\tau}|} \qquad (2.19)$$

Where:

G is shear elastic modulus,

m is plastic hardening exponent,

$\dot{\tau}$ is shear stress rate,

τ is shear stress,

τ^r = shear stress reversal point

τ^y = yield shear stress

$|\dot{\gamma}|$ = absolute value of shear strain rate,

$\frac{\dot{\tau}}{|\dot{\tau}|}$ = determine the point of the yield surface which is used to calculate the direction of yielding.

In equation 2.19 the ratio $\dot{\tau}/|\dot{\tau}|$is the unit vector that provides the stress direction of plastic flow, whereas, $|\dot{\gamma}|$ with the dimension of reciprocal time implicitly introduces the time factor in the formulation. In equation 2.19, the yield stress τ^yidentifies the onset of plastic flow, and τ^y is the state point on the stress surface where the stress direction rate ($\dot{\tau}$) was last reversed, i.e., changed from increasing to decreasing rate or vice-versa. The stress reversal point becomes a memory parameter, which is used to define the relative distance to the yield stress in the direction of stress rate (Ozdemir, 1976). The yield surface expands or contracts depending on the state of stress (Chen and Baladi, 1985). The volumetric strain rate ($\dot{\varepsilon}_v$) equation consists of two components: 1) the expansion strain rate ($\dot{\varepsilon}_v^x$)and 2) the collapse strain rate($\dot{\varepsilon}_v^c$). The expansion volumetric strain rate is due to the packing density change; whereas, the collapse volumetric strain rate is due to the grain reorientation. The volumetric strain rate equation is:

$$\dot{\varepsilon}_v = \dot{\varepsilon}_v^x + \dot{\varepsilon}_v^c = |\dot{\gamma}|[A(e - e_{cs})\lambda + B(1 - \lambda)] \qquad \ldots (2.20)$$

Where; A is volumetric expansion parameter, B is volumetric collapse parameter, e is current void ratio, e_{cs} is critical state void ratio, λ is relative structure change parameter ($0 \leq \lambda \leq 1$).

In equation 2.19, the yield stress τ^y in the direction of loading was hypothesized by Youngs (1982), based on experimental evidence, to be a function of the relative structure change parameter:

$$\tau^y = \tau^{f-} + \left(\tau^{f+} - \tau^{f-}\right) f(\lambda)$$

$$= \left(\tau^{f+} - \tau^{f-}\right)[1 - \exp(-5\lambda)] \quad \ldots (2.21)$$

Where;

τ^{f+} Is failure shear in the direction of shear (e.g., increasing or decreasing rate)

τ^{f-} Is failure shear stress in the opposite direction of shear (e.g., decreasing or increasing rate, respectively).

In equation 2.21, f(λ,) is an empirical function derived from experimental data. The function f(λ) for wheat was arrived at [1-exp (-5 λ,)] using the triaxial test data and Youngs (1982) linearity argument. For sands, exponents greater than 3 (compared to 5 for wheat) have been reported (Youngs, 1982). The relative structure change parameter λ is expressed as:

$$\lambda = 1 - \left[\{(\dot{\gamma}/|\dot{\gamma}|) - e^s\}/2\right] \qquad -1 \leq e^s \leq 1 \quad \ldots (2.22)$$

Where e^s is the variable used to measure the grain en masse structure.

The magnitude of the relative structure change parameter (λ) indicates the location of the failure stress state of the particulate material as the stress-strain path follows the limiting hardening curve, i.e., $\tau = \tau^y$ at all times. The value of λ varies from zero at the stress reversal point at the failure stress in one direction, to a value of unity as the failure stress, and is reached in the direction of shear. The magnitude of es measures the development of relative structure change and its sign determines the direction of the relative structure change. The absolute value of $e^s = 1$ implies that the particle rearrangement has been fully accomplished. This results in volumetric changes in collapse mode. Any further volumetric changes are due to the packing density adjustments. The rate of e^s is defined by:

$$\dot{e}^s = C\dot{\gamma}\,(1 - \lambda^l) \quad \ldots (2.23)$$

Where;

$\dot{e}^s$ is the rate of relative structure change,

C is structure modulus which controls the hardening rate,

l is exponent for the measure of linearity of relative structure change.

A useful interpretation of equation 2.23 is that initially $\dot{e}^s$is linearly proportional to $\dot{\gamma}$ since ($\gamma \approx 1$) no further changes in es occur during continued shear in that direction.

2.2.2. Three- Dimensional Constitutive Equation

Two assumptions, as postulated by Youngs (1982), are herein retained to expand the one-dimensional model described in the preceding section to a three-dimensional formulation. The assumptions are: 1) the granular material is isotropic, and 2) separate relationships can be developed for the response to deviatoric and hydrostatic (isotropic) loading.

The first assumption of isotropy simplifies the constitutive equations in that only two elastic material parameters (e.g., shear modulus and Poisson's ratio) are needed to completely describe the stress-strain relationship. In addition, invariants can also be effectively used to establish the state of stress. The evidence of structural anisotropy in sands has been demonstrated by Oda *et al.*, (1978). Tests by Lade (1972) and Oda *et al.*, (1972) with sand particles of various shapes showed that anisotropic behaviour decreases as the particle sphericity of the wheat particles tested in the present study was 55%. Hence, the load response of wheat en masse is expected to be anisotropic. The constitutive equation can be modified using the full elasticity tensor and introducing weighting factors in calculating the stress invariants as suggested by Sandler and DiMaggio (1973). The fully anisotropic constitutive equation requires 21 material constants for elastic component alone (Green-type linearly elastic material), which are extremely difficult if not impossible to determine. Therefore, as a first approximation and to keep the total number of material parameters at a reasonable number, the material response is assumed to be isotropic.

The deviatoric strain rate equation in three-dimensions similar in form to the one-dimension equation 2.19 is:

$$\dot{e}_{ij} = \frac{\dot{s}_{ij}}{2G} + \left\|\dot{e}_{ij}\right\| \left(\frac{\left\|s_{ij} - s_{ij}^r\right\|}{\left\|s_{ij}^y - s_{ij}^r\right\|}\right)^m n_{ij} \quad \ldots (2.24)$$

Where;

$\dot{e}_{ij}$ Is rate of deviatoric strain, $\left\|\dot{e}_{ij}\right\|$ is norm of deviatoric strain rate, which is also the length of the tensor $\dot{e}_{ij}$ projected on the octahedral plane and is defined by eq.2.24, m is shear yield exponent, n_{ij} is direction tensor, similar to the ratio $\frac{\dot{\tau}}{|\dot{\tau}|}$ in equation 2.19, S_{ij} is deviatoric stress, $\dot{S}_{ij}$ is rate of deviatoric stress, S_{ij}^r is deviatoric stress reversal point and S_{ij}^y is yield deviatoric stress,

$$\|\dot{e}_{ij}\| = \left(\dot{e}_{ij}\dot{e}_{ij}\right)^{1/2} = \left(2\|\dot{e}_{ij}\right)^{1/2} \quad \ldots (2.25)$$

$\|\dot{e}_{ij}$ Is second invariant of deviatoric strain

The double subscript notation has the usual meaning, i.e. the first index denotes the plane normal direction and the second index gives the direction of the tensorial quantity.

Both i and j subscripts can take on values 1, 2, and 3 which correspond to x, y, and z axis directions, respectively. In equation 2.25, repeated indices appearing in the subscripts imply summation, e.g. $e_{ii} = e_{11} + e_{22} + e_{33}$.

Since any hydrostatic (isotropic) stress change from a stress state containing a deviatoric component results in a movement relative to the failure surface (Lade and Duncan,1971), normalized deviatoric stress $\bar{S}_{ij}$, normalized deviatoric strain rate $\dot{\bar{e}}_{ij}$ and normalized shear modulus $\bar{G}$ are defined as follows (the overbar symbol, -, is used to denote normalized quantities):

$$\bar{S}_{ij} = \frac{S_{ij}}{(\sigma_m/P_a)^{\alpha}} \quad \ldots (2.26)$$

$$\dot{\bar{e}}_{ij} = (\sigma_m/P_a)^{\alpha}\dot{e}_{ij} \quad \ldots (2.27)$$

$$\bar{G} = \frac{G}{(\sigma_m/P_a)^{2\alpha}} \quad \ldots (2.28)$$

Where;

P_a Is atmospheric pressure, σ_m is mean stress which is defined as $\sigma_m = \frac{1}{3}\sigma_{kk}$

α Is failure surface curvature parameter

The deviatoric strain rate given by equation 2.24 then becomes:

$$\dot{e}_{ij} = \frac{\dot{S}_{ij}}{2G} - \propto \frac{\dot{S}_{ij}}{2G}\frac{\dot{\sigma_m}}{\sigma_m} + \|\dot{e}_{ij}\|\left(\frac{\|\bar{S}_{ij} - \bar{S}^r_{ij}\|}{\|\bar{S}^y_{ij} - \bar{S}^r_{ij}\|}\right)^m n_{ij} \quad \ldots (2.29)$$

In equation 2.29, normalized yield ($\bar{S}^y_{ij}$) and reversal ($\bar{S}^r_{ij}$) stresses appear because of the symmetry of response which results from the use of normal stresses. The directional tensor n_{ij} defines the direction of inelastic shear on the octahedral plane, and n_{ij} is the normal to the failure surface at a point defined by the direction of shear.

Using similar reasoning, a hydrostatic strain rate equation was derived by Youngs (1982):

$$\dot{\varepsilon}_{kk} = \frac{\dot{\sigma}_m}{K^e} + |\dot{\varepsilon}_{kk}|\, K^p \left(\frac{\sigma_m - \sigma^r_m}{\frac{\dot{\sigma}_m}{|\dot{\sigma}_m|}\sigma^{max}_m - \sigma^r_m}\right)^h \quad \ldots (2.30)$$

Where;

K^e Is elastic bulk modulus, K^p is plastic bulk modulus, h is plastic bulk exponent, $\dot{\varepsilon}_{kk}$ is hydrostatic volumetric strain rate, $\dot{\sigma}_m$ is mean stress rate, σ^{max}_m is past maximum mean stress rate.

The volumetric strains produced by three-dimensional shear straining are modelled the same way as the one-dimensional shear given by equation 2.20. The rate equation for volumetric strain becomes:

$$\dot{\varepsilon}_{kk} = \|\dot{e}_{ij}\|[A(e - e_{cs})\lambda + B(1 - \lambda)] \quad \ldots (2.31)$$

The total volumetric strain rate is the sum of hydrostatic (isotropic) volumetric strain rate (eq.2.30) and shear volumetric strain rate (eq. 2.31) In equation 2.24, the yield deviatoric stress S^y_{ij} is defined by equations 2.32 and 2.34 which is similar to the one-dimensional equation 2.21. The form of the empirical function f(λ) for the three: dimensional model suggested by experiments was $\lambda^{\bar{N}}$ (Youngs, 1982).

$$S^y_{ij} = S^{f+}_{ij} + \left(S^{f+}_{ij} - S^{f-}_{ij}\right)\lambda^{\bar{N}} \quad \ldots (2.32)$$

$$\bar{N} = N_1 + N_2\frac{\|S^{f+}_{ij}\|}{\|S^{f-}_{ij}\|} \quad \ldots (2.33)$$

Where;

S^{f+}_{ij} Is failure deviatoric stress in loading direction, S^{f-}_{ij} is failure deviatoric stress in

opposite loading direction, N_1 and N_2 are hardening curve exponents.

The structure change λ in the three-dimensional space is defined as:

$$\lambda = 1 - \frac{\|\lambda_{ij}\|}{2} \quad \ldots (2.34)$$

The structure change tensor λ_{ij} as in the one-dimensional case is defined in terms of the direction of shear strain. The tensor e_{ij}^{s} defines the current structure and $\dot{e}_{ij}$ the current strain rate. The continued shear in the direction of $\dot{e}_{ij}$ produces new structure in the direction $\dot{e}_{ij} / \|\dot{e}_{ij}\|$:

$$\lambda_{ij} = \frac{\dot{e}_{ij}}{\|\dot{e}_{ij}\|} - e_{ij}^{s} \quad \ldots (2.35)$$

Where;

e_{ij}^{s} Is the relative structure change

The rate equation for e_{ij}^{s} in three dimensions which is similar to the one dimension $\dot{e}^{s}$equation 2.23 is given by:

$$\dot{e}_{ij}^{s} = C\|\dot{e}_{ij}\|(1-\lambda^{l})\frac{\lambda_{ij}}{\|\lambda_{ij}\|} \quad \ldots (2.36)$$

Where C is the structure modulus

The structure modulus rate equation using the arguments similar to the one-dimensional model is given by:

$$\dot{C} = C\|\dot{e}_{ij}\|[(1-\lambda)D_2 - \lambda D_3] \quad \ldots (2.37)$$

Where D_2 and D_3 are relative structure change parameters.

Lee and Albaisa's (1974) experimental results showed that shear straining causes a reduction in the hydrostatic yield stress (σ_m^{max}). They also observed that volumetric strains for reconsolidated sand samples were the same under small shear strains. However, the volumetric strains exceeded the initial consolidation under large shear strains (Ishihara and Okada, 1978). These results imply that reorientation of granular material structure during shear erases the memory of previous overconsolidation. To account for this effect the following equation was proposed by Youngs (1982):

$$\dot{\sigma}_m^{max} = -D_1 P_a (OCR - 1)\|\dot{e}_{ij}\| \quad \ldots (2.38)$$

Where; $\dot{\sigma}_m^{max}$ is maximum mean stress rate, D_1 is plastic bulk modulus constant, OCR isoverconsolidation ration which is defined as:

$$OCR = \frac{\sigma_m^{max}}{\sigma_m} \quad \ldots (2.39)$$

The three- dimensional Youngs' EVP model for grain en loading is described by the deviatoric and hydrostatic strain rate equations 2.29 and 2.30, respectively, the volumetric strain rate (due to shear) equation 2.31, the structure change equation 2.35, and two structure change rate evolution equations 2.36 and 2.37.

Li *et al.*, (1990) made the following conclusions. Fifteen material parameters and their relationships for wheat en masse in Youngs' elastic-viscoplastic (EVP) model were determined from monotonic and cyclic triaxial test results. The single set of parameter values was used in the constitutive equations to successfully predict the cyclic load response in triaxial tests. The chi-square (χ^2) statistical test was used to evaluate the EVP model at the 0.05 level of significance. The following conclusions were drawn from this study:

1. Monotonic and cyclic triaxial tests can be used to determine all parameters and their relationships in the Youngs' EVP model.
2. The χ^2 test (at the 0.05 level of significance) established the goodness of Youngs' EVP model for predicting monotonic and cyclic stress (deviatoric and isotropic)-strain response of wheat en masse when data for all cycles were pooled in one set.
3. The χ^2 test (at the 0.05 level of significance) established the goodness of Youngs' EVP model for predicting monotonic volumetric strain response for all tests and cyclic volumetric strain response for the high-density test samples (849 kg/m^3) when data for all cycles were pooled in one set.

4. At the 0.05 level of significance, the χ^2 test demonstrated that the deviatoric and isotropic responses predicted by the EVP model and the triaxial data were not statistically different for the first two cycles in all tests.
5. At the 0.05 level of significance, the χ^2 test demonstrated that the EVP model predicted and the triaxial volumetric strain values were not statistically different for the first two cycles of loading at initial bulk density of 849 kg/m^3.

Table 2.1 Axial stress difference and isotropic stress χ^2 values for wheat en masse*

Confining pressure (kPa)	Monotonic loading		Cyclic loading	
	801kg/m^3	840 kg/m^3	801 kg/m^3	840 kg/m^3
Axial				
20.7	21.65	20.15	25.92	25.64
34.5	20.74	19.97	25.07	24.17
48.3	20.91	18.23	24.81	23.29
62.1	19.26	19.57	24.40	24.60
Isotropic				
0-82.2	25.86	25.47	30.91	31.14

* At 0.05 level of significance and 50 degrees of freedom, χ^2 value is 34.8

Table 2.2 Volumetric strain $\boldsymbol{\chi^2}$ values for wheat en masse for cyclyes*

Confining pressure (kPa)	Monotonic loading		Cyclic loading	
	801kg/m^3	840 kg/m^3	801 kg/m^3	840 kg/m^3
Axial				
20.7	34.09	33.05	37.01	34.49
34.5	32.71	34.28	38.24	33.50
48.3	33.23	31.05	34.82	34.79
62.1	31.78	31.22	38.76	33.26

* At 0.05 level of significance and 50 degrees of freedom, χ^2 value is 34.8

Table 2.3 Cycle by cycle χ^2 values for isotropic stress for wheat en masse

Cycle	**Isotropic pressure (kPa)**	**801 kg/m^3**	**849 kg/m^3**
1	0-20.7	27.6	29.3
2	0-41.4	27.1	28.5
3	0-62.1	35.0	36.7
4	0-82.8	36.2	38.2

* At 0.05 level of significance and 50 degrees of freedom, χ^2 value is 34.8

CONCLUSIONS

The mechanical behaviour of materials stored in silos and bunkers influence the flowability of the material and the forces that the material applies to the silo walls and bottom. The major problem in structural design of silos is to predict, with reasonable accuracy, the loads that these structures will be required to withstand during their service life.

This paper has reviewed elastoplastic, viscoelastic and elastoviscoplastic constitutive models for granular materials. Precise constitutive models and properly evaluated mechanical properties of granular materials are fundamental for proper design and control of storage, handling, and processing of those materials. More work remains in this crucial study area.

REFERENCES

Aklonis, J.J and W.J MacKnight. 1983. *Introduction to Polymer Viscoelasticity*. 2nd Ed. John Wiley and Sons, New York.

Balevičiu, R., I. Sielamowicz, Z. Mróz and Kačianauskas, R. 2011. *Investigation of wall stress and outflow in a flat-bottomed bin: a comparison of the DEM model results with the experimental measurements.* Powder Technology, 214, 322–336. doi: 10.1016/j.powtec.2011.08.042.

Briassou, D., and Curtis, J. **1985.** *"Design and Analysis of Silos for Friction Forces,"* Journal of Structural Engineering, 3 (6), June 1985, 1377-1398.

Chattopadhyay, A., R.K. Rao and M.A. Parameswaran. 1994. *On the classification of bulk solids.* Bulk Solids Handling, 14,339-344.

Chen, W.R and G.Y. Baladi. 1985. *Soil Plasticity.* New York: Elsevier**.**

Chi, L and Kushwaha, R.L. 1990. *Lade's elastoplastic model for granular soils.* American Society of Agricultural Engineers. Paper No. 90-1084.

Cundall, P.A., and O.D. Strack. 1979. *A discrete element model for granular assemblies.* Géotechnique, 29, 47–65.

Chung, T.J. 1988. *Continuum Mechanics.* Prentice-Hall International, Inc.

Dartevelle, S. 2003. *Numerical and granulometric approaches to geophysical granular flows***,** Ph.D. thesis, Michigan Technological University, Department of Geological and Mining Engineering, Houghton, Michigan.

Eurocode, L. 2003. *Actions on structures*. Part 4: Actions in silos and tanks. Ref. No. EN 1991-4.

Oranga, E. 2005. *Elastic and Viscoelastic Behaviour of Shelled Maize En Masse.* Master's thesis. University of Nairobi, Kenya.

Findley, W.N., J.S. Lai and K. Onaran. 1976. *Creep and Relaxation of Non- Linear Viscoelastic Materials*. Vol. 18 North-Holland Publishing Co., Amsterdam.

González-Montellano, C., E. Gallego, Á. Ramírez-Gómez and F. Ayuga. 2012. *Three dimensional discrete element models for simulating the filling and emptying of silos: Analysis of numerical results*. Computers and Chemical Engineering, 40, 22–32. doi: 10.1016/j.compchemeng.2012.02.007.

Gumbe, L.O. 1995. *Load deformation behaviour of soils and en-masse grains*. Paper Presented at the Symposium on Unsaturated Soil Behaviour and Applications. Nairobi, Kenya

Gumbe, L.O. 1993. *A Discussion on Constitutive Equation for Granular Materials En-masse*. East African Journal of Engineering. 1(1): 27 – 38.

Gumbe, L.O. 1990. *Material Characterisation and Prediction Equations for Loads in Silos Containing Granular Materials En-masse.* African Journal of Science and Technology, Series A: 8(1): 1 - 5.

Gumbe, L.O. and B.M. Maina. 1990. *Elastoplastic Constitutive Parameters for Rice En-masse*. African Journal of Science and Technology, Series A: 8(2): 15 - 25.

Harri, D. 2009. *An elastoplastic model for deformation and flow of granular materials and its connection with micro mechanical quantities.* In: Powders and Grains 2002:

Proceedings of the 6th international conference on micromechanics of granular media. 1145, 1085-1088. doi: 10.1063/1.3179833

Heinrich, M.J., R.N Sidney and P.B Robert. **1996.** *The Physics of Granular Materials*. In: Physics Today, pp 32

Herum, F.L., et al., **1979.** *"Viscoelastic Behavior of Soybeans Due to Temperature and Moisture Content,"* Transactions of ASAE, 22, (5), 1220-1224.

Horabik, J. and M. Molenda. **2014.** *Mechanical Properties of Granular Materials and Their Impact on Load Distribution in Silo: A Review*. Scientia Agriculturae Bohemica. *45*(4): 203–211

Ishihara, K. and S. Okada. 1978. *Effects of stress history on cyclic behavior of sand*. Soils and Foundation 18(4): 31-45.

ISO 3535. 1977. *Continuous mechanical handling equipment – Classification and symbolization of bulk materials*. International Agrophysics, 14,385-392

Janssen, H.A. 1895. *Experiments on grain pressure in silos.* Verein Deutscher Ingenieure, Zetschrift (Düsseldorf), 39, 1045–1049. (in German).

Jenike, A.W. 1961. *Gravity flow of bulk solids.* Bulletin of the University of Utah, 52, 1-309.

Kobyłka, R. and M. Molenda. 2014. *DEM simulations of loads on obstruction attached to the wall of a model grain silo and of flow disturbance around the obstruction.* Powder Technology, 256, 210–216. doi:10.1016/j.powtec.2014.02.030.

Kobyłka, R. and M. Molenda. 2013. *DEM modelling of silo load asymmetry due to eccentric filling and discharge.* Powder Technology, 233, 65–71. doi: 10.1016/j.powtec.2012.08.039.

Kou, H.P., P.C. Knight, D.J. Parker, Y. Tsuji, M.J. Adams and J.P.K. Seville. 2002. *The influence of DEM simulation parameters on the particle behaviour in a V-mixer*. Chemical Engineering Science, 57, 3621–3638.

Lade, P.V. 1977. *Elasto-plastic stress- strain theory for cohesionless soil with curved yield surface*. International Journal of Solids and Structure; 13: 1019-1035.

Lade, P.V. 1972. *The stress-strain and strength characteristics of cohesionless soils.* Ph.D. thesis. University of Califomia, Berkeley.

Lade, P.V. and J.M. Duncan. 1971. *Stress-path dependent behavior of cohesionless soil.* ASCE J. of Geotechnical Engineering Division 102(GT1): 51-68.

Lee, K.L. and F. Albaisa. 1974. *Earthquake induced settlements in saturated sands.* ASCE J. of Geotechnical Engineering Division 100(GT4): 387- 406**.**

Li, Y., Q. Zhang, V.M Puri and H.B Manbeck. 1989. *Elasto-plastic constitutive equation parameters and load response of wheat en-masse-part-I, initial density, moisture content and strain rate effects.* Trans. of ASAE 32(1): 194-202

Manbeck, H.B., and Nelson, G.L. 1975. *Three Dimensional Constitutive Equations for Wheat En Masse*. Transactions of ASAE, 18 (6) 1122-1127.

Manbeck, H.B., and Nelson, G.L. 1972. *Methods and Instrumentation for Evaluating the Stres-Strain Behavior of Wheat En Masse.* Transactions of ASAE, 919-922, American Society of Agricultural Engineers, St. Joseph, Michigan.

Masson, S. and J. Martinez. 2000. *Effect of particle mechanical properties on silo flow and stress from distinct element simulations.* Powder Technology, 109, 164–178. doi: 10.1016/ S0032-5910(99)00234-X.

Mensah, J.K., et al., 1981. *Effect of Drying Conditions on Impact Shear Resistance of Selected Corn Varieties.* Transactions of ASAE. 24(6), 1568-1572, American Society of Agricultural Engineers, St. Joseph, Michigan.

Mohsenin, N.N. 1980. *Thermal Properties of Foods and Agricultural Materials.* Gordon and Breach, New York

Moya, M., F. Ayuga, M. Guaita and P.J Aguado. 2002. *Mechanical properties of granular agricultural materials considered in silos*

design. ASCE Engineering Mechanics Conference; Colombia University, New York

McLaughlin, N.B. and R.E. Pitt. 1984. *Failure characteristics of apple tissue under cyclic loading*. Trans. of ASAE 27: SE 1984: 311-320

Oda, M., I. Koishikawa and T. Higiuchi. 1978. *Experimental study of anisotropic shear strength of sand by plane strain test*. Soils and Foundations 18(1): 26-38.

Ozdemir, H. 1976. *Nonlinear transient dynamic analysis of yielding structures*. Ph.D. thesis. University of California, Berkeley**.**

Parafiniuk, P., M. Molenda and J. Horabik. 2013. *Discharge of rapeseeds from a model silo: physical testing and Distinct Element Method simulation*. Computers and Electronics in Agriculture, 97, 40–46.

Peleg, M. 1985. *The role of water in rheology of hygroscopic food powders.* In: Simataos D, Multon JL (eds): Properties of water in foods. Martinus Nijhoff Publishers, Dordrecht, 394-404.

Stafford, J.V., E. Audsley and Sharp, J.R. 1986. *The determination of best fit linear failure envelopes to Mohr Circles*. J. Agric Eng. Res. (1986)33, 33-38.

Shelef, L. and N. N. Mohsenin. 1968. *Effects of Moisture Content on Mechanical Properties of Corn horny Endosperm*. Cereal chemistry 46 (3): 242-253.

Stinchcomb, W.W. 1989. *Damage and fracture of composite materials under cyclic loads. Advances in fracture research.* Salama, Ravi-Chandar, Taplin and Rama (eds); 4: 2939-2955

Schott, R.W., and Britton, M.G. **1984.** *Plane Strain Behavior of Bulk Grain.* ASAE Paper No. 84-503, American Society of Agricultural Engineers, St. Joseph, Michigan.

Kasap, S.O., S. Yannacopoulos, V. Mirchandani and J.R. Hildebrandt. 1992. *Ultrasonic Evaluation of Thermal Fatigue of Composites*. Journal of Kumar.

Magurno, A. 1999. *Vegetable fibres in automotive interior components.* Die Angew Makromol Chem. 272, 99–107.

Sykut, J., M. Molenda and J. Horabik. 2008. *Influence of filling method on packing structure in model silo and DEM simulations*. Granular Matter, 10, 273–278.

Ti, K.S. 2009. *A review of basic soil constitutive models for geotechnical application.* EJGE Vol. 14, Bund. J

Tordesillas, A. 2004. *The jekyl and hyde of granular materials uncovered*. www.unimelb.edu.au/

Vanel, L., P. Claudin, P.J. Bouchaud, M.E Cates, E. Clement and J.P Witterner. 2000. *Comparison between theoretical models and new experiments*. Physical Review Letters; 84(7): 1439-1442.

Youngs, R.R. 1982. *A three-dimensional effective stress model for cyclicly loaded granular soils.* Ph.D. diss. The University of California, Berkeley.

Zhang, Q., V.M Puri, H.B. Manbeck. 1994. *Applicability of a two-parameter failure criterion to wheat en masse.* Trans. of ASAE. 37(2): 571-575.

Zhang, Q., M.G. Britton and R. Jaremek. 1993. *Dynamic loads during discharge for wheat, barley and canola in a smooth and a corrugated-walled model bin.* Journal of Agricultural Engineering Research, 56, 111–119. doi: 10.1006/jaer.1993.1065

Zhang, Q., V.M, Puri and H.B. Manbeck. **1986.** *Determination of Elasto-plastic Constitutive Parameters for Wheat En Masse.* ASAE Paper No. 86-4073, American Society of Agricultural Engineers, St. Joseph, Michigan.

Zhang, Q., V.M. Puri and H.B. Manbeck. **1985.** *Finite Element Modelling of Thermally Induced pressures in Grain Bins Filled with Cohensionless Granular Material.* ASAE Paper No. 85-4002, American Society of Agricultural Engineers, St. Joseph, Michigan.

Maxwell, A.S., W.R Broughton, G. Dean and G.D Sims. 2005. *Review of accelerated ageing methods and lifetime prediction techniques for polymeric materials.* Engineering and Process Control Division, HMSO and Queen's Printer, NPL Report DEPC MPR 016 ISSN 1744-0270, Scotland.

Perrot, Y., C. Baley, Y. Grohens and P. Davies. 2007. *Damage Resistance of Composites Based on Glass Fibre Reinforced Low Styrene Emission Resins for Marine Applications*. Applied Composite Materials.14(1) 67-87.

Rapra.2012.
http://www.rapra.net/composites/material-selection/some-design-considerations.asp. Retrieved from http://www..net. On 24/02/2016

Wang, Y., S. Lim, J.L Luo and Z.H. Xu. 2006. *Tribological and Corrosion Behaviors of Al_2O_3/Polymer Nanocomposite Coatings.* Wear. **260**(9-10): 976-983.

INSTRUCTION TO JEAE CONTRIBUTORS

The editorial staff of the JEAE requests contributors of articles for publication to observe the following editorial policy and guidelines in order to improve communication and to facilitate the editorial process;

Criteria for article selection

Priority in the selection of articles for publication is that the articles:

a. Are written in the English language
b. Are relevant to the application in of engineering in agriculture and the environment
c. Have not been previously published elsewhere, or, if previously published are supported by a copyright permission
d. Deals with theoretical, practical and adoptable innovations applicable to agriculture and environment
e. Have a 150 to250 words abstract,preceeding the main body of the article
f. Are printed , double-spaced, under 4,000 words (approximately equivalent to 8 pages of JEAE-size paper)
g. Are supported by authentic sources, references or bibliography
h. Written on IBM formatted 3.5inch floppy discs or on recordable compact discs (CD-R) closed in the ISO 9660 standard format.

Rejected/accepted articles

a. As a rule, articles that are not chosen for JEAE publication are not returned unless writer (s) asks for their return and are covered with adequate postage stamps. At the earliest time possible, the writer (s) is advised whether the article is rejected or accepted.
b. When an article is accepted and requires revision/modification, the details will be indicated in the return reply from the JEAEChief Editor,in which case such revision/modification must be completed and returned to JEAE within three months from the date of receipt from the Editorial Staff.
c. The JEAE does not pay for articles published. However, the writers are given collectively 2 free copies (one copy airmailed, where applicable, and the other copy is sent by surface/sea mail) of the JEAE issue wherein their articles are published.in addition, a single writer is given 5 off-prints of the article and plural writters are given 10 off-prints (also sent by surface/sea mail).
d. Complementary copies: Following the publishing, three successive issues are sent to the author(s)

Procedure

a. Articles for publication (original and three copies) must be sent to JEAE on the following address:

The Chief Editor
Journal of Engineering in Agriculture and the Environment
P.O Box 10677-00100
GPO
Nairobi
Tel: +254 788 712 156
E-mail: info@kesebae.or.ke

b. The article must bear the writer (s) name, title/designation, office/ organization, nationality and complete mailing address. In addition, contributors with e-mail addresses are requested to forward the same to the Chief Editor for faster communication.

Format/ Style Guidance

a. Article must be sent on IBM formatted 3.5 inch floppy disks or on a recordable compact disc (CD-R) in a suitable word processor (e.g. WordPerfect, MS Word for Windows, etc.) along with one printed original and 3 copies.
b. The data for graphs and photographs (in the black & white) must be enclosed with the article.
c. Whether the article is a technical or popular contribution, lecture, research result, thesis or special report, the format must contain the following features:

i. A brief and appropriate title;
ii. The writer (s) name, designation/title, office/ organization; and mailing address;
iii. An abstract following (ii) above;
iv. Proper body (text discussion);
v. Conclusion (s)/ recommendation(s); and
vi. Bibliography

d. The printed copy must be numbered (Arabic numeral) successively at the top centre whereas the disc copy pages should not be numbered. Tables, graphs and diagrams must likewise be numbered. Table numbers must preced table captions, e.g., "**Table 1**: Hourly crushing capacities of mill A". Such table number and title must be typed at the top of the table and should be left-aligned. On the other hand, graphs, diagrams, maps and photographs are considered figures in which case the captions must be indicated below the figure and preceded by a number, e.g.,"**Figure 1**: Variation of compaction levels of the soil in increasing soil moisture content of the arable layers".
e. The data for the graph must also be included (both inhard and soft-copy form).
f. Tables and figures must be preceded by texts or discussions. Inclusion of such tables and figures not otherwise referred to in the text/ discussion must be avaoided.
g. Tables must be typed clearly without vertical lines or partitions. Horizontal lines must be drawn only to contain the subtitle heads of columns and at the bottom of the table.
h. Express measurements in the metric system and crop yields in metric tons per hectare (t/ha) and smaller units in kilogram or gram (kg/plot or g/row).
i. Indicate by footnotes or legends any bbreviations or symbols used in tables or figures.
Convert national currencies to US dollars and use the latter consistently
j. Round off numbers, if possible, to one or two decimal units, e.g., 5.5 tonnes/trip instead of 5.54762 tonnes/trip.
k. When numbers must start a sentence, such numbers must be written in words, e.g., "Forty-five workers…, or Five tractors" instead of 45 workers…, or, 5 tractors.

ARTICLES